Compact Waveguide Grating Couplers for Silicon Photonic Integrated Circuits

CHEN, Xia

A Thesis Submitted in Partial Fulfillment

of the Requirements for the Degree of

Doctor of Philosophy

in

Electronic Engineering

The Chinese University of Hong Kong

July 2010

ProQuest LLC.
789 East Eisenhower Parkway
P.O. Box 1346
Ann Arbor, MI 48106 - 1346

Abstract of Thesis Entitled:

Compact Waveguide Grating Couplers for Silicon Photonic Integrated Circuits

Submitted by CHEN, Xia

for the degree of Doctor of Philosophy in Electronic Engineering

at The Chinese University of Hong Kong in June 2010

Photonic integrated circuits (PICs) based on Silicon-on-insulator (SOI) substrate were proposed to make miniaturized photonic devices on chip, so that low-cost and compact devices for applications including sensing, inter/intra-chip communications and optical fiber communications could be made. One of the key challenges in the development of highly integrated PICs is efficient coupling of light between a submicron-sized nanophotonic wire and an optical fiber due to the large loss inherent from the mismatch in mode field size between the optical fibers and the nanophotonic wire waveguides. An attractive approach for efficient coupling is to use diffractive grating couplers which show many advantages over alternative approaches. However the angled alignment of the optical fiber to the grating as reported in the previous work is not desirable for a low-cost optical packaging process.

We demonstrated a simple technique to realize vertical fiber coupling with linearly chirped grating periods. No additional fabrication process is required yet a comparable coupling efficiency is achieved with the proposed chirped grating couplers with vertical optical fibers. Design and experimental results of one-dimensional (1D) gratings, two-dimensional (2D) gratings, focusing gratings and fully-etched nanoholes gratings are described in the thesis. We also describe the

waveguides and grating couplers fabricated on silicon-on-sapphire for mid-infrared applications.

The 2D grating couplers could be used as polarization splitter. Polarization insensitive coupling and polarization-diversity circuits are realized by the 2D grating couplers. We also demonstrated a novel silicon waveguide grating which serves dual functions: as a 1×2 variable integrated beam splitter/combiner and as an out-of plane diffractive element for coupling light. The split ratio can be tuned by changing the launch position of the optical fiber without introducing much excess loss. An integrated Mach-Zehnder interferometer (MZI) is implemented with this novel functional element. This MZI was demonstrated as a demodulator for differential phase-shift-keying (DPSK) signal.

An apodized grating coupler with the best coupling efficiency hitherto reported for shallow-etched waveguide grating couplers is described. By appropriate choice of waveguide/grating thicknesses and varying the coupling strength of the grating coupler via tailoring its fill factor to optimize the mode matching, a coupling loss of only 1.2dB was obtained for each fiber/silicon waveguide interface with a slightly titled optical fiber.

摘要

基於硅絕緣體（SOI）的光子集成電路（PICs）可用於製造晶片上的微型光子器件，這些低成本以及高度集成的器件能廣泛應用於遙感，晶片內部通信和光纖通信。實現高度集成的 PICs 的主要困難之一是如何高效率地耦合納米光波導和光纖，由於它們之間大小的巨大差異以及模式的不匹配造成大量的損耗。一個近幾年提出的有吸引力的方法是使用波導光柵耦合器。相對於其他的方法，它展示了許多優點。不過，之前設計的光珊偶合器需要光纖跟晶片垂直線成一個準確的角度，這不利於實現低成本的光封裝。

我們展示了一個利用線性啁啾光珊實現垂直光纖偶合的技術。這個技術可以在不需要額外的製造工藝的情況下，實現了跟傾斜光纖相似的偶合率。我們在論文中描述了一維（1D）光柵、二維（平面）光柵、聚焦光柵以及完全蝕刻的奈米結構光珊的設計和實驗結果。我們還描述了應用於中紅外領域的在 silicon-on-sapphire 上製備的光波導以及光珊偶合器。

2D 光珊還可用於偏振分光器，它們可用於實現偏振不敏感的耦合與光路。我們還展示了一種全新的有雙重功能的波導光柵結構。它可同時用作光分離/合成器和偶合器。它的分流比可以進行調節。我們還用它做成了可集成的 Mach-Zehnder 干涉儀（MZI），並用這個 MZI 來解調差分相移鍵控（DPSK）信號。

此外，我們還描述了一個變跡光柵耦合器。它實現了迄今所報告的淺層蝕刻波導光柵耦合器所達到的最高偶合效率。通過適當選擇波導/光柵的尺寸以及變化光柵的強度，我們優化了納米波導跟光纖之間的模式匹配。

Acknowledgement

First of all, I would like to express my deep and sincere gratitude to my supervisor, Prof. H.K. Tsang, for his patient guidance and encouragement during the four years of study. This thesis could not be finished without his helpful advices and support. I wish to thank Prof. K.T. Chan and Prof. Chester Shu for helpful discussions.

My sincere thanks are due to Ms. L.C. Ho for her technical assistance. Her countless help is the most critical thing for me to finish the experiments on time.

During my PhD study, a lot of friends and colleagues have offered help and useful discussions. My special thanks go to Dr. C. Li, Dr. T.K. Liang, Dr. Y.H. Luo, Dr. Mable Fok, Dr. P.S. Chan, Dr. Y. Liu, Dr. K.J. Chen, Dr. C.M. Sun, Dr. L. Xu, Ms. S.M. Wan, Mr. L.K. Cheng, Ms. K.Y. Fung, Mr. Y.H. Dai, Mr. J.B. Du, Mr. H. He, Mr. K.P. Lei, Mr. M.G. Lo, Mr. C.Y. Wong and Mr. Z.X. Zhang.

I thank ePIXfab (www.epixfab.eu) and NFF in HKUST for fabricating some of the devices included in this thesis.

I also thank all the technicians and administrative staff in the Department of Electronic Engineering, especially in the micro and nano-fabrication laboratory.

Finally, I would like to express my deepest gratitude to my family and my girlfriend Iris, for their love and support over these years.

Table of Contents

List of Figures

1. Introduction

Inspired by the huge successes of optical communication and integrated circuit (IC) industry, silicon-based photonic integrated circuits (PICs) were proposed to make miniaturized photonic devices on chips, so that low cost and compact devices for optical communications and sensing applications could be made. Besides, photonic integrated circuit (PIC) technology enables optical transmission systems for inter-chip or intra-chip connection with potential for larger bandwidth and lower power consumption, to overcome the physical limits of electrical interconnects that potentially limits the future development of IC industry. In this chapter, we first give an overview of PIC technology that is based on silicon-on-insulator (SOI) substrates. Then the motivation for the work presented in this thesis is introduced, with a brief review of the previous related work. A brief overview of the thesis is also included in the last part of this chapter.

1.1 Photonic integrated circuit (PIC)

Similar to electronic IC, the technology of PIC, sometimes also called optoelectronic integrated circuit (OEIC), is to integrate multiple functional photonic and electronic components together in a single semiconductor chip. Functional devices which may be integrated include lasers, modulators, detectors, attenuators, multiplexers/de-multiplexers, optical amplifiers, filters, etc. This technology would enable "parallel fabrication" process with numerous optical and electronic components fabricated simultaneously on the wafers [1]. Thus, high-speed, compact,

monolithically integrated devices combined with photonic and electronic circuits could be made to fulfill complex functions at low cost.

1.1.1 Reasons to develop PIC technologies

The concept of integrated optics was first described by S. E. Miller in 1969 [2]. It was proposed that sophisticate patterns of lightwave circuits for communication functions could be fabricated in a sheet of dielectric using photolithograph techniques. Various functional components could be fabricated simultaneously, which were connected with optical waveguides. Integration could save the cost for precise positioning of each optical component in a communication system, and reduce the sensitivity to acoustic as well as thermal effects. Development of IC industry now makes possible the integration of over one billion transistors in a single chip, and the mature processing technologies also facilitate the fabrication of silicon lightwave circuits in nanometer scale. PIC can refer to the further integration of lightwave circuits and electronic circuits either monolithically or using a hybrid approach [3].

PIC has potential for a huge market with the increasing use of various optical communication networks, which now extend to individual consumers. After the proposal of using glass fibers as optical data transmission medium in 1966 by Kao and Hockham [4], optical communication networks have established their domination at both the local and long-haul data transmission all over the world. Those networks include the well established dense wavelength division multiplexing (DWDM) networks, and also the emerging fiber-to-the-building (FTTB), fiber-to-the-home (FTTH) [5] and radio over fiber (ROF) systems [6]. We can envision that almost all the voice and video information we received in daily life, using whatever

tools (e.g. computers, televisions, mobile phones, radios), will be carried with optical signals in the near future. Devices with PICs that can generate, manipulate, and detect light will perform key functions in those networks, and they would have dominating cost-advantages over discrete optical components.

Besides those macro-scale networks, PIC technologies would also find applications for optical interconnects in computers. The exponential growth in information processing and transmission capacity, as summarized by Moore's law, has hitherto led to the integration of over one billion transistors on a single chip. Recently, the on-chip communication requirements of modern multi-core processors have already resulted in aggregate data rates in excess of 100Gb/s. The power consumption and heat generation from electrical signal transmission to/in the chip are increasingly the bottlenecks hindering the future advances of computers. Optics offers a potential solution to the increasing heat dissipation of on-chip communications [7]. Beside the limitation of transmission bandwidth and wiring density for electrical signaling in next-generation computers, substantial power would be consumed in the near future, which potentially contributes around 2.6% of the carbon emission worldwide. Therefore, there is an increasing need for an innovative technology (such as PICs) with large bandwidth, high density and low power consumption to replace the electrical signals in future inter-chip and possibly intra-chip communication networks.

1.1.2 Why silicon?

Silicon wafers have been the dominant platform for the electronic IC industry and driving the information revolution for over 50 years. Silicon is relatively cheap compared to other semiconductor materials, as it's the second most abundant

element after oxygen, making up 25.7% of the earth's crust by mass [8]. The development of complementary metal-oxide-semiconductor (CMOS) technology had made it possible to make transistors in high density and huge volume on silicon, which enables the complex microprocessors, dense memory circuits and other digital and analog electronics circuits with a low unit cost. Therefore, silicon has an enormous technological foundation, which makes it the material of choice for photonic circuits to be monolithically integrated with electronic circuits. The readily available fabrication facilities world wide and high quality silicon wafers available in the market are also attracting people to investigate the possibilities to fabricate the PICs on silicon. In addition, the high thermal conductivity and damage threshold would make silicon a superior substrate for PICs than group III-V materials [7].

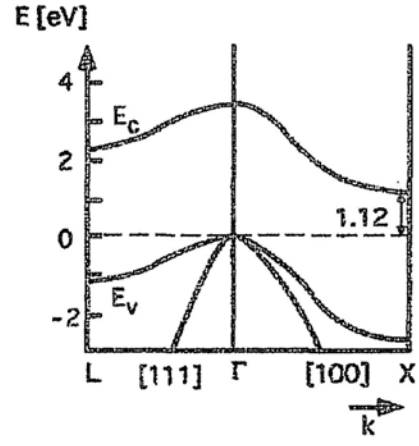

Fig. 1.1 Energy band diagram of silicon which is an indirect bandgap material with 1.12eV bandgap energy [11].

However, silicon photonics had only received a modest amount of attention at the early stage [9, 10]. There are mainly three reasons that limiting the development of PIC technology on silicon. One is that it's difficult to make efficient light emission form crystalline silicon because it's an indirect bandgap material. The energy band

diagram of silicon is shown in figure 1.1. The upper energy level is the conduction band and the lower level is the valence band. An electron will normally jump from minimal-energy state in the conduction band to the maximal-energy state in the valence band, and simultaneously emit a photon. The electron needs to satisfy conservation of energy and crystal momentum. For an indirect bandgap material such as silicon, the previous process must also involve the absorption or emission of a phonon at the same time, where the phonon momentum equals the difference of k-vector between the minimal-energy state in conduction band and the maximal-energy state in valence band. The involvement of the phonon makes this process much less likely to occur in a given span of time [11]. Thus, silicon is much more difficult to emit light than III-V compounds, which have a direct bandgap.

Another obstacle for the development of silicon photonics is silicon does not exhibit an electro-optic effect known as the Pockels effect, a traditional characteristic for fast modulation of light signal. Pockels effect is the second-order nonlinearity of semiconductors, causing a linear and relatively strong change of the refractive index with an applied electric field. Most optical modulators available in the market are based on the Pockels effect in lithium niobate or other III-V compound. However, Pockels effect occurs only in materials that lack inversion symmetry, which is not the case for silicon crystal. The diamond lattice of silicon implies that the Pockel effect simply does not exist. Some other techniques to change the refractive index or absorption of silicon for optical modulation would be required.

Monolithically integrated photo-detector on silicon would be another challenge for the research community. The wavelength used in various communication networks (1.3-1.6μm) also coincides with the low loss wavelength range in silicon. Silicon has an energy band gap of 1.12eV, so it is highly transparent for the

wavelength over 1.2μm. This is good for data transmission, but not suitable for light detection. It is challenging to make efficient photodetectors for the 1.3-1.6μm wavelength in crystalline silicon.

However, in recent years lots of work carried out shows a promising future of silicon as the mainstream platform for PICs. Similar to silicon electronic at the early stage, many possible solutions were proposed to tackle the obstacles listed previously, and different kinds of silicon based laser, modulator and photodetector were demonstrated successfully as introduced in the following paragraphs. More extended reviews of silicon photonics could be found in [12, 13].

The demonstration of silicon Raman amplifier [14] and laser [15-17] that can be fully integrated with CMOS circuits was one of the major milestones in the history of silicon photonics. Stimulated Raman scattering in bulk silicon is relatively strong and could be used for light amplification and generation. Yet the early attempts to achieve net gain by stimulated Raman scattering were limited by absorption of the free carrier generated by two-photon absorption (TPA) of the pump [18]. Pulse pumping was first used to achieve amplification and lasing, in which case the carriers cannot accumulate. Continues-wave amplification and lasing were then reported with increased carrier recombination by applying an electronic field across the silicon or increasing surface recombination with more surface area and internal defects. A wide variety of CMOS compatible lasers incorporated with materials other than silicon were also demonstrated. For example, growth or hybrid integration of group III-V on silicon, Erbium doping in silicon or silicon dioxide and silicon based quantum well structure could also make lasing in silicon achievable.

Although Pockels effect is not present in bulk silicon, the free-carrier plasma effect due to the electrons and holes in silicon was proposed to be able to produce

electro-optic modulation of both the absorption and refractive index [19]. 10GHz modulation was first reported by Intel Corporation with optimized metal-oxide-semiconductor (MOS) capacitor [20]. Ring cavity enhancement has further reduced the size of silicon modulators [21], and even higher modulation speed has been obtained by carrier-depletion type modulators [22]. On the other hand, high speed optical signal detection on silicon at the communication wavelength was realized by integrating with germanium (Ge) [23] or using ion-implantation induced defect states in silicon [24].

1.1.3 Silicon-on-insulator (SOI) waveguide devices

Silicon-on-insulator (SOI) is one special type of silicon wafers with a thin layer of buried oxide separating the top silicon layer from the bulk silicon. SOI was first used in the microelectronic industry to reduce parasitic capacitance of CMOS circuits, thus helping to reduce the power consumption and enhance the operating frequency. It was soon adopted by the photonic community because optical waveguides fabricated on SOI wafers would have two dimensional confinement of light. The large index step of the silicon (refractive index is around 3.48) and the cladding material (silicon dioxide with a refractive index of 1.46 or air) can now confine light not only in the lateral direction such as rib waveguide on bulk silicon, but also vertically between the cap and the buried oxide. Nanophotonic waveguides with a cross section of only about 0.1 μm^2 and a lost as low as 2.4dB/cm were made on SOI wafers using CMOS compatible technologies [25].

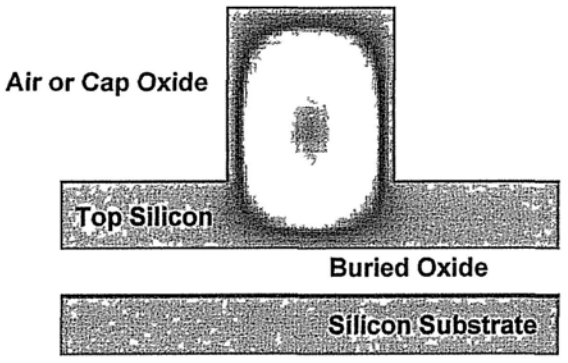

Fig. 1.2 Cross section of a SOI waveguide

The waveguide as illustrated in figure 1.2 is the most fundamental building block of PICs. Waveguides on SOI wafer work similarly to conventional fibers, trapping light in the core area of higher refractive index. The larger index step of silicon waveguide makes it possible to confine light beam in an area smaller than $0.1\mu m^2$. The bending radius of such nanophotonic waveguide could reach a few micrometers with negligible radiation loss [3]. Thus photonic devices could be integrated in a very compact way with a typical length of tens of micrometers.

Beside those fundamental research on the material properties of silicon, targeting at light generation, modulation and detection as described previously. Various structures based on silicon waveguide were studied to gain more superior functionalities. Ring resonator was used to improve the performance of modulators [21] originally based on Mach-Zehnder interferometer (MZI) structure [20]. It could also be used for wavelength filtering and routing, optical logic circuits, bio-sensing, etc. Arrayed waveguide grating (AGW) was also demonstrated on SOI with a footprint of only 0.07 mm^2 [26] for wavelength multiplexing and demultiplexing Recent development on photonic crystal structure [27] and plasmonic waveguide

[28] on silicon would also enrich the diversity of photonic devices on SOI. Figure 1.3 shows a picture of our fabricated photonic devices on an SOI wafer.

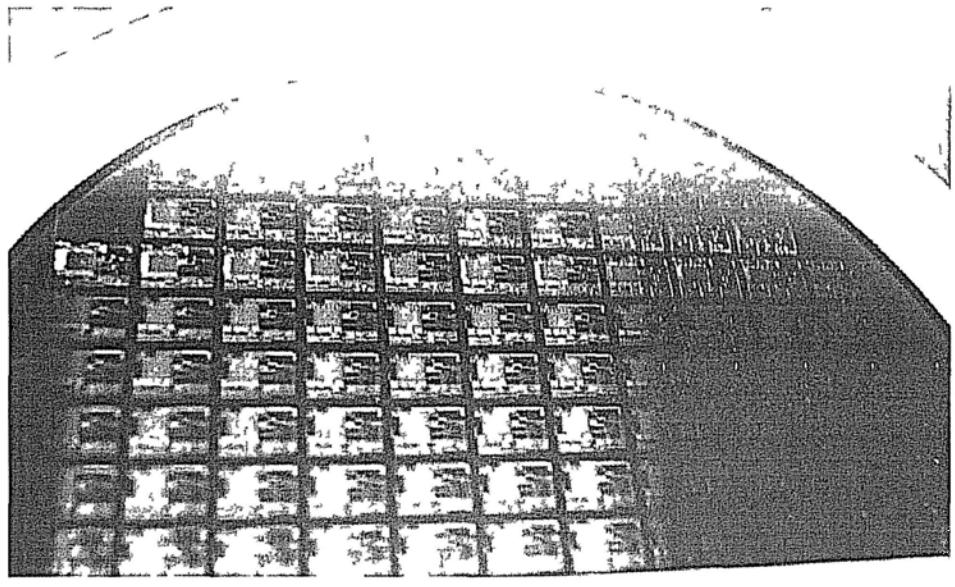

Fig. 1.3 Fabricated photonic devices on a silicon-on-insulator (SOI) wafer

1.2 Motivation

As we presented in the previous section, PIC devices based on SOI would gain a huge market for applications including sensing, inter/intra-chip communications and optical communications in various fiber-based networks.

A key challenge in the development of high density PICs is efficient coupling of light between a nanophotonic waveguide and an optical fiber because of the large loss inherent from the mismatch in mode field size between the optical fiber (~ 75μm^2 effective area) and the nanophotonic waveguide (~ 0.2μm^2 effective area). Coupling efficiency that is lower than 1% is expected from butt-coupling of an optical fiber and a nanophotonic waveguide. An attractive approach for efficient

coupling is to taper the waveguide width of the nanophotonic wire waveguide until it has the same size as the mode from the optical fiber and then to use an etched diffraction grating along the widened waveguide to diffract light between the fiber and the waveguide [29, 30]. The main advantages of such grating couplers over alternative techniques, such as using inverse adiabatic tapers and polished facets [31], include the capability to place the coupler anywhere on a chip (they need not be located at the edge of a die), no need for facet polishing, and compatibility with wafer-scale optical testing. Grating couplers are also much easier to fabricate with normally one shallow etching step, while the inverse taper approaches require patterning of an additional wave guiding layer (typically made of silicon nitride or polymer film) on top.

An off-normal alignment of optical fibers with respect to the die surface is required for grating couplers to reduce the significant second order back reflection of the waveguide grating to improve the coupling efficiency [30]. However the angled alignment of the optical fiber to the grating is not desirable for a low cost optical packaging process. Vertical coupling is more preferable because it enables a simpler optical alignment process that decouples adjustment of the fiber separation from the waveguide with the fiber position in the plane of the waveguide, and this can improve the speed for automatic alignment needed in low cost packaging. Grating couplers for vertical fiber coupling have also been proposed for low cost photonic packaging [32, 33]. However, those designs either include slanted grating which require non-standard fabrication methods or include additional polishing and etching steps to reduce the back reflection from the grating. A demand for a grating coupler design with no additional complication of fabrication process, yet could achieve high efficient coupling with a vertical optical fiber has be posted.

Another critical issue is the limited coupling efficiency of grating couplers hitherto demonstrated (~ 35%) [30], which is still below the expectation for applications in commercial products. Two main factors have limited the coupling efficiency of grating couplers. One is because a large fraction of the optical power in the SOI waveguide is coupled downwards into the substrate instead of upwards towards the optical fiber. Additional structures such as a substrate mirror [34] or a polysilicon overlay [35] is required to further improve the performance. Another factor that limits the coupling efficiency is the mode mismatch between the field profiles of diffracted light from waveguide grating and the fiber mode. An exponentially decaying field profile is generally expected when diffracted from a uniform grating, and this would theoretically limit the coupling efficiency to a maximum of 80% for coupling to the Gaussian-like mode profile of an optical fiber. Solutions to overcome these limitations are proposed in this thesis.

In addition, the waveguide gratings, as a versatile functional element, could be used for many other applications besides coupling of light. Novel multi-functional elements based on grating couplers are demonstrated, such as power splitters/combiners and polarization splitters. They will form a unique advantage promoting the grating couplers. For the applications of PICs in mid-IR region, which is an emerging field for chemical detection and remote sensing, we will also explore the characteristics of grating couplers and waveguides based on silicon-on-sapphire substrate.

1.3 Thesis overview and main innovations

In this thesis, we first propose a novel technique using chirped gratings to realize vertical fiber coupling without additional fabrication process. It can reduce the cost

of the packaging process of PIC devices. A detailed theoretical model for calculation of the 2D grating is presented. A novel tunable grating splitter/combiner is reported. Most importantly, we demonstrated the best coupling efficiency to date for waveguide grating couplers with apodized gratings. We also extended our work to mid-infrared wavelength, using silicon-on-sapphire wafers.

Chapter 2 introduces a novel technique to realize vertical fiber coupling to nanophotonic waveguides with linearly chirped grating periods, including the design, simulation and experimental results of one-dimensional (1D) chirped grating couplers. Focusing chirped grating couplers are also demonstrated that dramatically reduce the device footprint of the grating couplers.

Chapter 3 describes two-dimensional (2D) chirped grating couplers. Polarization-diversity circuit with ring resonators for differential phase-shift-keying (DPSK) demodulation was realized by the 2D grating couplers.

Chapter 4 introduces a novel silicon waveguide grating which serves dual functions: as a 1×2 variable integrated beam splitter/combiner and as an out-of plane diffractive element for coupling light between a optical fiber and a nanophotonic waveguide. Experimental characterization results of an integrated MZI implemented with this novel functional element are presented. This MZI was demonstrated as a demodulator for DPSK signal in an optical transmission system.

In chapter 5, simulation and experimental results of grating couplers composed of arrays of nanoholes are presented. This subwavelength grating coupler can be fabricated using the same photolithography mask and etching process as used for the silicon-on-insulator waveguides, which dramatically reduces the fabrication cost. Effective index model is applied to the subwavelength structure.

Chapter 6 describes the simulation and experimental results of an apodized grating coupler coupling between an optical fiber and a nanophotonic waveguide. The design parameters were optimized and the coupling strength was engineered to obtained Gaussian-like output profile. 1.2dB coupling loss is achieved to slightly titled optical fibers. Preliminary results for coupling with vertical fibers with chirped gratings are also introduced.

Chapter 7 presents extended work of silicon photonic devices on silicon-on-sapphire wafer in mid-infrared region. The implementation of a mid-infrared fiber laser is introduced and we also present the waveguides and grating couplers for mid-infrared wavelength.

Chapter 8 summaries the main results of my research work with suggestions of some possible further work.

References

[1] L. Tsybeskov, D. J. Lockwood, and M. Ichikawa, "Silicon photonics: CMOS going optical," Proc. IEEE, vol.97, no.7, pp.1161-1165, July 2009.

[2] S. E. Miller, "Integrated optics: an introduction," Bell Syst. Tech. J., vol.48, pp.2059-2068, Sept. 1969.

[3] G. T. Reed, "Silicon photonics: the state of the art," Wiley, 2008

[4] C. K. Kao and G. A. Hockham, "Dielectric fiber suface waveguides for optical frequencies," Proc. IEE, vol.133, no.7, pp.1151-1158, July 1966

[5] K. Wada, S. Park, and Y. Ishikawa, "Si photonics and fiber to the home," Proc. IEEE, vol.97, no.7, pp.1329-1335, July 2009.

[6] Z. Jia, J. Yu, and G-K Chang, "A full-duplex radio-over-fiber system based on optical carrier suppression and reuse," IEEE Photon. Technol. Lett., vol.18, no.16, pp.1726-1728, Aug. 2006.

[7] D. A. B. Miller, "Device requirement for optical interconnects to silicon chips," Proc. IEEE, vol.97, no.7, pp.1166-1185, July 2009.

[8] Wikipedia, http://en.wikipedia.org/wiki/Silicon

[9] R. A. Soref, "Silicon-based optoelectronics," Proc. of the IEEE, vol.81, no.12, pp.1687-1706, Dec. 1993.

[10] G. T. Reed, "The optical age of silicon," Nature, vol.427, no.6975, pp.595-596, Feb. 2004.

[11] Y. Liu, Optoelectronic Characteristics and Application of Helium Ion-implanted Silicon Devices, PhD Thesis, The Chinese University of Hong Kong, 2007.

[12] R. Soref. "The past, present, and future of silicon photonics," IEEE J. Sel. Topics Quantum Electron., vol.12, no.6, pp.1678-1687, Nov. 2006.

[13] B. Jalali, "Can silicon change photonics?" Phys. Stat. Sol. (a), vol.205, no.2, pp.213-224, Feb. 2008.

[14] R. Claps, D. Dimitropoulos, V. Raghunathan, Y. Han, and B. Jalali, "Observation of stimulated Raman amplification in silicon waveguides," Opt. Express, vol.11, no.15, pp.1731-1739, July 2003.

[15] Boyraz and B. Jalali, "Demonstration of a silicon Raman laser," Opt. Express, vol.12, no.21, pp.5269-5273, Oct. 2004.

[16] H. Rong, A. Liu, R. Jones, O. Cohen, D. Hak, R. Nicolasecu, A. Fang, and M. Paniccia, "An all-silicon Raman laser," Nature, vol.433, pp.292-294, Jan. 2005

[17] H. Rong, R. Jones, A. Liu, O. Cohen, D. Hak, A. Fang, and M. Paniccia, "A continuous-wave Raman silicon laser," Nature, vol.433, pp.725-728, Feb. 2005.

[18] T. K. Liang and H. K. Tsang, "Role of free carriers from two-photon absorption in Raman amplicfication in silicon-on-insulator waveguides," Appl. Phys. Lett., vol.84, no.15, 2745, Apr. 2004.

[19] R. A. Soref and B. R. Bennett, "Electrooptical effects in silicon," IEEE J. Quantum Electron., vol.QE-23, no.1, pp.123-128, Jan. 1987.

[20] L. Liao, D. Samara-Rubio, M. Morse, A. Liu, D. Hodge, "High speed silicon Mach-Zehnder modulator," Opt. Express, vol.13, no.8, pp.3129-3135, Apr. 2005.

[21] Q. Xu, B. Schmidt, S. Pradhan, and M. Lipson, "Micrometre-scale silicon electro-optic modulator," Nature, vol.435, pp.325-327. May 2005.

[22] A. Liu, L. Liao, D. Rubin, H. Nguyen, B. Ciftcioglu, Y. Chetrit, N. Izhaky, and M. Paniccia, "High-speed optical modulation based on carrier depletion in a silicon waveguide," Opt. Express, vol.15, no.2, pp.660-668, Jan. 2007.

[23] M. Morse, O. Dosunmu, T. Yin, Y. Kang, G. Sarid, E. Ginsburg, R. Cohen, and M. Zadka, "Progress toward competitive Ge/Si photodetectors," Proc. SPIE, vol.6996, 699614, May 2008.

[24] M. W. Geis, S. J. Spector, M. E. Grein, J. U. Yoon, D. M. Lennon, and T. M. Lyszczarz, Opt. Express, vol.17, no.7, pp.5193-5204, Mar. 2009.

[25] W. Bogaerts, R. Baets, P. Dumon, V. Wiaux, S. Beckx, D. Taillaert, B. Luyssaert, J. Van Campenhout, P. Bienstman, and D. Van Thourhout, "Nanophotonic waveguides in silicon-on-insulator fabricated with CMOS technology," J. Lightw. Technol., vol.23, no.1, pp.401-412, 2005

[26] P. Dumon, W. Bogaerts, D. Van Thourhout, D. Taillaert, R. Baets, J. Wouters, S. Beckx, and P. Jaenen, "Compact wavelength router based on a silicon-on-insulator arrayed waveguide grating pigtailed to a fiber array," Opt. Express, vol.14, no.2, pp664-, Jan. 2006.

[27] J. D. Joannopoulos, S. G. Johnson, J. N. Winn, and R. D. Meade, Photonic crystals: molding the flow of light (second edition), Princeton university press, 2008

[28] E. Ozbay, "Plasmonics: merging photonics and electronics at nanoscale dimensions," Science, vol.311, no.5758, pp.189-193, Jan.2006.

[29] D. Taillaert, et al., "An out-of-plane grating coupler for efficient butt-coupling between compact planar waveguides and single-mode fibers," *IEEE J. Quantum Electron.*, vol.38, pp.949-955, July 2002.

[30] D. Taillaert, et al., "Grating couplers for coupling between optical fibers and nanophotonic waveguides," *Jap. J. Appl. Phys.*, vol.45, no.8A, pp.6071-6077, Aug. 2006.

[31] T. Shoji, T. Tsuchizawa, T. Watanabe, K. Yamada, and H. Morita, "Low loss mode size converter from 0.3μm^2 Si wire waveguides to singlemode fibers," *Electron. Lett.* Vol.38, pp.1669-1670, Dec. 2002.

[32] B. Wang, J. Jiang, and G. P. Nordin, "Embedded slanted grating for vertical coupling between fibers and silicon-on-insulator planar waveguides," *IEEE Photon. Technol. Lett.*, vol.17, no.9, pp.1884-1886, Sept. 2005.

[33] G. Roelkens, D. V. Thourhout, and R. Baets, "High efficiency grating coupler between silicon-on-insulator waveguides and perfectly vertical optical fibers," *Opt. Lett.*, vol.32, pp.1495-1497, Jun. 2007.

[34] F. Van Laere, G. Roelkens, M. Ayre, J. Schrauwen, D. Taillaert, D. Van Thourhout, T. F. Krauss, and R. Baets, "Compact and highly efficient grating couplers between optical fiber and nanophotonic waveguides," *J. Lightw. Technol.* **25**, 151-156 (2007).

[35] G. Roelkens, D. Vermeulen, D. Van Thourhout, R. Baets, S. Brision, P. Lyan, P. Gautier, and J.-M. Fedeli, "High efficiency diffractive grating couplers for interfacing a single mode optical fiber with optical fiber with a nanophotonic silicon-on-insulator waveguide circuit," Appl. Phys. Lett. **92,** 131101 (2008).

2. One-dimensional chirped grating couplers

Waveguide grating couplers for coupling between optical fibers and nanophotonic waveguides are of immense practical interest because of their many advantages. However, orientating the fibers at a small angle from normal to the wafer surface would be required to reduce the back reflection and achieve a high coupling efficiency. In this chapter, a novel technique to realize vertical fiber coupling to nanophotonic waveguides with linearly chirped grating periods is proposed. A brief introduction of the grating couplers is first presented, followed by design and simulations for the proposed 1D chirped grating coupler. Experimental measurement results for the normal chirped grating couplers and the focusing ones with reduced device footprint are also included.

2.1 Introduction

Diffraction gratings are studied for utilizing various functionalities, including light coupling for a few tens of years. Early work was reviewed by Gaylord, et al in 1985 [1]. After PICs were introduced, grating couplers were proposed to couple light into/out of waveguides [2-4]. However, the early work concentrated on weak gratings which typically have a length longer than 100μm. They were used to couple light beams in free space with relative large diameters, and occupy a large area compared to photonic devices. But for the high density PIC technology nowadays, the chip area is a valuable resource. Light beams in free space will also pose many difficulties for the packaging process.

In 2002, the first work using strong grating to butt-couple a vertical optical fiber with a nanophotonic waveguide was reported [5]. Finite difference time-domain (FDTD) simulation was used to design such shallow etched strong second-order gratings on waveguides [6]. However, only a maximum of 19% coupling efficiency is measured for this waveguide grating coupler. A strong resonance in the obtained spectrum indicates that there is a large second-order back reflection into the waveguide when coupling light into an optical fiber, which greatly limits the overall coupling efficiency. A new design of grating coupler with around 90% coupling efficiency was proposed by the same group in 2004 [7]. The optical fiber was tilted with respect to the surface normal of the SOI wafer, in order to prevent the large second-order Bragg back reflection encountered previously. Each grating period in the grating coupler was carefully calculated to achieve a Gaussian-like output field profile to match with the fiber mode. A substrate back reflector was also included in the simulation to have nearly all the light power diffracted upwards into the optical fiber. However, such grating couplers have not been experimental implemented so far due to difficulties in fabrication. Around 30% coupling efficiency was demonstrated by 2006 [8], and there was some work reported with higher coupling efficiencies thereafter. 69% was demonstrated for the grating coupler bonded with gold bottom mirror [9]. A poly-silicon overlay was also shown to be able to improve the directionality of the grating diffraction [10-12]. The most recent coupling efficiency reported using poly-silicon overlay was also -1.6dB (69%) [12].

Although grating couplers have already been demonstrated with such high coupling efficiency and reduced back reflection by placing the fiber at an off-normal alignment with respect to the die surface, the angled alignment of the optical fiber to the grating is undesirable for a low cost optical packaging process. Vertical coupling

is more preferable because it enables a simpler optical alignment process that decouples adjustment of the fiber separation from the waveguide grating with the fiber position in the plane of the waveguide, and this can improve the speed for automatic alignment needed in low cost packaging. Recently, grating couplers for coupling with vertical fibers without small angle tilting have also been proposed [13-16]. However, those designs either include slanted gratings which require the development of angled dry etching processes or additional polishing and etching steps to reduce the back reflection from the grating. A novel technique to realize vertical fiber coupling to nanophotonic waveguides was reported by our group [17-19]. A section of grating with linearly chirped periods was applied to suppress the Bragg back reflection and enhance the coupling efficiency. A coupling efficiency of over 34% was achieved for the vertical fiber grating coupler, which could be fabricated with only a shallow etch step same as the one for normal titled fiber grating couplers. The design, simulation and experimental results of one-dimensional (1D) chirped grating couplers are presented in this chapter. Focusing chirped grating couplers that dramatically reduce the device footprint of the grating couplers are also introduced.

2.2 Design and simulations

2.2.1 Device layout and theoretical calculation

The chirped grating coupler is designed for SOI wafers with 220nm top silicon layer and 2μm thick buried oxide. There is 750nm top oxide deposited, which is optimized to direct more light upwards to enhance the coupling efficiency [8], similarly to an anti-reflection layer. The fundamental mode propagating in a

nanophotonic waveguide fabricated on SOI may be expanded by an adiabatic taper to a width of about 12μm and coupled out vertically by diffraction of a 70nm shallow etched grating structure on top of the waveguide as shown in Fig. 2.1. This etch depth is also optimized for coupling to a single mode fiber [8] at the operation wavelength. The taper to a 12μm-width produces a lateral TE mode profile that is well-matched with the mode of conventional single mode optical fibers and allows a theoretical matching efficiency as high as 97% in y-z plane [7]. The mode field parameter (MFD) of the single mode optical fiber is set to be 10.4 μm in calculation, which is the typical value for single mode fibers in the market. The proposed design is optimized for coupling to the TE mode in the waveguide.

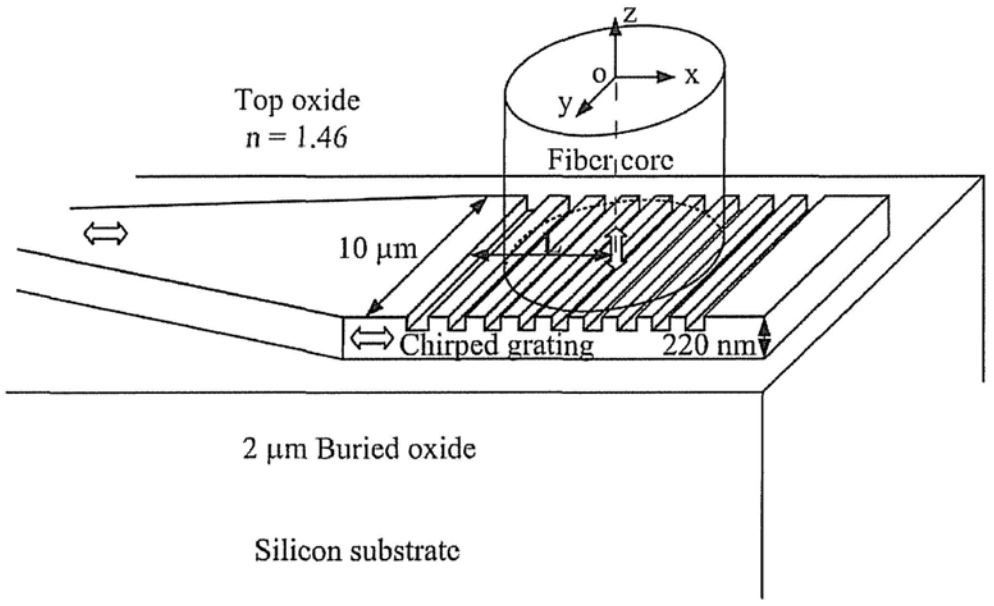

Fig. 2.1: Schematics of the proposed grating coupler with chirped gratings

The period needed for vertical out-of-plane coupling is calculated by the phase matching condition, which could be derived simply by considering the path difference of light scattered out from different periods:

$$k_o n_{eff} = k_o n_c \sin\theta + q\frac{2\pi}{\Lambda}, \qquad (2.1)$$

where $k_o=2\pi/\lambda$, n_c is the refractive index of the cladding (equals to 1.46 for silicon dioxide), θ is the angle of the output light to the surface normal of the SOI wafer (equals to zero for vertical coupling), n_{eff} is average effective index of the grating, q is a integer representing the diffraction order (typically equals to 1 for grating couplers mentioned in this thesis), and Λ is the period of the waveguide grating.

Among those parameters in Eq. 2.1, the n_{eff} is a critical one that needs to be determined before calculating the period. During FDTD simulations, we can observe the optical power confined in the fundamental mode of waveguide for both the teeth (non-etched) and grooves (etched) of the grating region. This implies the phase change of the wave along one period is approximately the combination of phase changes in the tooth and groove region. Thus an almost linear relationship between average effective refractive index n_{eff} and fill factor f (defined as the ratio of the shallow-etched groove's width to the grating period) could be obtained.

$$n_{eff} = n_{tooth}(1-f) + n_{groove} f \qquad (2.2)$$

The n_{tooth} and n_{groove} are the effective indices of the optical mode in the tooth and a groove region of the grating respectively. The teeth and grooves (220 nm and 150 nm thick silicon slabs, respectively) have the same importance in contributing to the n_{eff} of the whole grating region in the light propagation direction. FDTD simulations were carried out to verify the Eq. 2.2. We measured the diffractive angle θ from the simulations and calculated the n_{eff} based on Eq. 2.1. The results obtained from FDTD simulations are plotted in Fig. 2.2, which roughly match with the approximated solution (straight line) derived by Eq. 2.2.

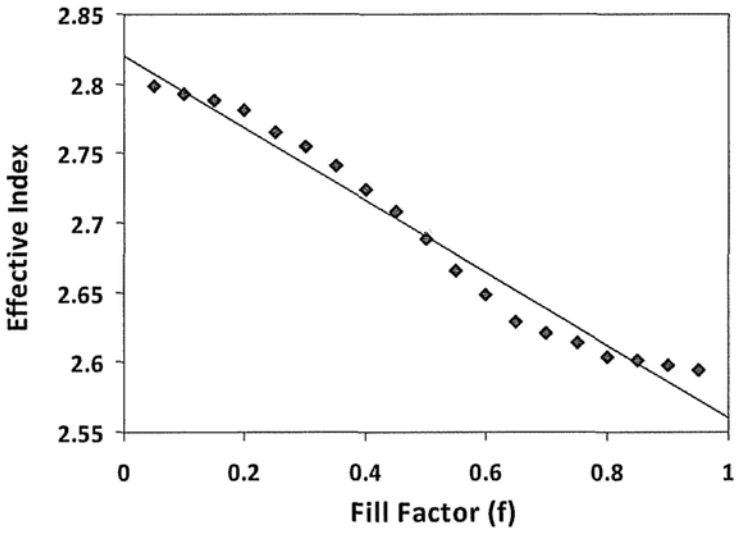

Fig. 2.2: The average effective indices n_{eff} of 1D gratings obtained by 2D FDTD simulation were plotted (dots) against f, with 220nm thick top silicon and 70nm shallow-etched gratings. The solution derive by a linear approximation in Eq. 2.2 is also plotted (in line) for comparison.

2.2.2 Simulations and design optimization

Two dimensional (2D) FDTD simulations were used for such grating structures as shown in Fig. 2.3 because the waveguides are sufficiently wide. To calculate the coupling efficiency, a Gaussian waveform with 1/e width of 10.4μm was employed to represent the fiber mode. The fiber mode propagates vertically and is diffracted by the grating. Light can couple into the waveguide mode by Bragg diffraction. Coupling efficiency between the fiber and waveguide was calculated using the power in the waveguide mode coming out from the front end of the grating coupler. The back reflection into the waveguide when coupling light from waveguide to optical fiber was also monitored. Calculations for uniform grating with tilted fiber were

done to validate our simulation method. The results were consistent with those reported previously [8]. During simulations, the fiber position L (illustrated in Fig. 2.3) which is the horizontal distance from the center of fiber core to the front-end of the grating coupler was adjusted to maximize the coupler efficiency.

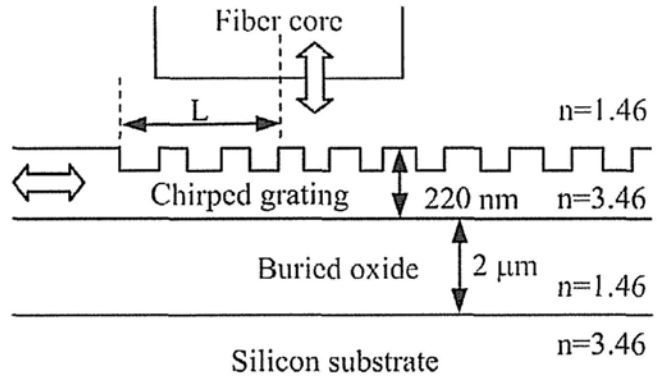

Fig. 2.3: Cross-section schematic of the proposed grating coupler for FDTD simulation. The position of fiber was represented by L: the horizontal distance from the center of fiber core to the front-end of the grating coupler

In our design, the 22 periods are divided into two sections. The total length is about 13μm. The grating in the front section is linearly chirped. Grating period Λ varies linearly with p (0, 1, 2, p_{total}-1) according to:

$$\Lambda_p = \Lambda_0 + \frac{p}{p_{total} - 1}\Delta, \quad (2.3)$$

where Δ is the grating chirp parameter (defined as the max grating period deviation), Λ_0 is the period of first grating at the front end. The average period is 580nm with a fill factor (or duty cycle) of 0.53 for front chirped section. This fill factor minimizes the back reflection, because of the destructive interference of the wave reflected by the front and rear surfaces of each slot.

The rear section is a uniform grating. The fill factor *f* for the rear section is changed in simulation to optimize the design. We found that a large reflection from the rear grating would increase the light coupled into the fiber. The simulation results for grating coupler design with different fill factors for the rear section were shown in Fig. 2.4. A 0.66 fill factor would give the best coupling efficiency according to our simulations.

Coupling efficiency and back reflection for our proposed design (Design II) with different Δ were shown in Fig. 2.4. For comparison, the results of coupler with *f=0.53* for both front and rear grating sections (Design I) are also plotted. Only about 25% of light is coupled into the fiber mode from the waveguide with uniform grating, because of the large Bragg back reflection into waveguide, which approaches 35% for the uniform grating. The back reflection is reduced by chirping of the grating periods in the front section, either positively or negatively. The coupling efficiency between fiber and waveguide is over 42% when grating chirp parameter Δ equals to *-120nm*. The asymmetry of coupling efficiency for positive and negative chirping is due to the different beam profiles diffracted from the grating coupler.

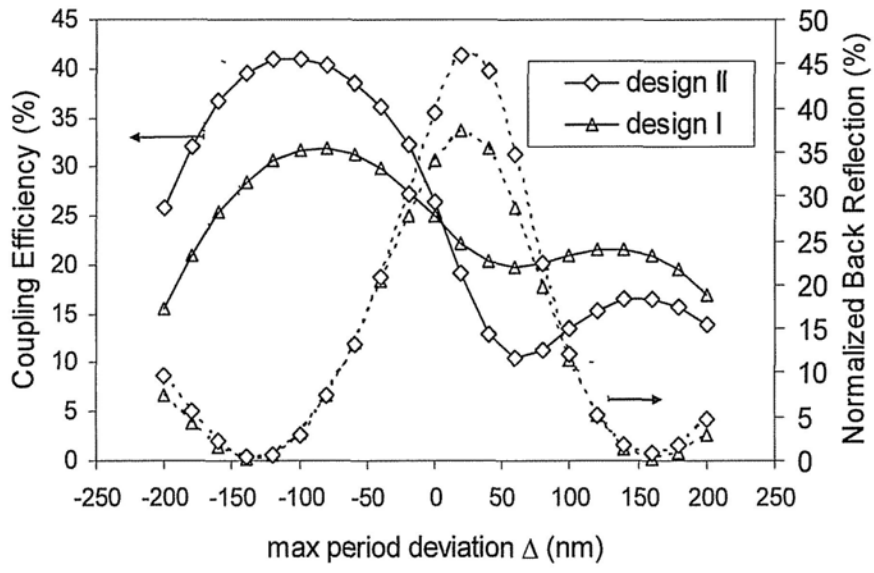

Fig. 2.4 Coupling efficiency (solid) and back reflection into waveguide (dashed) for designs with different grating chirp parameters Δ. Design I: *f=0.53* across the whole grating. Design II: *f=0.53* for the front chirped section, and *f=0.66* for the rear uniform section.

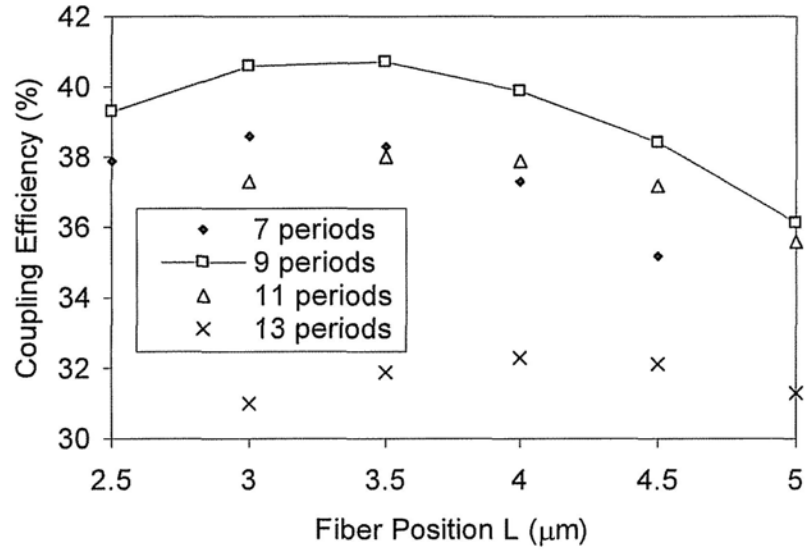

Fig. 2.5: Coupling efficiency with different fiber position *L* and number of chirped grating periods (*Δ= -120nm*). Optimum coupling efficiency achieved with 9 periods chirped in the front grating section.

The tolerance of the fiber position L (illustrated in Fig. 2.3) was also studied in calculating the coupling efficiency. The simulation results are shown in Fig. 2.5. Best coupling efficiency was obtained with 9 periods linearly chirped in the front grating section, while fiber was fixed at a horizontal position of 3.5μm away from the front end the grating coupler. For this optimized configuration, coupling efficiencies and back reflection for different wavelength between 1505nm and 1595nm are presented in Fig. 2.6. Results for optimized uniform grating coupler at 1550nm are also plotted for comparison. The back reflection into waveguide is dramatically suppressed and coupling efficiency is improved by the chirped grating. The maximum coupling efficiency is about 42% with a 3dB bandwidth of 48nm. The coupling efficiency of this grating coupler is mainly limited by the directionality of diffraction, as almost half of the optical power was diffracted downward.

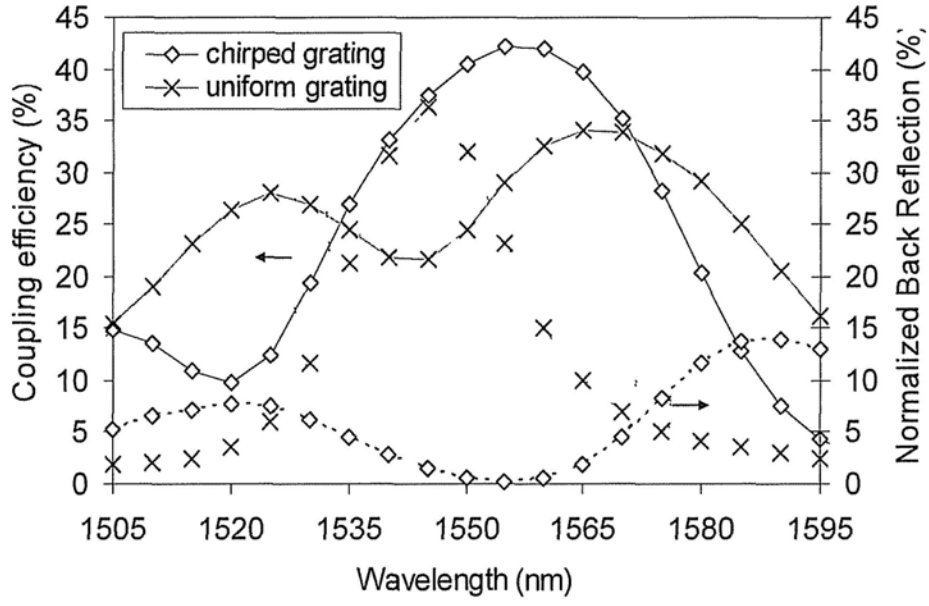

Fig. 2.6: Comparison on coupling efficiency (solid) and back reflection (dashed) between our proposed design and the optimized uniform grating coupler.

2.3 Experimental measurements and discussions

These devices were fabricated using Deep-UV lithography at ePIXfab (www.epixfab.eu). The fabricated devices consisted of a section of 500nm-width waveguide with the adiabatic tapers and grating couplers as described above for input and output coupling. The SEM image of the fabricated chirped grating coupler is shown in Fig.2.7. The measured coupling efficiency of the grating coupler is shown in Fig. 2.8 assuming that the waveguide and tapers are lossless and that the input and output grating couplers have the same coupling loss. The maximum coupling efficiency is over 34% with a 3dB bandwidth of 45nm. The peak coupling efficiency is similar to the 31% peak coupling efficiency reported for the uniform gratings with angled optical fibers [8]. However, the 1dB bandwidth is only about 25nm for the chirped grating couplers, which is small than the one (40nm) for the uniform gratings with angled optical fibers. The actual coupling efficiency of the grating would be higher if the propagation loss of the waveguide is included. The coupling efficiency for standard vertical uniform grating coupler is also presented in Fig. 2.8 for comparison. 3dB improvement is achieved by applying the chirped grating for coupling to a vertical optical fiber.

Measurements of the angular alignment tolerance in x-z plane give <0.5dB change of coupling efficiency for 2.9° deviation from normal alignment as shown in Fig. 2.8 (ii). From the SEM image shown in Fig. 2.8 (i), we could find that there are random variations of about 20nm in the width of the etched slots of the nominal uniform grating.

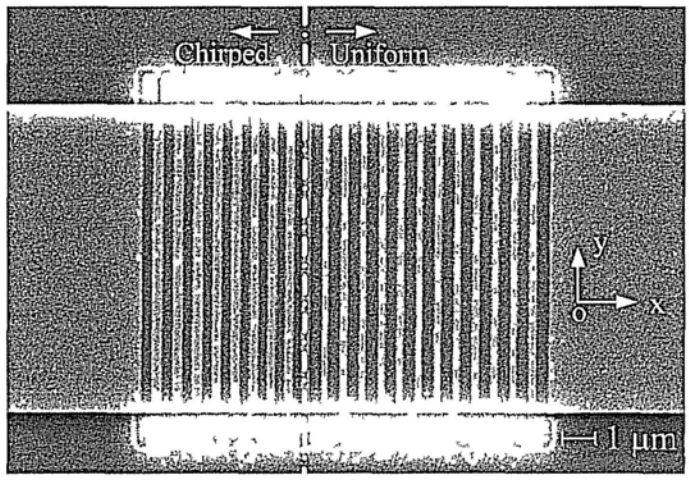

Fig. 2.7: SEM image of the fabricated chirped grating coupler.

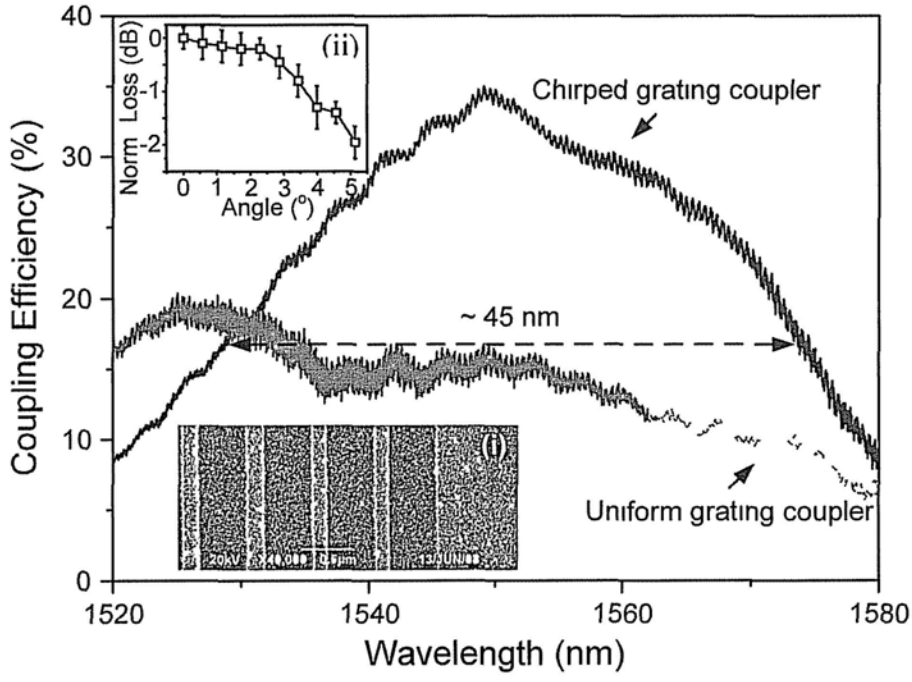

Fig. 2.8: Measured coupling efficiency versus wavelength. (i) A SEM image of the rear section a grating coupler that should be uniform. Over 20nm random fluctuations were induced during fabrication. (ii) Measured angular alignment tolerance in x-z plane.

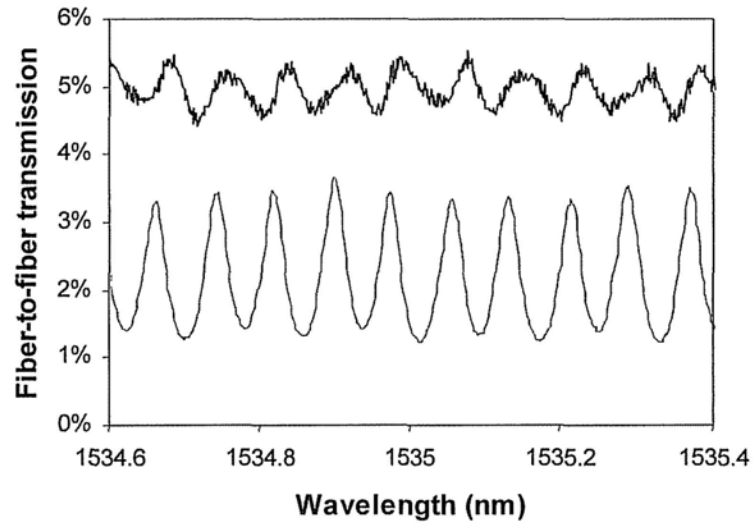

Fig. 2.9: Transmission spectra of the waveguide with two grating coupler. Strong Fabry-Perot interference was found for the couplers with uniform granting.

The measured Fabry-Perot interference fringes for both uniform and chirped grating coupler are shown in Fig. 2.9. As the length between two grating couplers is 4mm including adiabatic tapers and a section of 500nm-width waveguide, the period of the transmission spectrum is calculated to be 0.1nm, assuming the average index of the fundamental mode is 2.9. This agreed well with the experimental result. The Fabry-Perot interference oscillation of the waveguide with uniform grating couplers is much stronger than the one with chirped grating coupler because of their larger reflection. The optical intensity transmission I of a Fabry-Perot cavity of length L, internal loss coefficient α, effective index n_{eff} , interface reflectivity R and transmission T is given by:

$$I = \frac{T^2 \exp(-\alpha L)}{1 + R^2 \exp(-2\alpha L) - 2R \cdot \exp(-\alpha L)\cos(\frac{4\pi n_{eff} L}{\lambda})}. \qquad (2.4)$$

Thus the uniform grating has a reflection of about 22% while the chirped grating has about 4% reflection, calculated form Fig. 2.9 by Eq. 2.4. The chirped grating coupler has ~5dB reduction of the back reflection back into waveguide compared with the uniform grating. Direct measurement of the back reflection into fiber from grating surface at 1550nm, by connecting a circulator in the input fiber, yielded -12dB for the chirped grating and -8dB for the uniform grating.

The alignment tolerance of the chirped grating couplers to fiber positioning in x-y plane was studied by scanning the fiber position. The results shown in Fig. 2.10 indicate good tolerance to the fiber position, with less than 1dB additional loss from misalignment by 1μm.

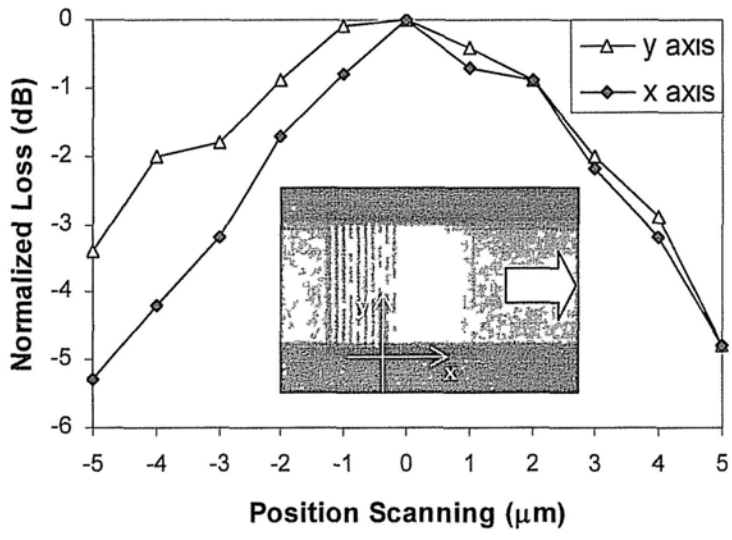

Fig. 2.10: Coupling loss versus fiber position along x and y axis. A photograph of the grating coupler is shown in the inset.

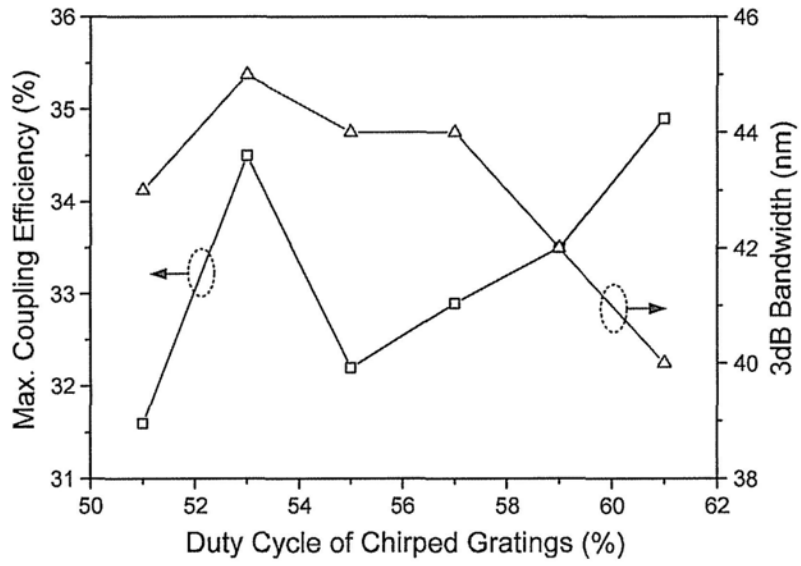

Fig. 2.11: Maximum coupling efficiency of the grating coupler with 51%, 53%, 55%, 57%, and 61% duty cycle (or fill factor) for the front section, the duty cycle of the rear section were 64%, 66%, 68%, 70%, 72%, and 74% respectively. The different duty cycles were obtained by using different exposure energies in the photolithography of each sample.

We also varied the duty cycle (or fill factor) of the grating couplers by changing the exposure energy during photo lithography process. Fig. 2.11 shows that the measured maximum coupling efficiency and the 3dB bandwidth for couplers with different duty cycles (51% to 61%) for the front section chirped grating, and different duty cycles (64% to 74%) in the rear grating section. Despite such large variations in actual slots width and duty cycles, coupling efficiency remained over 31%. The measured bandwidth in Fig. 2.11 matched with simulation results quite well. We think the change from 31.5% to 35% variation in coupling efficiencies for the different samples comes from fabrication errors (~20nm random variations in

slot widths are present in Fig. 3(i)) as simulations suggest only <1% change for the above mentioned duty cycle variations. Pictures of the experimental setup for the testing of the grating couplers are shown in Fig. 2.12.

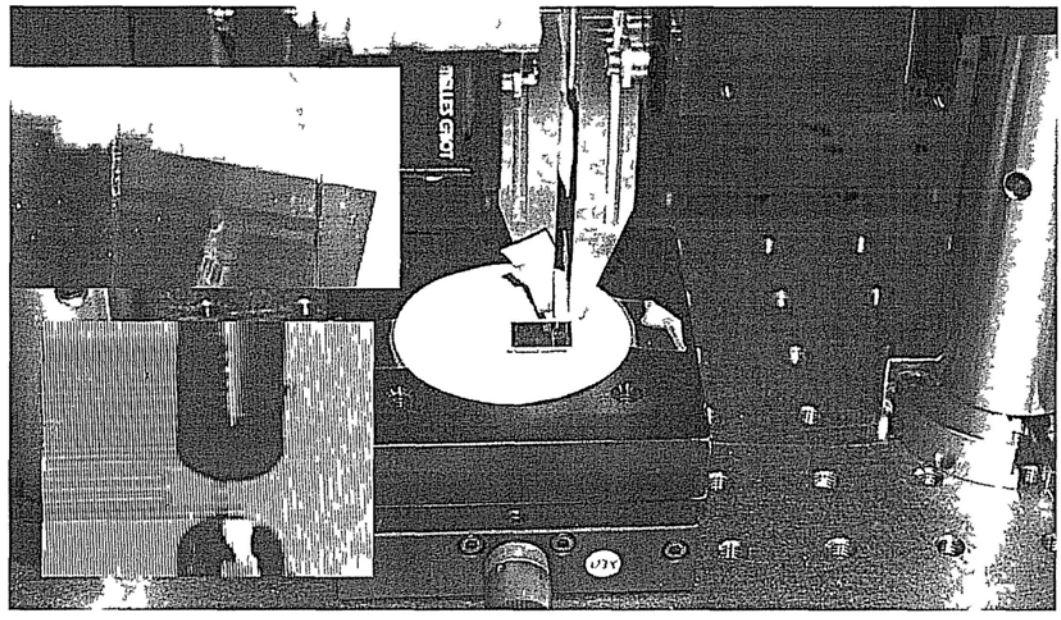

Fig. 2.12: Pictures of the experimental setup

2.4 Focusing chirped grating couplers

Compact focusing grating couplers with curved grating structure was reported to significantly reduce the size of coupler structure [20, 21]. Light could coupled directly into the 500nm wide waveguide from single-mode fiber with focusing grating without passing though a adiabatic taper separately, which may occupy over 20μm× 300μm area of the valuable die space as shown in Fig. 2.13, which shows the losses for tapers with different lengths. Here we applied linearly chirped grating structure introduced previously to a curved grating and fabricated a focusing grating coupler on silicon-on-insulator for coupling light between 500nm wide waveguide and perfectly vertical single mode optical fiber. The footprint of the coupler was

reduced to 18μm × 30μm with the same coupling efficiency as the grating with 300μm long taper.

The devices were fabricated using deep UV photolithography at ePIXfab (www.epixfab.eu) on a SOI wafer, which had a 220nm thick top silicon layer (device layer) and 2μm thick buried oxide layer. A 750nm thick oxide layer was deposited on top. The waveguides were formed by etched to the buried oxide and the grating structure was fabricated by a separate 70nm shallower etch. This depth was optimized and widely used to make grating coupler on SOI as introduced previously in this chapter.

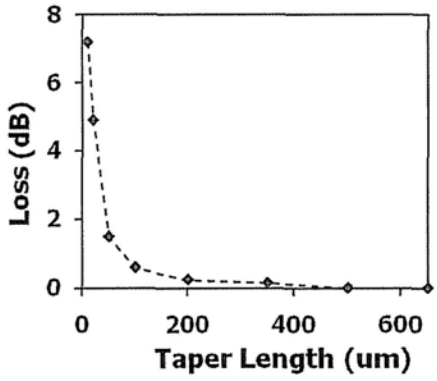

Fig. 2.13: Loss of each taper with different length for chirped grating couplers with non-curved gratings.

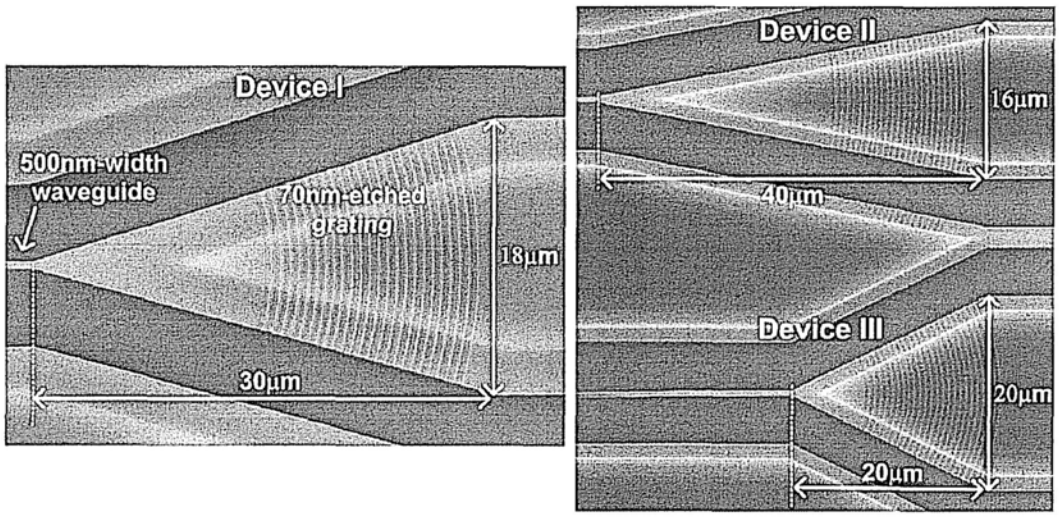

Fig. 2.14: SEM images of the fabricated focusing chirped grating couplers with curved grating. Similar coupling efficiency was achieved by Device I & II. Additional loss for Device III is < 0.5dB.

The SEM images of the fabricated focusing grating couplers are shown in Fig. 2.14. Standard single mode fiber with a MFD of ~10μm would be attached perfectly perpendicular to the surface of wafer. Light comes from the fiber would be diffracted by the shallow etched grating into the waveguide. This grating was designed to couple the corresponding polarization into TE mode of the waveguide only. Detail design parameters (period and fill factor) are the same as the optimum design for chirped grating coupler introduced previously in section 2.2.

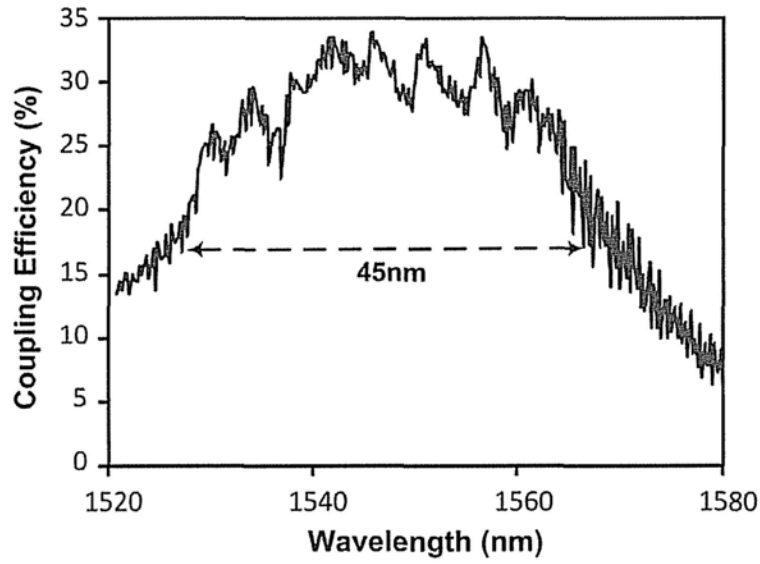

Fig. 2.15: Coupling efficiency of Device I is plotted for the proposed focusing grating coupler between silicon waveguide and vertical fiber. The bandwidth is larger than 45nm with a maximum coupler efficiency of 33%.

We measured the optical loss passing through a 2mm long 500nm-width waveguide with the proposed coupler at both end. The coupling efficiency was then calculated from the fiber-to-fiber loss, assuming that the waveguide is lossless. Using this approximation we obtained a maximum coupling efficiency of 33% and measured an optical 3dB bandwidth of 45nm for Device I as shown in Fig. 2.15. The non-periodic fluctuation of the efficiency profile may be attributed to mechanical noise during the experimental measurement.

2.5 Conclusion

In summary, we proposed and analyzed a linearly chirped grating for coupling light between a SOI waveguide and a vertical optical fiber. Optimization of the design can suppress the back reflection and increase coupling efficiency to about

42% with a 3dB bandwidth of 48nm by FDTD simulation. The fabrication steps required for the proposed chirped grating couplers are the same as the uniform grating couplers with titled fiber.

The optimized chirped grating couplers were fabricated with deep-UV photolithography. Experimental measurements showed that the optimized chirped grating design is robust and tolerant to variations in fabrication process parameters which may lead to a large (~20nm) random fluctuations in slot width and vary the duty cycle of the fabricated grating. Using a two section design with a negative linear chirp in the front section, we obtained over 34% coupling efficiency for coupling light between TE mode in submicron-sized SOI waveguide and a perfectly vertical optical fiber. The 3dB bandwidth was 45nm with center wavelength around 1550nm. The coupling efficiency of this grating coupler was mainly limited by the bi-directional nature of diffraction from the grating. Further improvement may be obtained by improving the diffraction directionality of the grating, such as adding waveguide bottom mirrors or optimize the thickness and etching depth

We also presented the design and measurement results of the focusing grating couplers between SOI waveguide and perfectly vertical optical fiber employing a section of linearly chirped grating. The footprints of the grating couplers can be significantly reduced yet similar coupling efficiencies were obtained. These compact couplers are suitable for low cost packaging process of SOI chip using cleaved fiber or fiber array.

References

[1] T. K. Gaylord and M. G. Moharam, "Analysis and applications of optical diffraction by gratings," Proc. IEEE, vol.73, pp.894-937, 1985

[2] N. Eriksson, M. Hagberg, and A. Larsson, "Highly directional grating outcouplers with tailorable radiation characteristics," IEEE J. Quantum Electron., vol.25, pp.1038-1047, Jun. 1996.

[3] A. Mekis, A. Dodabalapur, R. E. Slusher, and J. D. Joannopoulos, "Two-dimensional photonic crystal couplers for unidirectional light output," Opt. Lett., vol.25, pp.942-944, July 2000.

[4] T. W. Ang, G. T. Reed, A. Vonsovici, A. G. R. Evans, R. R. Routley, and M. R. Josey, "Effects of grating heights on highly efficient unibond SOI waveguide grating couplers," IEEE Photon. Technol. Lett., vol.12, pp.59-61, Jan. 2000.

[5] D. Taillaert, W. Bogaerts, P. Bienstman, T. F. Krauss, P. Van Daele, I. Moerman, S. Verstuyft, K. De Mesel, and R. Baets, "An out-of-plane grating coupler for efficient butt-coupling between compact planar waveguides and single-mode fibers," *IEEE J. Quantum Electron.*, vol.38, pp.949-955, July 2002.

[6] A. Taflove, Computational Electrodynamics, the Finite-Difference Time-Domain Method. Norwood, MA: Artech House, 1995.

[7] D. Taillaert, P. Bienstman, and R. Baets, "Compact efficient broadband grating coupler for silicon-on-insulator waveguides," *Opt. Lett.*, vol.29, no.23, pp.2749-2751 Dec. 2004.

[8] D. Taillaert, F. Van Laere, M. Ayre, W. Bogaerts, D. Van Thourhout, P. Bienstman and R. Baets, "Grating couplers for coupling between optical fibers and nanophotonic waveguides," *Jap. J. Appl. Phys.*, vol.45, no.8A, pp.6071-6077, Aug. 2006.

[9] F. Van Laere, G. Roelkens, M. Ayre, J. Schrauwen, D. Taillaert, D. Van Thourhout, T. F. Krauss, and R. Baets, "Compact and highly efficient grating couplers between optical fiber and nanophotonic waveguides," *J. Lightw. Technol.*, vol.25, no.1, pp.151-156, Jan. 2007.

[10] G. Roelkens, D. Van Thourhout, and R. Baets, "High efficiency silicon-on-insulator grating coupler based on a poly-silicon overlay," Opt. Express, vol.14, no.24, pp.11622-11630, Nov. 2006.

[11] G. Roelkens, D. Vermeulen, D. Van Thourhout, R. Baets, S. Brision, P. Lyan, P. Gautier, and J.-M. Fedeli, "High efficiency diffractive grating couplers for interfacing a single mode optical fiber with optical fiber with a nanophotonic silicon-on-insulator waveguide circuit," *Appl. Phys. Lett.*, vol.92, no.13, 131101, Mar. 2008.

[12] D. Vermeulen, S. Selvaraja, P. Verheyen, G. Lepage, W. Bogaerts, G. Roelkens, "High-efficiency Silicon-On-Insulator Fiber-to-Chip Grating Couplers Using a Silicon Overlay," IEEE 6th International Conference on Group IV Photonics, PDPF1, Sept. 2009.

[13] B. Wang, J. Jiang, and G. P. Nordin, "Compact slanted grating couplers," Opt. Express, vol.12, no.15, July 2004.

[14] B. Wang, J. Jiang, and G. P. Nordin, "Embedded slanted grating for vertical coupling between fibers and silicon-on-insulator planar waveguides," *IEEE Photon. Technol. Lett.*, vol.17, no.9, pp.1884-1886, Sept. 2005.

[15] G. Roelkens, D. V. Thourhout, and R. Baets, "High efficiency grating coupler between silicon-on-insulator waveguides and perfectly vertical optical fibers," *Opt. Lett.*, vol.32, pp.1495-1497, Jun. 2007.

[16] J. Feng and Z. Zhou, "Polarization beam splitter using a binary blazed grating coupler," Opt. Lett., vol.32, no.12, June 2007.

[17] X. Chen, C. Li, and H. K. Tsang, "Chirped Grating for Efficient Coupling from a Silicon Waveguide to a Vertical Optical Fiber," IEICE Photonics in Switching Conference, Sapporo Japan, Aug. 2008.

[18] X. Chen, C. Li, and H. K. Tsang, "Characterization of silicon-on-insulator waveguide chirped grating for coupling to a vertical optical fiber," IEEE/LEOS International Conference on Optical MEMs and Nanophotonics, Germany, pp.56-57, Aug. 2008.

[19] X. Chen, C. Li, and H. K. Tsang, "Fabrication-tolerant waveguide chirped grating coupler for coupling to a perfectly vertical optical fiber," *IEEE Photon. Technol. Lett.,* vol.20, no.23, pp.1914-1916, Dec. 2008.

[20] F. Van Laere, T. Claes, J. Schrauwen, S. Scheerlinck, W. Bogaerts, D. Tailaert, L. O'Faolain, D. Van Thourhout, and R. Baets, "Compact Focusing Grating Couplers for Silicon-on-Insulator Integrated Circuits," *IEEE Photon Technol. Lett.*, vol.19, no.23, pp.1919-1921, Dec. 2007.

[21] X. Chen, C. Li, and H. K. Tsang, "Non-uniform focusing grating for coupling between silicon waveguide and vertical optical fiber," The 22nd Annual Meeting of IEEE Photonics Society, Antalya, Turkey, pp.305-306 (TuV3), Oct. 2009.

3. Two-dimensional chirped grating couplers and the polarization-diversity scheme

In this chapter, the design and experimental measurement results of shallow etched 2D gratings for coupling light between silicon-on-insulator nanophotonic waveguides and vertical optical fibers are presented. We show that the large second order back reflection could be suppressed effectively by applying a linear chirp in the grating period for 2D grating couplers. The total coupling efficiency from an optical fiber to two orthogonal silicon waveguides is independent of the input polarization. We also report an approach to estimate the average effective index for the two dimensional gratings, supported by the effective medium theory (EMT) when the lateral fill factor of the etched holes is larger than 0.5. In addition, we describe the design and experimental results of an integrated polarization-diversity DPSK demodulator. The integration of 2D chirped grating couplers enables polarization-diversity operation with two micro-ring resonators which convert the phase modulation to intensity modulation.

3.1 Introduction

As mentioned in the previous chapters, efficient coupling of optical signals between standard single-mode optical fibers and nanophotonic waveguides on SOI chips is one of the major obstacles that need to be solved before SOI becomes the mainstream platform for PICs. Compared to the approach using end-fire coupling between fibers and waveguides and an adiabatic taper for mode size matching [1], waveguide grating couplers are superior from the perspective of the fabrication

process [2]. Various types of 1D grating couplers were demonstrated in the past few years [3-5]. 2D grating couplers were also studied as polarization splitters [6], which are the key component to realize polarization-diversity scheme and facilitate polarization independent operation for PICs [7, 8].

Polarization independence has been a critical issue yet to be solved for some applications of SOI devices [9]. The (in principle) polarization independent waveguides with a square cross section embedded in silica will impose stringent requirements on the design and fabrication process, which are almost impossible to achieve with the current technologies and fabrication facilities. For example, the uniformity of SOI wafers, the tolerance of the line width from lithography and the fairly controllable sidewall slope of the dry etching. Those will induce dimensional errors in nanometer scale, which is sufficient to demolish the polarization independence. In a polarization-diversity scheme, the two polarizations of the fiber input are split into the quasi-transverse electric (TE) mode of two waveguides. The unified polarization in those two waveguides can thus be processed in separate circuits to achieve polarization-independent operation [10, 11]. Thus polarization independent operation could be realized in such a way that both polarizations passing through the same device in opposite directions [7], or fine-tuning the two circuits for different polarization separately.

The earlier works of grating couplers relied on an off-normal tilt (typically 8° to 10°) of the optical fiber with respect to the surface normal of the SOI wafer in order to reduce the second order back reflection and improve the coupling efficiency [2]. Vertical coupling is more preferable because it enables a simpler optical alignment process for low cost packaging. Moreover, the fibers with off-normal tilt are out of the diffraction plane of the 2D gratings, inducing additional coupling loss [6-8]. We

describe the design, experimental characterization results and analysis of 2D chirped grating couplers for the coupling of light between waveguides and optical fibers without an off-normal tilt as illustrated in Fig. 3.1 in this chapter. The back reflection into waveguide is suppressed by the linearly chirped grating section, which requires no additional fabrication process compared to other vertical coupling scheme [12, 13]. The coupling efficiency is also improved to -5.2dB, compared to -6.7dB in [7] and -5.6dB in [8] demonstrated by the Baets's group in Belgium. An almost linear relationship between the average effective index of the grating region and the fill factor is first proposed and verified experimentally. We also proposed to use effective medium theory (EMT) to estimate the effective index of the 2D grating region. These results would be very useful in design process of the grating couplers.

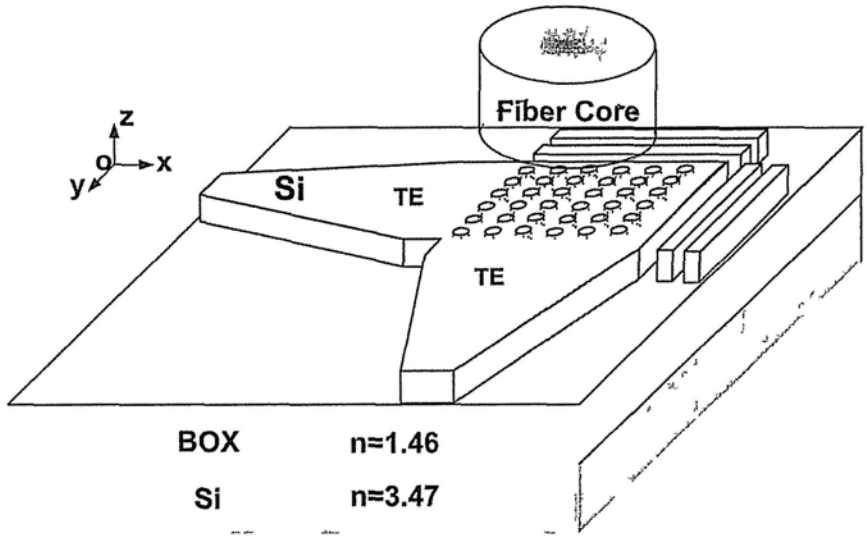

Fig. 3.1: Schematic diagram of the fabricated 2D chirped grating coupler.

We also describe the design and experimental results of an integrated polarization-diversity DPSK demodulator. The integration of 2D chirped grating couplers enabled polarization-diversity operation with two micro-ring resonators which converted the phase modulation to intensity modulation.

3.2 Design of the 2D grating coupler

The grating couplers were optimized for coupling between optical fibers and the fundamental quasi-TE mode in the nanophotonic waveguides. Similar to the 1D grating couplers, they were fabricated on a SOI wafer using Deep-UV (193nm) lithography with 220nm top silicon layer and 2μm thick buried oxide. There is 750nm top oxide deposited, which was optimized to direct more light upwards to enhance the coupling efficiency [5]. The fundamental optical mode of the nanophotonic waveguide was first expanded laterally by an adiabatic taper to a wider waveguide which have a lateral mode size similar to the fundamental mode of normal single mode optical fiber. The light would then be diffracted vertically upwards into the fiber by the 70nm shallow etched grating structure on top of the waveguide, according to the phase matching condition (see Eq. 2.1).

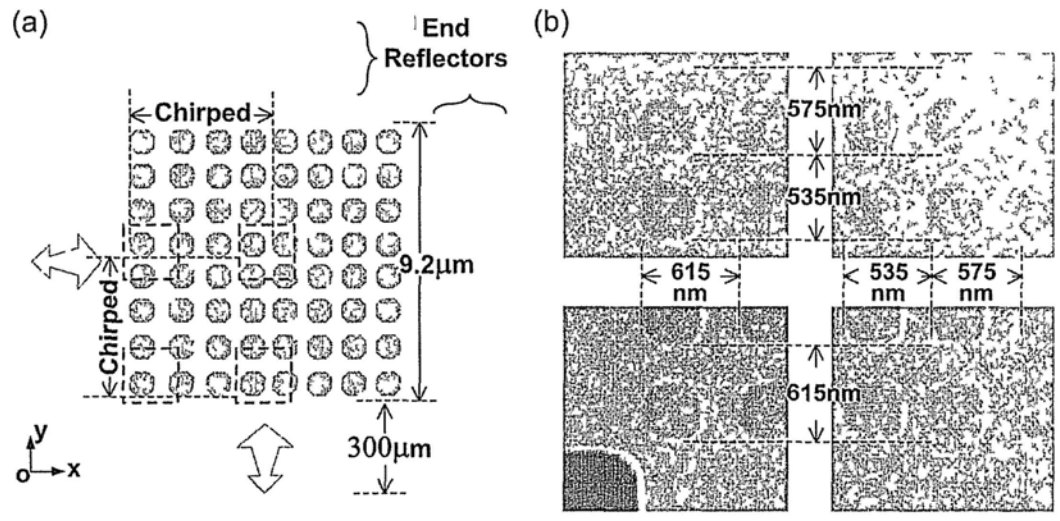

Fig. 3.2: (a) Schematic diagram shows the top view of the proposed 2D grating coupler. The grating periods at the front end were linearly chirped to reduce the back reflection. (b) SEM images of a fabricated 2D chirped grating coupler with the maximum and minimum grating periods indicated.

The detailed design of the fabricated 2D grating couplers for vertical optical fiber is shown in Fig. 3.2a. They consist of a rectangular lattice of octagonal holes covering an area of $9.2\times9.2\mu m^2$, including 16 rows and columns. Octagonal holes (Fig. 3.2b) were used because they are easier to fabricate using optical lithography than rectangular holes (which have sharper angled corners), whilst circular holes would take much more memory for the design file (The circular shaped holes need much more points to define and it is possible to use have many thousands of such holes on a chip). The average grating period is calculated to be 575nm for communication band. Two orthogonal 500nm width nanophotonic waveguides are connected to the front end of 2D grating with 300μm long linear adiabatic tapers. At the back end of the grating coupler, two end reflectors are used to improve the coupling efficiency. They consist of two rectangular shaped silicon slabs

(0.15×9.2μm) at a spacing of 240 nm with each other and with the edge of grating coupler. Those parameters were optimized by 2D FDTD simulation to give a wide-band reflection (over 70% reflection with a 100nm 1dB bandwidth) around 1530nm wavelength.

In order to reduce the second order back reflection that limits the coupling efficiency between waveguides and vertical optical fibers, we introduced linear chirp in the grating period at the front end of the grating coupler as shown in Fig. 3.2a. The design, simulation and measurement results of a 1D chirped grating coupler [14] were described in the previous chapter. The chirped grating couplers are easier to fabricate compared to other vertical coupling schemes previously reported: for example, the slanted gratings in [12] require focused ion beam etching that is not commonly used in SOI fabrication; and the proposed grating couplers in [13] would require an additional overlay of silicon.

For the proposed 2D grating couplers, we introduced a linear chirp in the first 9 periods of the gratings, with the period varying from 615 nm at the front end to 535 nm. The average period Λ_{avg} is 575 nm. The grating chirp parameter Δ (defined in [14] as the maximum period deviation) is equal to 80nm. 2D FDTD simulation shows the back reflection into waveguide is reduced to less than 10% across the whole bandwidth because the destructive interference of light from the chirped periods, whilst the curved phase front of the diffracted light from the chirped periods still matches the optical fiber's numerical aperture (NA). Around -4dB coupling efficiency was achieved with 1D chirp grating structure by simulation.

3.3 Experimental characterization of the grating couplers

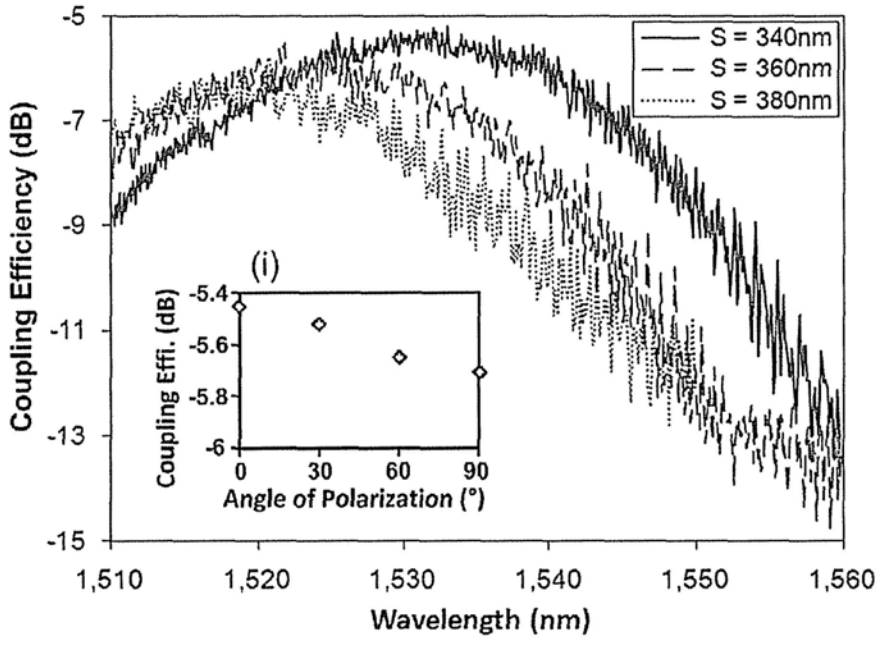

Fig. 3.3: Experimentally measured total coupling efficiency for 2D chirped grating couplers with different span S of the octagonal holes ($S = f\Lambda_{avg}$). The total coupled power to the two orthogonal waveguides is almost polarization independent as shown in the inset.

We characterized the fabricated 2D chirped grating couplers by measuring the fiber-waveguide-fiber insertion loss of light coupled via a pair of grating couplers separated only by the 500nm wide waveguides. The coupling efficiency is assumed to be the same for the chirped grating couplers at both ends. The loss of the 300μm long taper and the short waveguides were almost zero according to our experimental measurements. Coupling efficiency was then obtained for grating couplers with different span of the shallow etched octagonal holes ($S = f\Lambda_{avg}$ = 340nm, 360nm and 380nm, where f is the fill factor of holes as illustrated in the inset of Fig. 3.4c) and

plotted in Fig. 3.3. With S = 340nm, we obtained 10.4dB fiber-to-waveguide-to-fiber loss (corresponding to over 30% coupling efficiency per fiber-waveguide interface) at the wavelength of 1532nm. The Fabry-Perot resonance at the center wavelength of the grating coupler was less than 0.5dB, indicating the back reflection into waveguide was largely suppressed.

We also varied the polarization of the light input. The sum of the coupling efficiency into the orthogonal waveguides was confirmed to be independent of the input polarization. The coupling efficiency against different polarization was plotted in the inset of Fig. 3.3. The variation is under 0.4dB for a 90° rotation in polarization, which may be caused by the fiber being positioned not exactly at the center of the grating coupler. The alignment tolerance of an optical fiber for 1dB polarization dependent loss of each fiber/waveguide interface is measured to be better than 2μm. Thus polarization diversity circuits on SOI can be implemented with the proposed 2D chirped grating coupler, and polarization independent operation of photonic integrated circuits, packaged with vertically attached fiber arrays could be made.

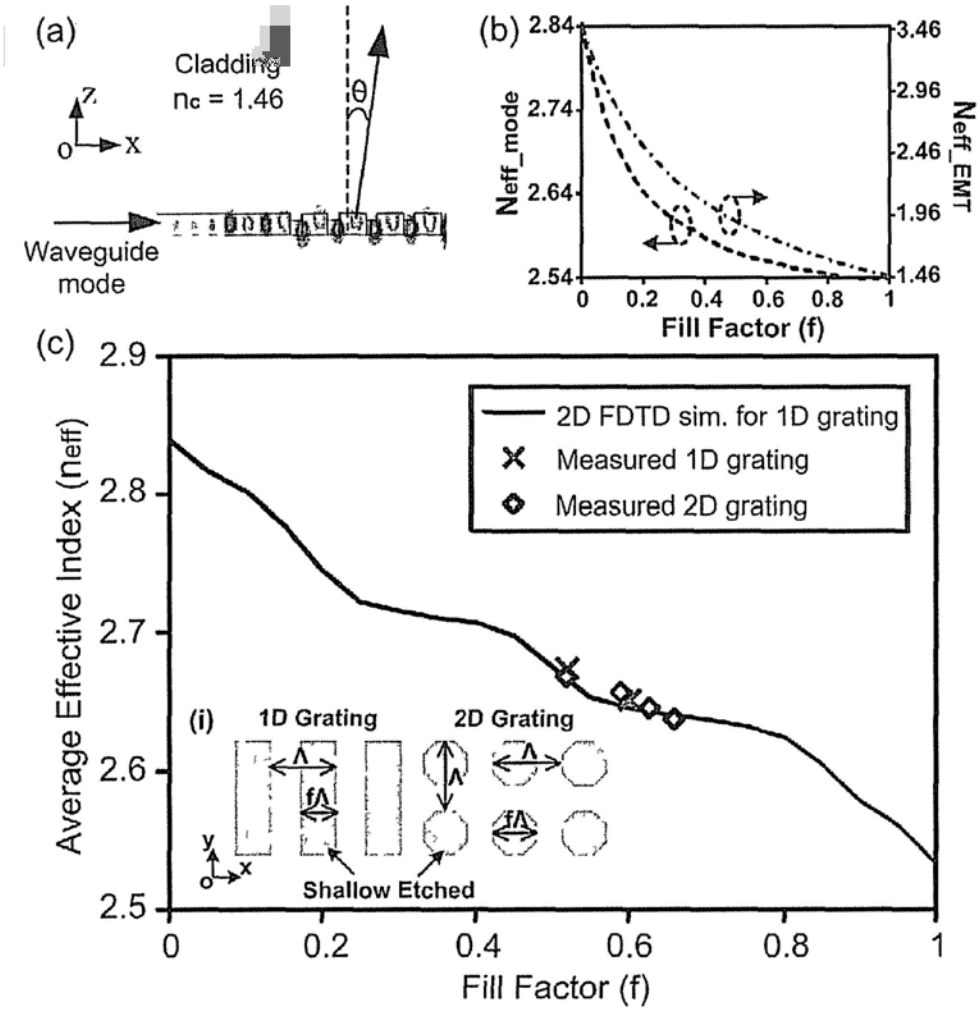

Fig. 3.4: (a) Schematic picture of the 2D FDTD simulation. (b) One array of shallow etched holes can be approximated as a groove filled with a homogenous medium with effective index n_{eff_EMT}. The effective index of the fundamental TE mode for the approximated groove region (n_{eff_mode}) was then calculated. (c)The average effective index of the grating n_{eff} of 1D grating obtained by 2D FDTD simulations were plotted against *f*. Experimental data for both 1D and 2D grating couplers was also plotted. (i) Schematic diagram shows the shallow etched 1D and 2D grating with fill factor *f* indicated.

Preliminary simulations show that the fabrication process can be simplified further by utilizing deep etched subwavelength nanoholes structure instead of the shallow etch holes [15], as there would be no need for additional shallow etch process dedicated for the gratings. Further enhancement of the coupling efficiency could be achieved by adding the substrate mirror [16] or a polysilicon overlay [17] to improve the directionality of the grating and guide more light upwards into optical fiber. We previously demonstrated focusing 1D grating coupler with chirped grating for perfectly normal optical fiber [18], which could also be implemented into 2D grating coupler as presented in this paper following a similar designing process described in [8].

3.4 Theoretical analysis and discussions

2D FDTD simulation is needed to design the shallow etched waveguide grating couplers instead of perturbation methods [2]. The angle θ of diffracted light by 1D grating with different fill factor is calculated by simulation as shown in Fig. 3.4a, by measuring the angle between the wave front of diffracted light and wafer surface. The fill factor f is defined as the ratio of shallow etched slits for 1D and 2D gratings shown in the inset of Fig. 3.4c. The average effective index (n_{eff}) of the grating region is then calculated by the phase matching condition (Eq. 2.1) and plotted in Fig. 3.4c. An almost linear relationship between n_{eff} and f is obtained. Thus the teeth and grooves (220nm and 150nm thick silicon slabs, respectively) have the same importance in contributing to the n_{eff} of the whole grating region in the light propagation direction as introduced in the previous chapter. We can also observe that the optical power is confined in the fundamental mode of waveguide for both the teeth (non-etched) and grooves (etched) sections during FDTD simulation.

Experimentally measured results for 1D grating structures with different f are also plotted in Fig. 3.4c, which are consistent with the simulation data.

The measured n_{eff}, derived from the measured wavelength of peak coupling efficiency of the 2D gratings, is also plotted in Fig. 3.4c. We found the measured n_{eff} for 2D gratings also have good agreement with the simulation result for 1D grating. When considering the TE mode propagating along x-axis, this result means that the f_y (fill factor along y-axis, $f_y = f_x = f$ for those fabricated samples) has insignificant effect on the n_{eff} of the 2D grating (when $f_y > 0.5$). Because the feature size of shallow etched holes in y direction is smaller than the dimensions of fundamental mode and also the wavelength of the propagating light, we can use the first-order effective medium theory (EMT) [15, 19] to estimate the effective refractive index of 2D gratings. According to EMT, the array of shallow etched holes can be approximated as a groove filled with a homogenous medium along y-axis for light propagating in x direction, whose effective index is given by:

$$\frac{1}{n_{eff\_EMT}} = [\frac{f_y}{n_{hole}^2} + \frac{(1-f_y)}{n_{Si}^2}]^{1/2} \qquad (3.1)$$

where n_{eff_EMT} is the effective refractive index of the approximated groove for TE wave, n_{hole} equals to 1.46 (the holes are filled with silicon dioxide), n_{Si} equals to 3.47 (refractive index of silicon). The result is shown in Fig. 3.4b. The calculated effective index of the fundamental quasi-TE mode for the approximated groove region (n_{eff_mode}) is shown also in Fig. 3.4b (for light propagating in x direction). The n_{eff_mode} decreases rapidly with the increase of fill factor f. When f is larger than 0.5, the difference in the effective index of fundamental mode in groove region for 1D and 2D grating is smaller than 0.032. Thus, the shift of the peak wavelength would

be smaller than 10nm, which is insignificant when compared to the tolerances of the fabrication process.

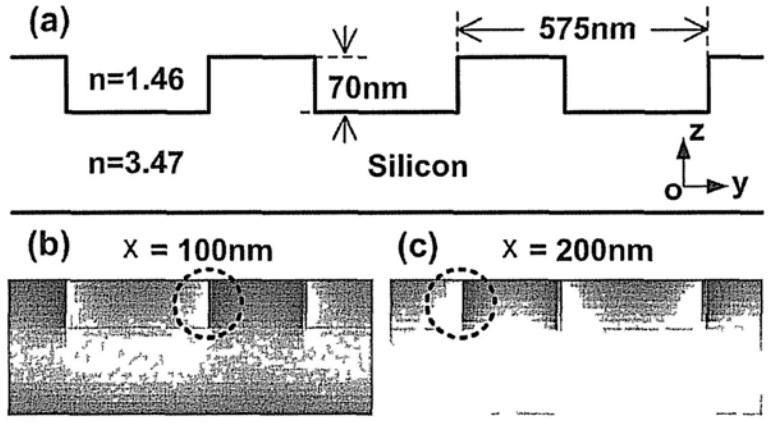

Fig. 3.5: (a) Schematic diagram of the grating structure for 3D FDTD simulation, f = 0.6. (b) E field distribution after propagating 100nm along x-axis with a quasi-TE mode input. (c) E field distribution after propagating 200nm along x-axis.

In lateral direction to the light propagation (e.g. y direction for light propagating in x-axis), the lower refractive index region accounts for a relatively larger portion in the averaged refractive index for TE mode according to EMT because the normal component of the electric displacement field D is continuous across the interface, which leads to a larger E field intensity in the material with lower permittivity, whilst the corresponding magnetic field H is continuous. Thus a larger percentage of power is present in the lower index region, as can be confirmed in the 3D FDTD simulation result shown in Fig. 3.5. The calculated ausi-TE slab mode was inputted to the grating structure along x-axis, and we monitored the E field distribution in the y-z plan of the shallow etched grating.

3.5 Polarization-diversity DPSK demodulator

Differential phase-shift keying (DPSK) has the advantage of 3dB lower optical signal-to-noise ratio (SNR) with balanced detection to reach a given bit-error rate (BER) compared with on-off-keying (OOK) [20, 21]. DPSK has also been shown to be quite robust to nonlinear effect in fibers. Integrated Mach-Zehnder interferometers (MZIs) and micro-ring resonators on SOI have been used for DPSK modulation and demodulation [22-24]. The high index contrast and compatibility with the mature CMOS technologies of SOI make it a promising platform for making PICs, but their strong polarization dependence typically prevent their use in practical optical fiber communication systems since the received optical polarization may drift randomly. One possible solution to the issue of polarization dependence is the integrated polarization-diversity scheme [7, 10, & 11].

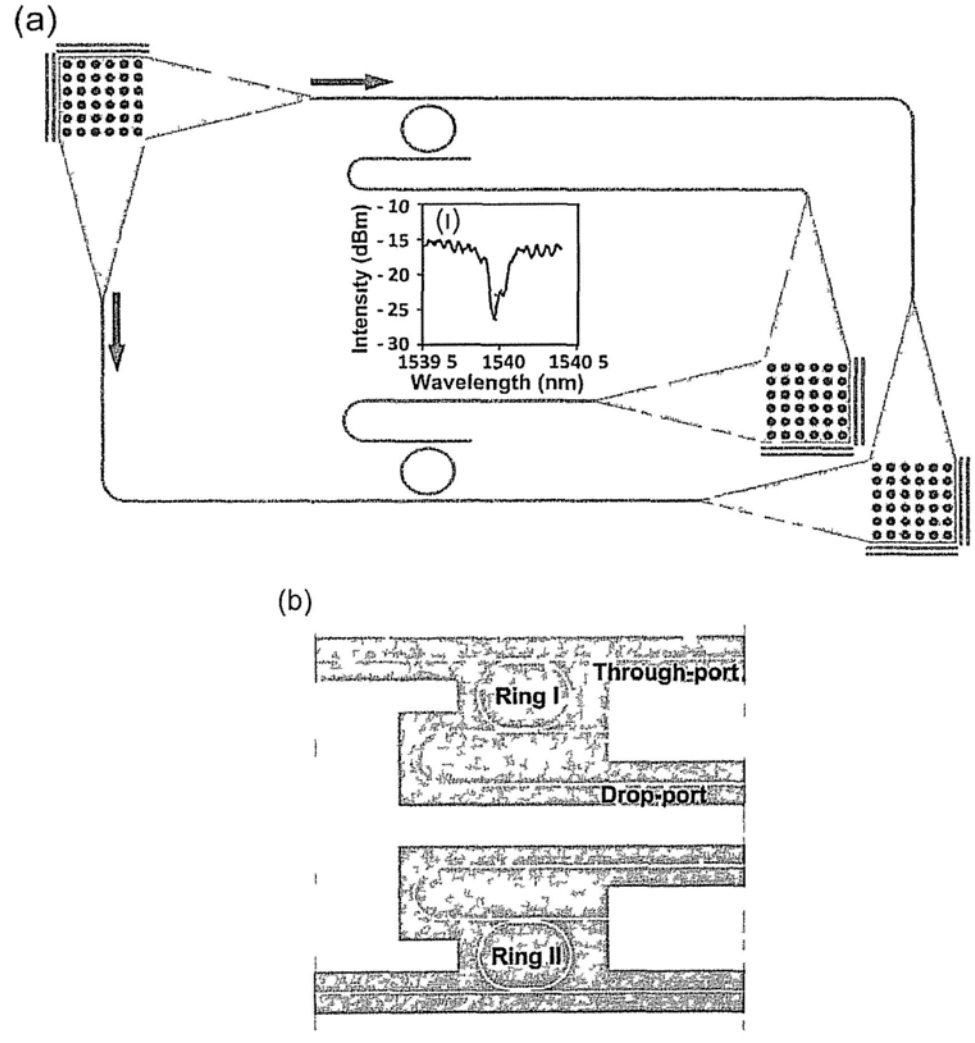

Fig. 3.6 (a) Schematic diagram of the integrated polarization-diversity DPSK demodulator with chirped 2D grating couplers and racetrack micro-ring resonators, the inset shows a typical transmission spectrum at the through-port of the fabricated microrings (b) Image of those micro-rings by optical microscope

The proposed polarization-diversity DPSK demodulator was fabricated using Deep-UV (193nm) lithography on a SOI wafer, which had 220nm thick top silicon layer and 2μm thick buried oxide 2D chirped grating couplers introduce preciously with around 30% coupling efficiency were used to connect with the fibers [25]. The

integrated microrings have already been proposed for modulation and demodulation of DPSK and differential-quadrature-phase-shift-keying (DQPSK) [23, 26], and we previously demonstrated DPSK demodulation with a single microring resonator [24]. Alternate mark inversion (AMI) and duobinary output may be obtained from the through-port and drop-port respectively, when the DPSK signal passes through the ring resonator. We demonstrated polarization-diversity operation using two nominally identical light paths for the orthogonal fiber polarizations as shown in Fig. 3.6. The arc radii of the two racetrack microrings were both 8μm and the length of the straight light coupler was 6μm. The gap between the micro-ring and the waveguide is 200nm. A typical transmission spectrum of the through-ports of those microrings was measured and is shown in the inset of Fig. 3.6a. The quality factor (Q) is about 10,000. Despite nominally identical design there may however be small differences in the two fabricated microrings because of fabrication tolerances. We observed that the resonance wavelength differences of the two microrings may vary from less than 0.1nm to as high as 0.5nm for different dies because of fabrication variations across the wafer. In order to achieve polarization insensitive operation for DPSK demodulation, fine tuning of the resonances of the two microrings by metal wire heaters may be needed.

Preliminary measurement results of the proposed integrated polarization-diversity DPSK demodulator in an optical transmission link were obtained [27]. The experimental setup is shown in Fig. 3.7a. The CW light at the wavelength of 1540nm was generated by a tunable laser. It was then phase modulated with the data generated from a pseudo-random binary sequence (2^{31}-1 PRBS) pattern generator at 10Gb/s data rate. After amplification and filtering, the DPSK signal was coupled into and out of the integrated DPSK demodulator using cleaved single mode fibers. Open

eye diagrams were obtained after demodulation as shown in Fig. 3.7c, which is a typical result at the through-port of ring resonators.

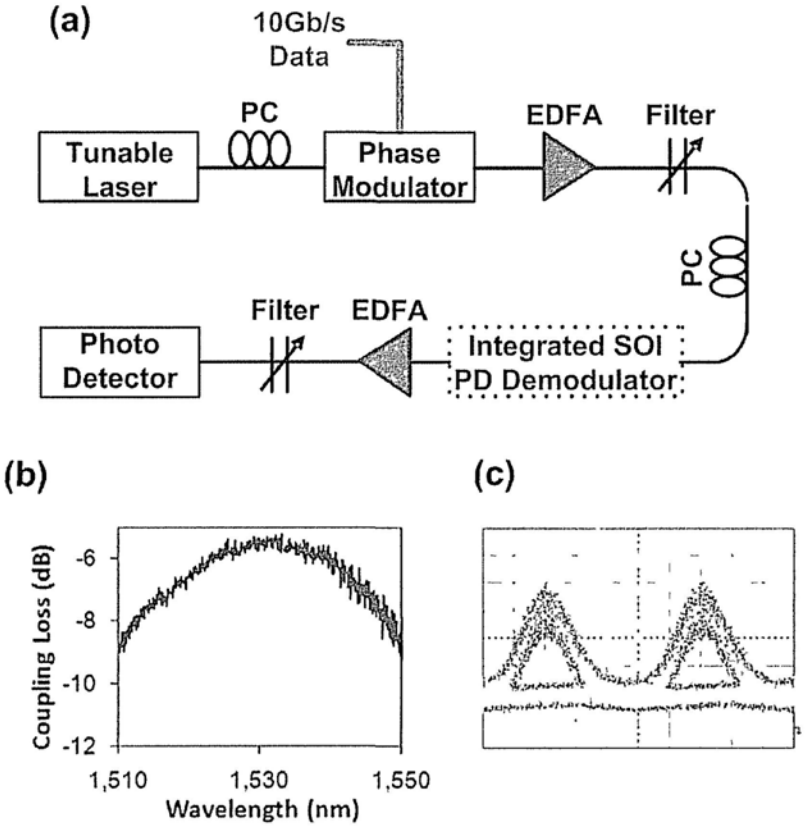

Fig. 3.7: (a) Experimental setup for DPSK demodulation (b) Measured fiber-waveguide coupling loss of the 2D chirped grating coupler, which is polarization independent (c) Measured eye diagram at the through-port after 10Gb/s DPSK demodulation using the polarization-diversity microrings

3.6 Summary

We demonstrated 2D chirped grating couplers fabricated using deep-UV photolithography. Polarization independent operation was obtained. Measurements show that the chirped grating design could successfully suppress the second order

back reflection into waveguide and enhance the coupling efficiency for 2D gratings couplers. Thus the couplers may be used with perfectly vertical optical fibers, which are more preferable for low-cost photonic packaging process. We obtained over 30% coupling efficiency for coupling light between the quasi-TE mode in SOI nanophotonic waveguides and optical fibers. The coupling efficiency is slightly higher than the 2D grating couplers with tilted off-vertical optical fibers [7, 8]. According to the measurement results, we found that the effective index of the grating region of the 2D grating could be predicted by simulation results for the 1D grating, when lateral fill factor of the shallow etched holes is larger than 0.5. This was explained by the effective medium theory and verified by 3D FDTD simulation. The coupling efficiency of the demonstrated 2D grating couplers was mainly limited by the bi-directional nature of diffraction from the grating. Further improvement may be obtained by improving the diffraction directionality of the grating.

We also described the design and preliminary experimental results of an integrated polarization-diversity DPSK demodulator on SOI, which consist of the proposed 2D chirped grating couplers and two nominally identical microring resonators. It could potentially achieve polarization insensitive operation. The polarization-diversity scheme however places stringent fabrication tolerances on the microring resonators and we expect that thermal tuning of the micro-rings would be needed for the typical device fabricated using 193nm lithography in order to achieve fully polarization independent operation.

References:

[1] T. Shoji, T. Tsuchizawa, T. Watanabe, K. Yamada, and H. Morita, "Low loss mode size converter from 0.3μm^2 Si wire waveguides to singlemode fibers," *Electron. Lett.*, vol.38, pp.1669-1670, Dec. 2002.

[2] D. Taillaert, W. Bogaerts, P. Bienstman, T. F. Krauss, P. Van Daele, I. Moerman, S. Verstuyft, K. De Mesel, and R. Baets, "An out-of-plane grating coupler for efficient butt-coupling between compact planar waveguides and single-mode fibers," *IEEE J. Quantum Electron.*, vol.38, pp.949-955, July 2002.

[3] D. Taillaert, P. Bienstman, and R. Baets, "Compact efficient broadband grating coupler for silicon-on-insulator waveguides," *Opt. Lett.*, vol.29, no.23, pp.2749-2751 Dec. 2004.

[4] S. Scheerlinck, J. Schrauwen, F. Van Laere, D. Taillaert, D. Van Thourhout, and R. Baets, "Efficient, broadband and compact metal grating couplers for silicon-on-insulator waveguides," *Opt. Express,* vol.15, no. 15, pp. 9625-9630, 2007.

[5] D. Taillaert, F. Van Laere, M. Ayre, W. Bogaerts, D. Van Thourhout, P. Bienstman and R. Baets, "Grating couplers for coupling between optical fibers and nanophotonic waveguides," *Jap. J. Appl. Phys.*, vol.45, no.8A, pp.6071-6077, Aug. 2006.

[6] D. Taillaert, H. Chong, P. I. Borel, L. H. Frandsen, R. M. De La Rue, and R. Baets, "A compact two-dimensional grating coupler used as a polarization splitter," *IEEE Photon. Technol. Lett.*, vol.15, no.9, pp.1249-1251, Sept. 2003.

[7] W. Bogaerts, D. Taillaert, P. Dumon, D. Van Thourhout, and R. Baets, "A polarization-diversity wavelength duplexer circuit in silicon-on-insulator photonic wires," *Opt. Express*, vol.15, no.4, pp.1567-1578, Feb. 2007.

[8] F. Van Laere, W. Bogaerts, P. Dumon, G. Roelkens, D. Van Thourhout, and R. Baets, "Focusing polarization diversity grating couplers in silicon-on-insulator," *J. Lightw. Technol.*, vol.27, no.5, pp.612-618, Mar. 2009.

[9] G.T. Reed, G.Z. Mashanovich, W.R. Headley, B. Timotijevic, F.Y. Gardes, S.P. Chan, P.Waugh, N.G. Emerson, C.E. Png, M.J. Paniccia, A. Liu, D. Hak, V.M.

Passaro, "Issues associated with polarization independence in silicon photonics," J. Sel. Top. Quantum Electron., vol.12, no.6, pp.1335-1344, 2006

[10] C.R. Doerr, M. Zirngible, C.H. Joyner, L.W. Stultz, and H. Presby, "Polarization diversity waveguide grating receiver with integrated optical preamplifiers," IEEE Photon Technol. Lett., vol.9, no.1, pp.85-87, Jan.1997.

[11] T. Barwicz, M.R. Watts, M.A. Popovic, P.T. Rakich, L. Socci, F.X. Kartner, E.P. Ippen, and H. Smith, "Polarization-transparent microphotonic devices in the strong confinement limit," Nature Photonics, vol.1, no.1, pp.57-60, 2007.

[12] B. Wang, J. H. Jiang, and G. P. Nordin, "Embedded slanted grating for vertical coupling between fibers and silicon-on-insulator planar waveguides," *IEEE Photon. Technol. Lett.*, vol.17, no.9, pp.1884-1886, Sept. 2005.

[13] G. Roelkens, D. V. Thourhout and R. Baets, "High efficiency grating coupler between silicon-on-insulator waveguides and perfectly vertical optical fibers," *Opt. Lett.*, vol.32, pp.1495-1497, Jun. 2007.

[14] X. Chen, C. Li, and H. K. Tsang, "Fabrication-tolerant waveguide chirped grating coupler for coupling to a perfectly vertical optical fiber," *IEEE Photon. Technol. Lett.,* vol.20, no.23, pp.1914-1916, Dec. 2008.

[15] X. Chen and H. K. Tsang, "Nanoholes grating couplers for coupling between silicon-on-insulator waveguides and optical fibers," IEEE Photon. J., vol.1, pp.184-190, Sept. 2009.

[16] F. Van Laere, G. Roelkens, M. Ayre, J. Schrauwen, D. Taillaert, D. Van Thourhout, T.E. Krauss and R. Baets, "Compact and highly efficient grating couplers between optical fiber and nanophotonic waveguides," *J. Lightw. Technol.*, vol.25, no.1, pp.151-156, Jan. 2007.

[17] G. Roelkens, D. Vermeulen, D. Van Thourhout, R. Baets, S. Brision, P. Lyan, P. Gautier, and J.-M. Fedeli, "High efficiency diffractive grating couplers for interfacing a single mode optical fiber with optical fiber with a nanophotonic silicon-on-insulator waveguide circuit," *Appl. Phys. Lett.*, vol.92, no.13, 131101, Mar. 2008.

[18] X. Chen, C. Li, and H. K. Tsang, "Non-uniform focusing grating for coupling between silicon waveguide and vertical optical fiber," The 22nd Annual Meeting of IEEE Photonics Society, Antalya, Turkey, pp.305-306 (TuV3), Oct. 2009.

[19] S. M. Rytov, "Electromagnetic properties of a finely stratified medium," Sov. Phys. JETP, vol.2, pp.466-475, 1956.

[20] M. Rohde, C. Caspar, N. Heimes, M. Konitzer, E.-J. Bachus, and N. Hanik, "Robustness of DPSK direct detection transmission format in standard fibre WDM systems," Electron. Lett., vol.36, no.17, pp.1483-1484, 2000

[21] A.H. Gnauck, and P. J. Winzer, "Optical phase-shift-keyed transmission," J. Lightwave Technol., vol.23, no.1, pp.115-130, 2005

[22] X. Chen, C. Li, L. Xu, and H. K. Tsang, "DPSK Demodulation Using Mach-Zehnder Delay-Interferometer on Silicon-on-Insulator Integrated with Diffractive Grating Structure," Asia Optical Fiber Communication and Optoelectronic Exposition and Conference (AOE) 2008, paper SuF3.

[23] L. Zhang, J.Y. Yang, M. Song, Y. Li, B. Zhang, R. G. Beausoleil, and A.E. Willner, "Microring-based modulation and demodulation of DPSK signal," Opt. Express, vol.15, no.18, pp.11564-11569, 2007

[24] L. Xu, C. Li, C. Wong and H.K. Tsang, "Optical differential-phase-shift-keying demodulation using a silicon microring resonator," IEEE Photon. Technol. Lett., vol.21, no.5, pp.295-297, Mar.2009.

[25] X. Chen, C. Li, and H.K. Tsang, "Two dimensional silicon waveguide chirped grating couplers for vertical optical fibers," Optics Communications, vol.283, no.10, pp.2146-2149, May 2010.

[26] L. Zhang, J.Y. Yang, Y. Li, R. G. Beausoleil, and A. E. Willner, "Silicon Microring-Resonator-Based Modulation and Demodulation of DQPSK Signals," OFC/NFOEC 2008, paper OWL5.

[27] X. Chen, C. Li, Y. Gao, L. Xu, H.K. Tsang, and C. Shu, "Characterization of integrated polarization-diversity DPSK demodulator with two-dimensional chirped grating couplers and ring resonators," OFC/NFOEC 2010 in San Diego, California, USA, JWA26, Mar. 2010.

4. Variable grating splitter/combiner and Mach-Zehnder interferometer (MZI)

In addition to the coupling of optical signal between optical fibers and nanophotonic waveguides, more functionality could be implemented with specially designed gratings. We propose and test a silicon waveguide grating in this chapter, which serves dual functions: as an 1×2 variable integrated beam splitter/combiner and as an out-of plane diffractive element for coupling light between a single mode optical fiber and a 500nm wide silicon-on-insulator waveguide. An integrated Mach-Zehnder interferometer (MZI) made with this novel functional element was demonstrated with tunable splitting ratio. We also demonstrated a DPSK demodulator using the proposed MZI in a communication system.

4.1 Introduction

The high index contrast and mature fabrication facilities available from silicon-based CMOS technology make the SOI a promising platform for making photonic integrated devices for communication networks [1, 2]. Beam splitters/combiners are a basic element in constructing PICs, such as for the MZIs and hybrid-integrated optical transceivers. 1×2 waveguide splitters/combiners include Y-branches [3], multimode interference couplers [4] and star coupler [5]. Since 2002, waveguide grating couplers are becoming a popular technique for interfacing between PICs and optical fibers. Their key advantages over alternative approaches include large alignment tolerance, allowing wafer scale testing and avoiding the need for waveguide facet polishing [6]-[9].

A lot of effort was put into enhancing the coupling efficiency of those grating couplers in recent years. Meanwhile, various novel functions were proposed, such as polarization splitter [10, 11] and duplexer [12]. In this chapter, we describe the design and experimental characterization of a MZI based on novel 1×2 waveguide splitter/combiners, which employed etched gratings to couple light between the optical fibers and waveguides and also split (or combined) the light to (or from) different waveguides. No excess loss is introduced compared to normal vertical grating coupler.

The split ratio of the grating splitter/combiners can be adjusted by changing the fiber position without decreasing the coupling efficiency. We achieved over 20dB extinction ratio for the integrated MZI made with this novel functional element. The grating coupler had over 36% coupling efficiency and a 1dB spectral bandwidth of 37nm. An opened eye-diagram was observed when applying the proposed MZI in a communication link for demodulation of the DPSK signal.

4.2 Design and fabrication of the grating splitter/combiner

The schematic diagram of the fabricated waveguide splitter/combiner is shown in Fig. 4.1(a) with a SEM image in Fig. 4.1(b). The device was fabricated using deep UV photolithography at IMEC on a SOI wafer which had a 220 nm thick top silicon layer (device layer) and 2-μm-thick buried oxide layer. A 750-nm-thick oxide layer was deposited on top of the grating structure to improve coupling efficiency. The round trip optical path length in the top oxide layer is equal to about one and a half wavelength and thus the 750nm oxide acts like an antireflection coating for the silicon grating. The waveguides were formed by etching to the buried oxide. And the grating structure was fabricated by a separate shallow etch, to a depth of 70 nm. This

depth was optimized and widely used to make grating coupler on SOI [7], [9]. A standard single mode fiber, orientated perfectly perpendicular to the wafer surface, is attached to the center of the grating structure on top of the 10-μm-wide waveguide. As illustrated in Fig. 4.1(a), light coming from optical fiber will be diffracted bi-directionally, and coupled into the fundamental mode of the 10-μm-wide waveguides on each end of the grating. The mode field profile of the waveguide in the grating region was designed to match well with the fundamental mode of optical fiber. The optical mode in the waveguide was then compressed laterally by an adiabatic taper to a 500-nm-wide nanophotonic waveguide. The design was optimized for coupling to the quasi-TE mode in the waveguide.

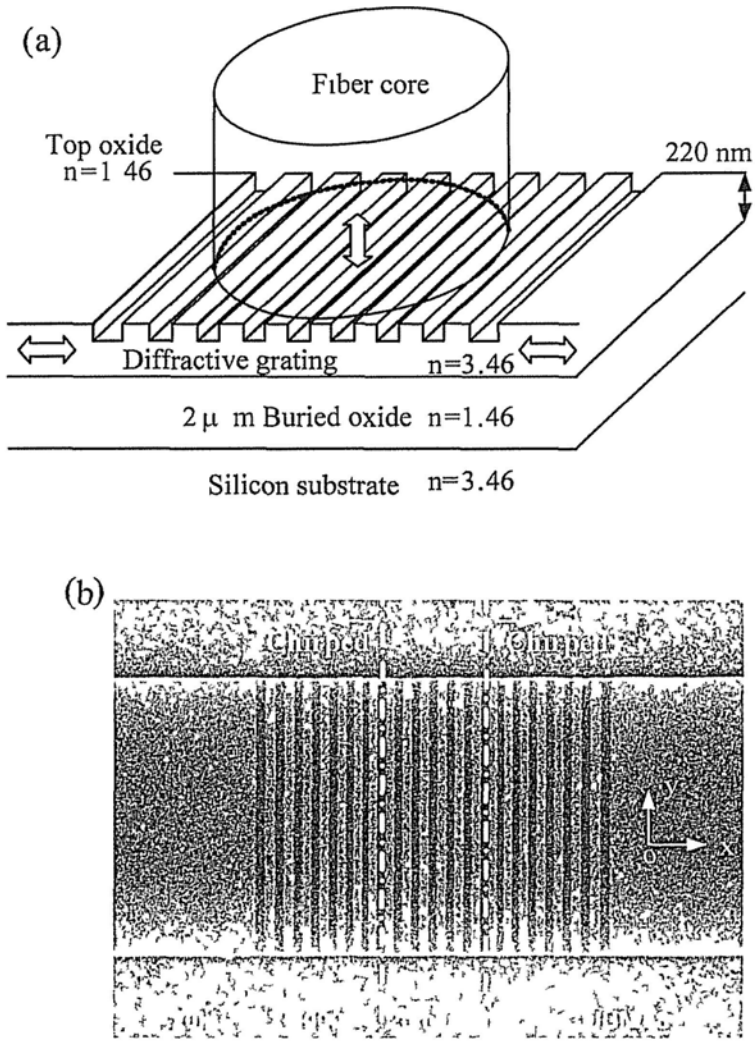

Fig. 4.1: (a) Schematic diagram of the fiber-waveguide coupler and splitter/combiner. (b) Scanning electron microscope (SEM) image of the shallow etched diffractive grating on planar waveguide for coupling and splitting light. This symmetric structure include uniform grating in the middle and 7 slits linearly chirp at both ends.

One of the potential problems in having a grating for coupling to a vertical optical fiber is the presence of a large back reflection from the grating structure back

into waveguide. Such reflection is often undesirable and may lead, for example to large Fabry-Perot spectral oscillations. This Fabry-Perot feedback can be observed experimentally and can have an adverse affect on the performance of many functional components in PICs. To reduce the back reflection, we chirped the grating period at each end of the grating structure as introduced in the previous chapters.

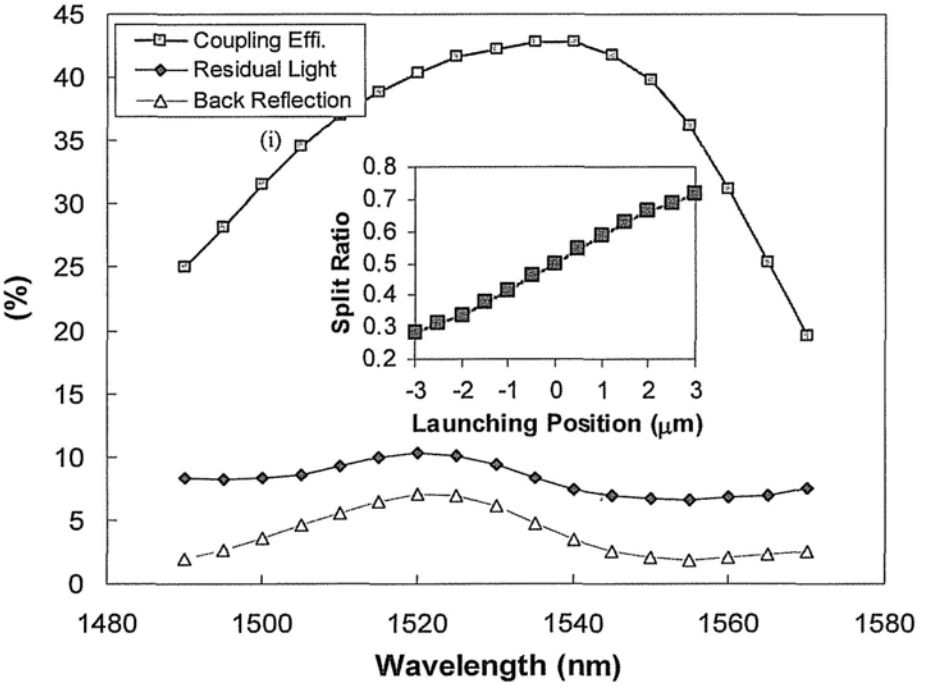

Fig. 4.2: Coupling efficiency, back reflection into waveguide and residual light transmitting through the grating from waveguide for different wavelength are plotted. The inset shows that an almost linear relationship was obtained between the split ratio and the launching position of one optical fiber (moving along x axis as shown in Fig. 4.1).

Two dimensional finite-difference time-domain (2D FDTD) simulations were employed to optimize the grating structure [6]-[9]. The fiber mode was represented by a Gaussian waveform with 1/e full width of 10.4 μm. For our final design, the

grating contains 21 etched slits with 0.53 fill factor (or 53% duty cycle, defined as the ratio of the slit width to the grating period). The number of etched slits was optimized to minimize the residual light transmitting through the grating from waveguide at the opposite side, whilst keeping a good coupling efficiency between the fiber and waveguides.

The total length of the grating is about 12μm and the average period is 580 nm. In order to reduce the large back reflection (>30%) when the light is coupling from the waveguide into the optical fiber, 7 periods were linearly chirped at both ends of the grating. The chirp introduced a maximum grating period deviation of 120nm in the structure. Those periods are thus 640 nm, 620 nm, 600 nm, 580 nm, 560 nm, 540 nm, 520 nm respectively, counting from the ends towards the center. The widths of the 7 slits at the center were uniform with 305 nm width and 275 nm spacing (f = 0.53). The simulation results for the final design are shown in Fig. 4.2. The coupling efficiency, back reflection into waveguide and residual light transmitting through the grating from waveguide were calculated. The split ratio for the proposed splitter/combiner could be tuned almost linearly from 0.28 to 0.72 by adjusting the position of either one of the optical fiber along x-axis. The variation of the overall coupling efficiency was less than 0.65dB across this range of split ratios. The calculated split ratio as a function of fiber position is plotted in the inset of Fig. 4.2.

4.3 Experimental results and discussion of the MZI

The experiment results were published in [13]. A schematic diagram of the fabricated MZI with the proposed waveguide grating splitters/couplers is shown in Fig. 4.3(a). It is a compact device and has potential for many practical applications. For example, we successfully employed the fabricated MZI for DPSK signal

demodulation in a communication system [14]. This device comprises two waveguide splitter/combiner mentioned previously for input and output coupling with optical fibers. Each splitter/combiner has a grating structure in the center and a 1.05-mm-long adiabatic taper at each side to convert the mode into the 500-nm-wide nanophotonic waveguides. The lengths of the two submicron-sized waveguide arms are 1.72mm and 9.16mm respectively (ΔL = 7.44mm), which was designed to introduce one bit delay (100ps) for 10Gb/s signal. The coupling efficiency was measured with broad-band ASE source coupled with a standard single mode optical fiber. Transmission loss for 500-nm-widewaveguide is estimated to be 0.2dB/mm, similar to the result in [15]. The measured coupling efficiency with ~0.5 split ratio is shown in Fig. 4.3(b). Over 36% coupling efficiency was achieved with ~37nm 1dB bandwidth.

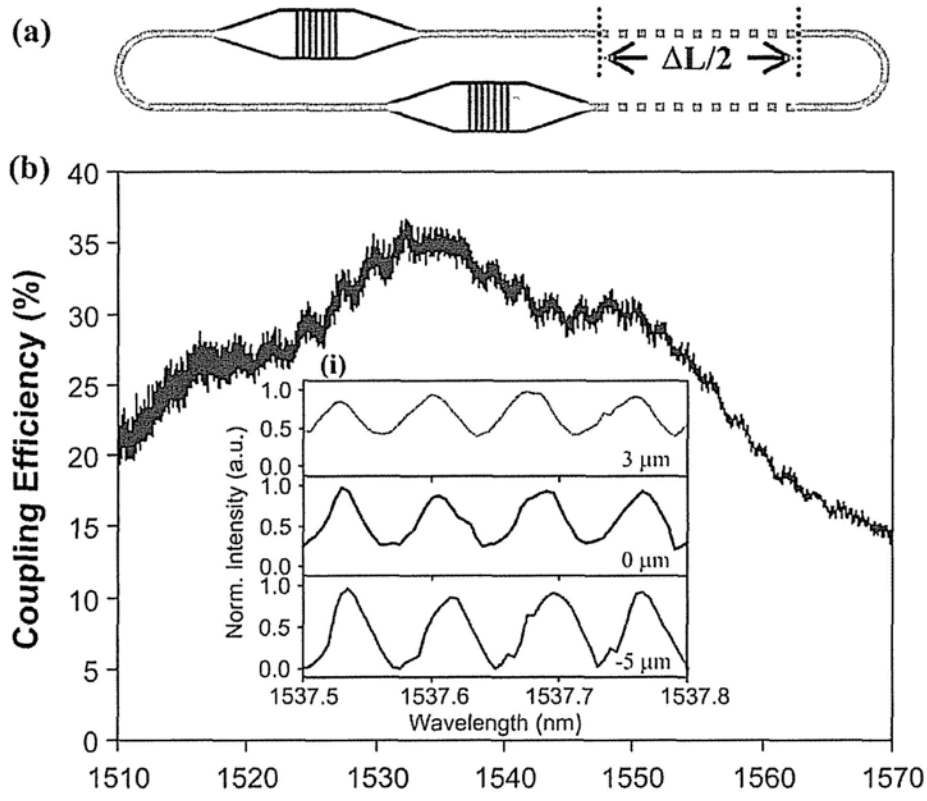

Fig. 4.3: (a) Schematic diagram of the fabricated MZI. (b) Measured coupling efficiency versus wavelength while the inset (i) shows the MZI responses when moving one of the fiber positions to +3μm, 0 and -5μm. We changed the split ratio by adjusting the fiber position in order to balance the difference in the propagation losses of the two nanophotonic waveguide arms.

The performance of the MZI was characterized using tunable laser scanning around 1537nm. Strong interference beating was observed. By slightly tuning of fiber position to change the splitting ratio, we could compensate the transmission loss difference of the two arms. The extinction ratio of the interference pattern can experimentally exceed 20dB when the optical power in the arms of MZI is well matched, as shown in the inset of Fig. 4.3(b). Our simulations give a group index of

4.18 for the silicon nanophotonic waveguides. So the calculated FSR at 1537nm should be 0.076nm. This fits well with the experimental results of 0.075nm.

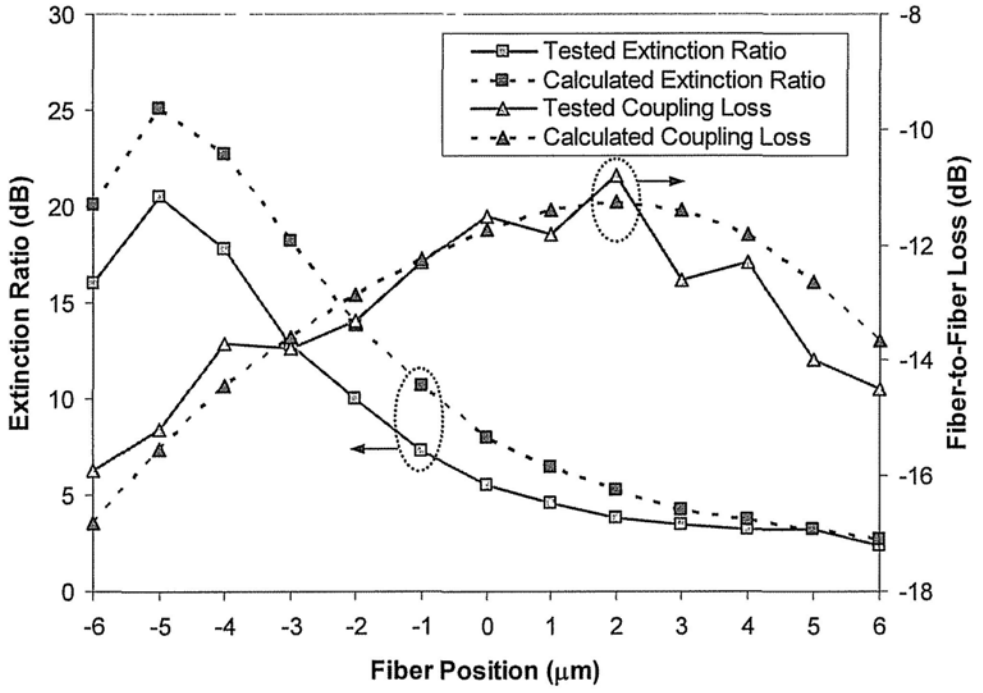

Fig. 4.4: Experimentally measured fiber-to-fiber loss and extinction ratio are presented while scanning the output fiber position along x-axis. The calculated results were also plotted for comparison.

In order to verify the split ratio of the splitters/combiners, we monitored the coupling loss and the extinction ratio of the MZI while keeping the input fiber at one random position and moving the output fiber along x-axis on top of the grating structure. As the split ratio would change with the fiber position as shown in the inset of Fig. 4.2, and the estimated waveguide loss is 0.2 dB/mm for the two arms, we could calculate the coupling loss and extinction ratio of the MZI with different positions of the output fiber. The calculated results are shown in Fig. 4.4, and agree well with the experimental data, albeit the tested extinction ratio is slightly lower

than the calculated one. This is probably due to the actual split ratio of the fabricated grating structure was slightly different from the simulation one (Fig. 4.2(i)), because of fabrication errors, which introduced about 20nm random variation in the grating slit width (as measured in SEM images).

4.4 DPSK demodulation using the MZI

Integrated MZI could be used to demodulate DPSK signal as introduce in [16]. Fig. 4.5(a) shows the experimental setup for DPSK demodulation in a simple optical transmission link. The CW light at the wavelength of 1535nm was generated by a tunable laser. It was then phase modulated with the data generated form a pseudo-random binary sequence (PRBS) pattern generator at 10Gb/s data rate. After amplification and filtering, the light signal would be coupled into and out of the integrated MZI on SOI chip using cleaved single mode fibers. Clearly opened eye diagrams were obtained after demodulation as shown in Fig. 4.5(b), indicating the DPSK signal was successfully demodulated by the fabricated device.

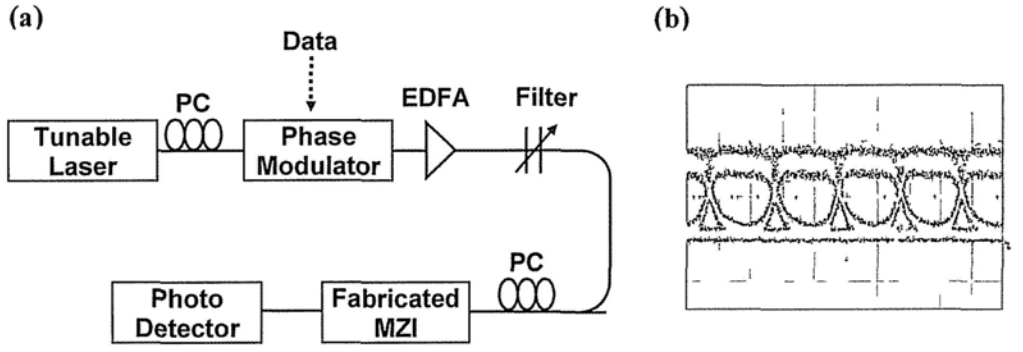

Fig. 4.5. (a) Experimental setup for DPSK demodulation testing. (b) Measured eye diagram after DPSK demodulation using the proposed MZI at 10Gb/s.

4.5 Summary

We demonstrated a Mach-Zehnder interferometer (MZI) on silicon-on-insulator (SOI) wafer. The extinction ratio of the fabricated MZI was experimentally measured to be over 20dB. The MZI was formed using novel 1×2 waveguide splitters/combiners that are based on an etched chirped grating on the waveguide. The grating could couple light directly from/into a cleaved optical fiber while splitting/combining the light power without excess loss. Over 36% coupling efficiency was experimental measured. The splitting ratio was widely tunable by adjusting the fiber position. The performance of the variable split ratio was verified experimentally. The proposed splitter/combiner is a promising component for photonic integrated circuits because of its high efficiency and tunable splitting ratio. The coupling efficiency is mainly limited by the bi-directionality of the grating diffraction. Further improvement to coupling efficiency may be achieved by adding a bottom mirror beneath the buried oxide or a further optimizing the waveguide thickness and etch depth to enhance the directionality of the grating.

In addition, we demonstrated a DPSK demodulator at 10Gb/s data rate using the proposed MZI. Opened-eye diagram was obtained after demodulation. The device can be easily packaged with cleaved fibers or fiber arrays vertically attached to the wafer surface. This potentially low-cost packaging process and its good performance would make the proposed device a promising choice for the commercial market.

References:

[1] B. Jalali, S. Yegnanarayanan, T. Yoon, T. Yoshimoto, I. Rendina, and F. Coppinger, "Advances in silicon-on-insulator optoelectronics," *IEEE J. Sel. Top. Quantum Electron.,* vol.4, pp.938-947, Nov. 1998

[2] W. Bogaerts, R. Baets, et al., "Nanophotonic waveguide in silicon-on-insulator fabricated with CMOS technology," *J. Lightw. Technol.*, vol.23, pp.401-412, Jan. 2005

[3] L. H. Frandsen, et al., "Ultralow-loss 3-dB photonic crystal waveguide splitter," *Opt. Lett.*, vol.29, pp.1623-1625, July 2004

[4] C. S. Hsiao and L. Wang, "Design for beam splitting components employing silicon-on-insulator rib waveguide structures," *Opt. Lett.*, vol.30, pp.3153-3155, Dec. 2005

[5] A. Koster, E. Cassan, S. Laval, L. Vivien, and D. Pascal, "Ultracompact splitter for submicrometer silicon-on-insulator rib waveguides," *J. Opt. Soc. Am. A*, vol.21, pp.2180-2185, Nov. 2004

[6] D. Taillaert, et al.: "An out-of-plane grating coupler for efficient butt-coupling between compact planar waveguides and single-mode fibers," *IEEE J. Quantum Electron.* vol.38, pp.949-955, July 2002

[7] D. Taillaert, et al: "Grating couplers for coupling between optical fibers and nanophotonic waveguides," *Jap. J. Appl. Phys.* vol.45, pp.6071-6077, Aug. 2006

[8] G. Roelkens, et al. "High efficiency diffractive grating couplers for interfacing a single mode optical fiber with a nanophotonic silicon-on-insulator waveguide circuit," Applied Physics Letters, vol. 92, 131101, Mar. 2008

[9] X. Chen, C. Li, and H. K. Tsang, "Fabrication-tolerant waveguide chirped grating coupler for coupling to a perfectly vertical optical fiber," *IEEE Photon. Technol. Lett.*, vol.20, no.23, pp.1914-1916, Dec. 2008

[10] D. Taillaert, H. Chong, P.I. Borel, L.H. Frandsen, R.M. de la Rue, and R. Baets, "A compact two-dimentional grating coupler used as a polarization splitter," IEEE Photon. Technol. Lett., vol.15, no.9, pp.1249-1251, Sept.2003.

[11] Y. Tang, D. Dai, and S. He, "Proposal for a grating waveguide serving as both a polarization splitter and an efficient coupler for silicon-on-insulator nanophotonic circuits," IEEE Photon. Technol. Lett., vol.21, no.4, pp.242-244, Feb.2009.

[12] G. Roelkens, D. Van Thourhout, and R. Baets, "Silicon-on-insulator ultra-compact duplexer based on a diffractive grating structure," Optics Express, vol.15, no.16, pp.10091-10096, 2007

[13] X. Chen, C. Li, H.K. Tsang, "Etched waveguide grating variable 1×2 splitter/combiner and waveguide Coupler," IEEE Photon. Technol. Lett., vol.21, no.5, pp.268-270, Mar.2009.

[14] X. Chen, C. Li, L. Xu, and H.K. Tsang, "DPSK demodulation using mach-zehnder delay-interferometer on silicon-on-insulator integrated with diffractive grating structure," Asia Optical Fiber Communication and Optoelectronic Exposition and Conference, Shanghai, China, SuF3, Oct. 2008

[15] P. Dumon, et al., "Low-loss SOI photonic wires and ring resonators fabricated with deep UV lithography," *IEEE Photon. Technol. Lett.,* vol.16, no.5, pp.1328-1330, May 2004

[16] A.H. Gnauch and P.J. Winzer, "Optical phase-shift-keyed transmission," J. Lightw. Technol., vol.23, pp.115-130, 2005.

5. Grating couplers with subwavelength structure

In this chapter, simulation and experimental results of grating couplers composed of arrays of subwavelength nanoholes are presented. The use of an array of fully-etched holes instead of the conventional waveguide gratings provides an additional degree of freedom in the design of the coupler, thus enabling fabrication using the same photolithography mask and etching process as used for the silicon-on-insulator (SOI) waveguides. A grating coupler with coupling efficiency as high as 34% for coupling between the quasi-TE mode of the silicon nanophotonic waveguide and a single-mode optical fiber, and with 3dB bandwidth of 40nm was fabricated. A theoretical model is presented and three-dimensional finite-difference time-domain simulations are used to optimize the coupler design.

5.1 Introduction

SOI is a promising platform for PLCs due to its high refractive index contrast and compatibility with the mature fabrication facilities for complementary metal–oxide–semiconductor (CMOS) technology. Various kinds of devices on SOI wafers have been demonstrated in recent years using nanophotonic waveguides which have cross sectional dimensions of only a few hundred nanometers. The large coupling loss from the mode mismatch between optical fibers and the nanophotonic waveguides is one important problem that must be solved before silicon can replace silica as a mainstream platform for planar lightwave circuits. Recently, waveguide grating couplers defined by shallow-etched grooves [1-3], metallic lines [4] and slanted grooves [5] have been used for efficient coupling to optical fibers. They have

many advantages over alternative approaches that use adiabatic tapers and polished facets [6], including freedom for placement anywhere on a chip, avoiding need for facet polishing, enabling wafer-scale optical testing and potentially facilitating low cost packaging. Grating couplers also offer additional functionality such as polarization or power splitters [7-10].

For those grating couplers mentioned previously, the lithography and etching processes needed to fabricate the grating structures must be distinct from the corresponding waveguide fabrication steps because of the different etch depths required for the grating couplers. Applying grating couplers that could be made with the same fabrication steps as used for the waveguides will reduce the total number of fabrication steps and the cost of the PLC. However, for conventional gratings formed by continuous lines which are etched to the depths typically needed for waveguide fabrication (to the buried oxide of the SOI wafers), the refractive index step introduced would normally be too large. For example almost 50% of the light coming from the waveguide would be reflected by the first period. The grating strength in this case would be too strong for efficient coupling of light between waveguides and optical fibers. Subwavelength structures may be used to reduce the effective index step without distortion of the phase front of waveguide mode [11]. A single-etch grating coupler which could be fabricated by the same etch step as the waveguides, was recently proposed for coupling into the TM mode of the waveguide using subwavelength microstructures, and three-dimensional finite-difference time-domain (3D FDTD) simulation results were reported in [12], but no devices were fabricated.

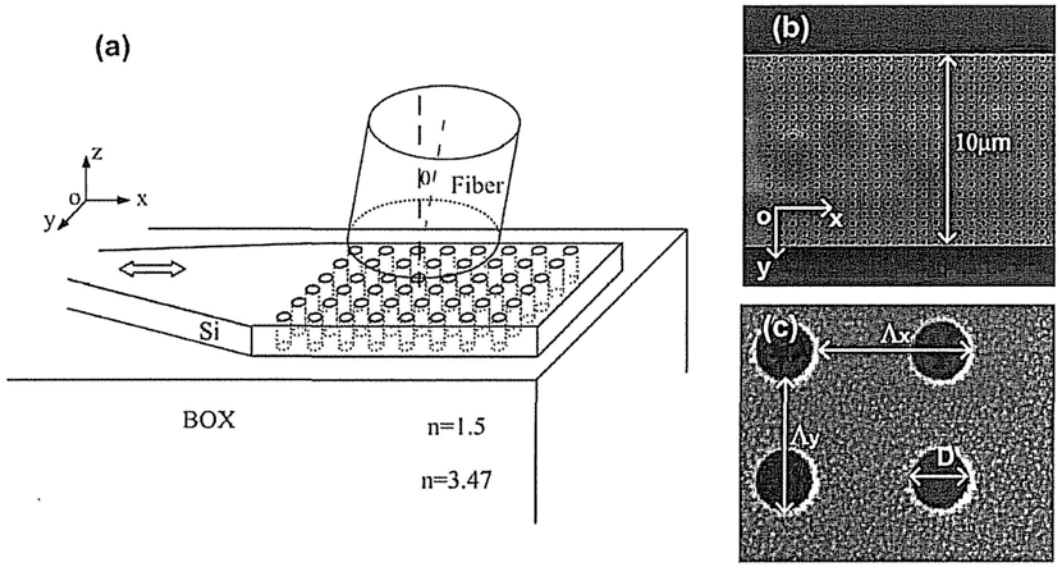

Fig. 5.1: (a) Schematic picture of the grating coupler for coupling between fibers and nanophotonic wire waveguides on SOI, $\theta = 8°$. (b) Scanning electron microscope (SEM) image of the fabricated array of nanoholes on the 10μm-width waveguide. The silicon dioxide on top was removed. (c) Nanoholes array with the holes diameter D, grating period Λ_x and transversal holes period Λ_y defined ($D = 200nm$, $\Lambda_x = 610nm$ and $\Lambda_y = 500nm$).

In this chapter, we present both the simulation and experimental characterization results of a single-etched (or fully-etched) grating coupler formed by an array of subwavelength nanoholes for coupling into the quasi-TE mode of a SOI waveguide as shown in Fig. 5.1. Nanoholes have less stringent photolithography requirements than the square-shaped microstructure proposed in [12] and can be produced using the standard deep-UV photolithography commonly used for CMOS devices. The coupling efficiency attained using the array of nanoholes (34% for TE polarization) is comparable to those obtained with other grating couplers [2-4], which were fabricated using additional photolithography and shallow etch steps. We also

describe a two dimensional (2D) model for the proposed nanoholes grating coupler in this chapter.

5.2 Theoretical model

Fig. 5.1(a) shows the schematic of the proposed single-etch nanoholes grating coupler. The device was fabricated using deep UV photolithography (193nm) on a SOI wafer, which has a 220nm thick top silicon layer (device layer) and 2000nm thick buried oxide layer. A 750nm thick oxide layer was deposited on top after fabrication of nanoholes array. This silicon dioxide layer can provide protection of devices and also slightly increase the percentage of light coupled upwards [2]. The waveguides and grating couplers were formed together by the single-step dry etching to the buried oxide. Fig. 5.1(b) and (c) are SEM images of the fabricated nanoholes grating coupler taken with the top oxide removed. Fig. 5.1(c) is a close up view of the nanoholes array. The holes diameter D, grating period Λ_x and transversal holes period Λ_y are defined as indicated in the figure. The holes diameter D was chosen to be 200nm in the device design. Smaller holes diameter would give smaller back reflection into waveguide, but 200nm was the minimum value that could be guaranteed by this specific fabrication technology. A single-mode optical fiber with 10.4μm mode field diameter (MFD) was used for the input and output coupling. Following the approach used in conventional grating coupler designs [2], the coupling fiber is oriented at an angle of 8 degrees off-vertical in the x-z plane defined by the surface normal (z axis) of SOI wafer and the waveguide direction (x-axis) in order to minimize second order Bragg reflection, which would otherwise limit the performance of the grating coupler as shown in Fig. 5.1(a). The width of the

planar waveguide of the grating region was designed to be 10μm, in order to have a good match with the mode field diameter from the optical fiber laterally (in y axis). The grating period could be calculated using the phase matching condition [9], [13] by the following equation, which is simply derived from equation 2.1:

$$q\lambda = \Lambda_x(n_{eff} - n_{cladding}\sin(\theta)). \qquad (5.1)$$

In equation 5.1, λ is the center wavelength; n_{eff} is the effective index of the grating region with nanoholes array; θ is the off-vertical tilt angle of the fiber ($\theta = 8°$); $n_{cladding}$ is the refractive index of the cladding material ($n_{cladding} = 1.5$); q is the diffraction order (set equal to 1 for the first order diffraction); and Λ_x is the grating period in the beam propagating direction.

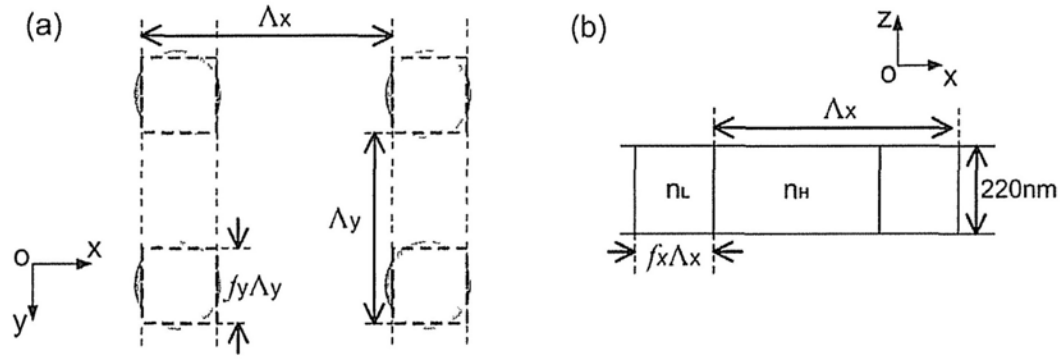

Fig. 5.2. (a) Top view of the nanoholes array. Square shape holes with same area were used in calculation. First order EMT was then applied to estimate the effective refractive index of the shaded region with nanoholes. (b) 2D model of the waveguide grating with nanoholes array based on a slab structure.

We initially used Eq. 5.1 to estimate the grating period Λ_x. The average effective index of the nanoholes grating region could be calculated using a 2D modal

based on a slab structure shown in Fig. 5.2(b). The section with higher index is made of 220nm thick silicon slab with refractive index of 3.47 and a cladding refractive index of 1.5. The effective index n_H for the fundamental mode was calculated to be 2.89 for a wavelength of 1450nm. The sections with lower effective index n_L are made from silicon with nanoholes that are filled with cladding material (silicon dioxide) as shown in Fig. 5.2(a). The refractive indices are 3.47 and 1.5 for silicon and nanoholes, respectively.

For ease of calculation, we use square shape holes to represent the 200nm diameter round shape holes. The side length of the square shape holes is set to be 177nm in order to have the same area as the round shape holes. Similar to the subwavelength structure in [11], the first-order effective medium theory (EMT) [14] could be used to estimate the effective refractive index of the shaded region in Fig. 5.2(a). According to EMT, a composite medium comprising two different materials interleaved at the subwavelength scale can be approximated as a homogenous medium. The first-order expressions for anisotropic refractive index are given by:

$$n^{TM} = [f_y n_{hole}^2 + (1-f_y) n_{Si}^2]^{1/2}, \qquad (5.2a)$$

$$\frac{1}{n^{TE}} = [\frac{f_y}{n_{hole}^2} + \frac{(1-f_y)}{n_{Si}^2}]^{1/2}, \qquad (5.2b)$$

where the symbol n_{hole} is the refractive index of the nanoholes (equals to 1.5), and n_{Si} is the refractive index of silicon slab (equals to 3.47). By assuming the transversal holes period Λ_y equals to 500nm, transversal fill factor of nanoholes f_y would be equal to 0.35. In our geometry, the electric field of the TE mode of waveguide is perpendicular to the nanoholes. Eq. 5.2b should be used to calculated the refractive index of the shaded region, which equals to 2.18. The effective

refractive index for the fundamental TE mode of the slab in the shaded region is then calculated, and in this case it is equal to 1.76.

For the fundamental mode in the grating structure shown in Fig. 5.2(b), the average effective index of the grating region n_{eff} for the fundamental mode was obtained using a roughly linear relationship as explained in chapter 2 for one-dimensional gratings:

$$n_{eff} = f_x n_L + (1 - f_x) n_H . \qquad (5.3)$$

Thus the value of n_{eff} is about 2.6 for grating structure with $\Lambda_y = 500nm$ and $\Lambda_x = 610nm$. The center wavelength of light coupling is 1450nm for a grating period of 610nm based on Eq. 5.1.

5.3 3D FDTD simulation and measurement results

The 2D model mentioned in section 5.2 requires the transversal holes period Λ_y to be as small as possible compared to the effective wavelength in the medium. A more precise result would be obtained using 3D FDTD simulations. The results of the 3D FDTD simulations, such as shown in Fig. 5.3(a), allowed the transversal period Λ_y of the nanoholes to be varied and the coupler design for the desired wavelength to be optimized. The fundamental waveguide mode was calculated and propagated into the grating region containing the nanoholes array (holes diameter $D = 200nm$). The percentage of power reflected back from grating into waveguide for different transversal period Λ_y of the nanoholes and different wavelengths was calculated and plotted in Fig. 5.3(b). The wavelength of peak reflection varied with the transversal period Λ_y as shown in the figure.

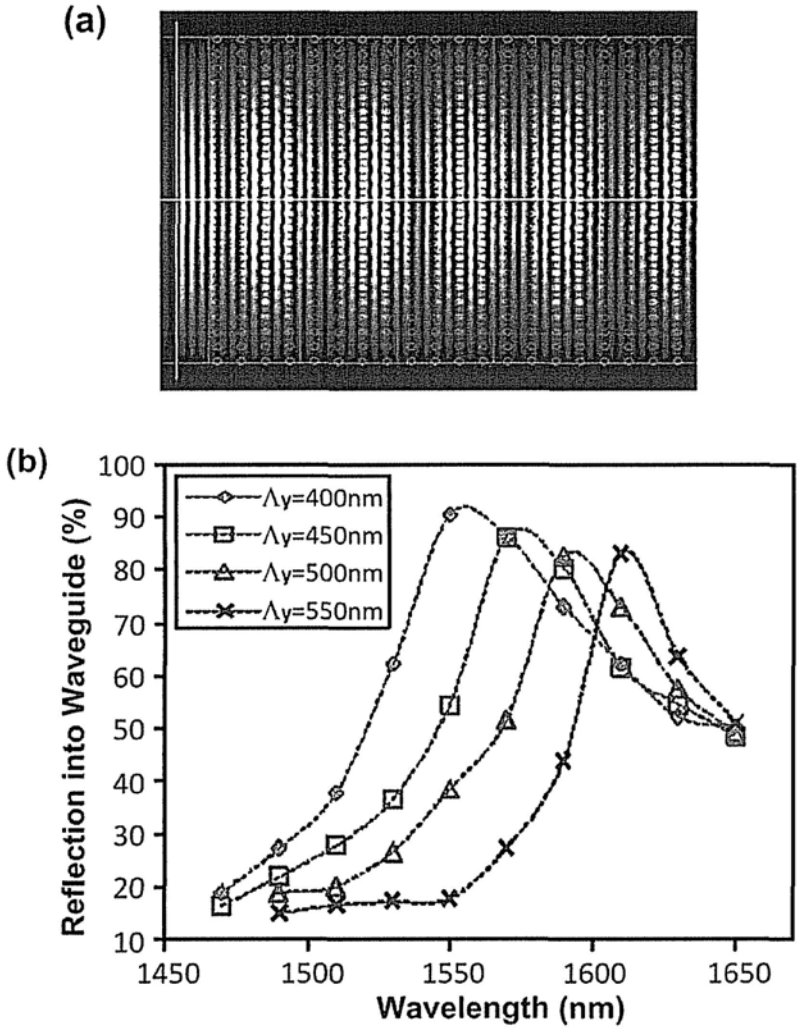

Fig. 5.3. (a) Color graded representation of the mode field amplitudes in the grating region obtained from 3D FDTD simulation of the nanoholes grating coupler with $\lambda = 1490nm$, $\Lambda_y = 450nm$, $\Lambda_x = 610nm$ and $D = 200nm$. (b) Simulation results of the back reflection into waveguide from the nanoholes grating ($D = 200nm$ and $\Lambda_x = 610nm$) as a function of wavelength for Λ_y between 400nm and 550nm. The wavelength of the 2nd order Bragg reflection shifts with change of Λ_y.

The peak reflection occurs at the wavelength of second order Bragg back reflection (phase matching condition). The wavelength of peak reflection could also be determined by the simple equation $\lambda_p = \Lambda_x \times n_{eff}$ [2]. Using this equation, we calculated the effective index of the grating region with nanoholes array. We found that the effective index obtained from the 3D FDTD simulations varied almost linearly from 2.64 to 2.55 with the transversal period Λ_y, which was varied from 550nm to 400nm. From Eq. 5.1, the center wavelength for coupling with $\theta = 8°$ may be calculated and this is plotted in Fig. 5.4 together with the experimental data. The center wavelength calculated using the 2D model described in section 5.2 is also plotted in the same figure. We can see that the results obtained by 3D FDTD simulations are smaller than the experimental data. This is because the refractive index will increase slightly when the wavelength was reduced (from around 1560nm to around 1450nm). Higher effective refractive index will lead to longer center wavelength. We can also observe that the result obtained by the proposed 2D model would become more and more inaccurate with the increasing of transversal period Λ_y, as the EMT used in the model requires the transversal period Λ_y as small as possible compare to the wavelength in the medium [11], [14].

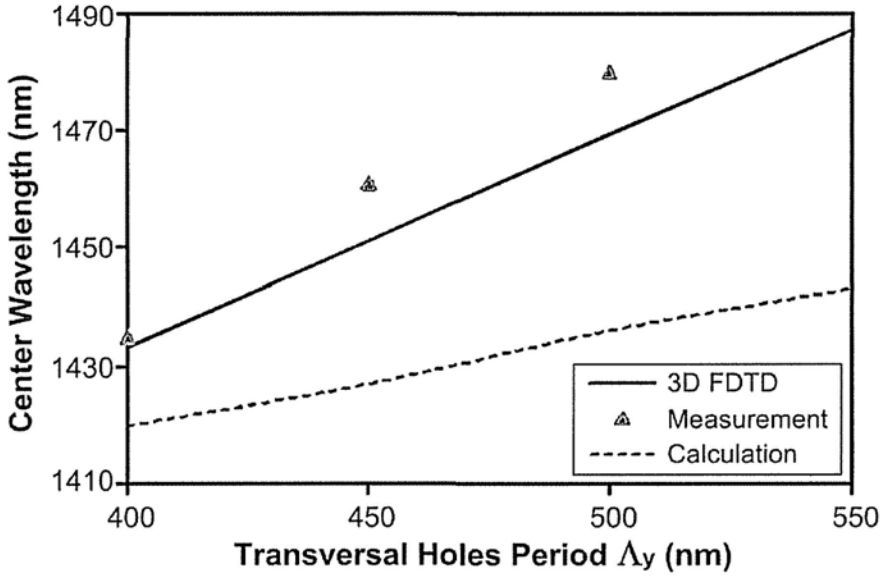

Fig. 5.4. The center wavelength of the nanoholes grating coupler with $\theta = 8°$ was calculated based on 3D FDTD simulations for different transversal holes period Λ_y. The experimentally measured data and calculated result by the 2D model described in section 2 are also presented.

From Fig. 5.3(b), it can be seen that as the transversal period Λ_y is reduced, the bandwidth of reflection increases, and the back reflection at the coupling wavelength would also increase. This bandwidth of reflection would become even larger for the fabricated devices when incorporated with the fabrication errors. We measured the Fabry-Perot (FP) resonances around the center wavelength for different nanoholes grating couplers as shown in Fig. 5.5.

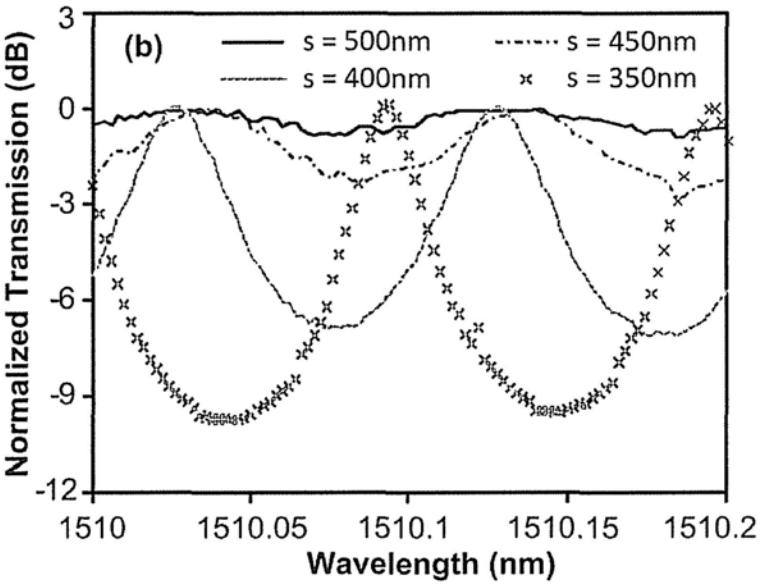

Fig. 5.5. (a) Coupling efficiency was plotted for the proposed grating coupler with deep etched holes array (s = 500nm). (b) Normalized fiber-to-fiber transmission of waveguides with the proposed couplers at both ends. Strong Fabry-Perot effect was observed when the holes spacing s increased.

Strong FP resonances (3.8dB peak to trough extinction ratio) with about 0.1nm free spectral range (FSR) were observed for the grating coupler with $\Lambda_y = 400nm$. This extinction ratio was reduced to 1.6dB and 0.8dB for 450nm and 500nm transversal period respectively. Using the well known expression for FSR of FP cavity:

$$\Delta\lambda \approx \lambda_o^2 / 2n_g L . \qquad (5.4)$$

For a cavity length L (equal to 3mm for the fabricated devices), and the calculated average group index $n_g \approx 4$ at wavelength around 1460nm, the calculated FSR is about 0.09nm. This agrees with the measurements and confirms that spectral oscillations are from FP resonances formed by the reflections between the grating

couplers at each end of the waveguide. The large back reflection for grating coupler with $\Lambda_y = 400nm$ leads to a lower coupling efficiency.

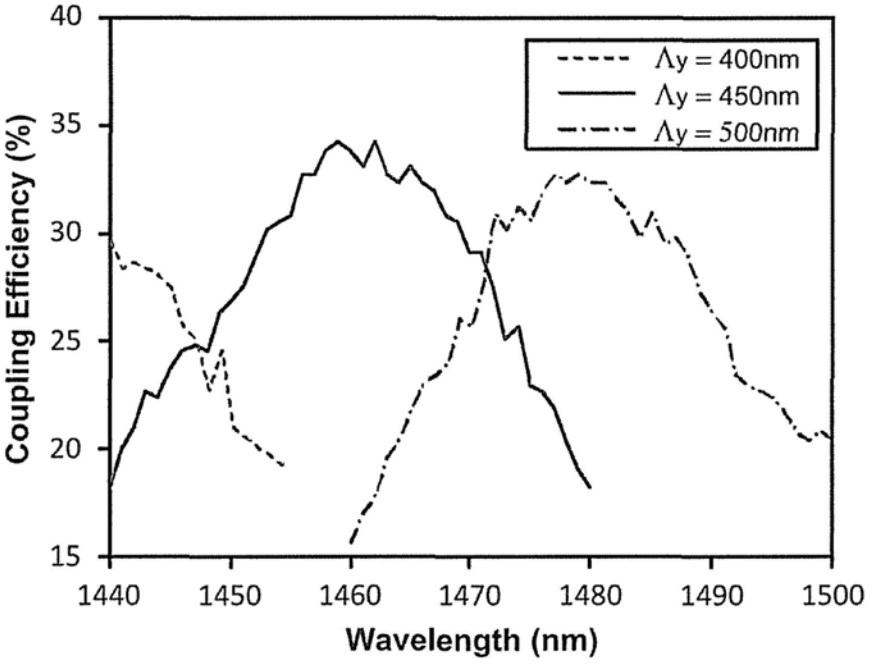

Fig. 5.6. Experimentally measured coupling efficiencies are plotted for the proposed nanoholes grating couplers with different transversal period Λ_y. 34% coupling efficiency was measured with 40nm 3dB bandwidth with $\Lambda_y = 450nm$.

We characterized the fabricated nanoholes grating couplers by measuring the fiber-waveguide-fiber insertion loss of light coupled via a pair of grating couplers separated by a 500nm wide waveguide of 2mm length. The grating with nanoholes array in x-direction would diffract light into/from a cleaved single-mode optical fiber with 8 degree tilt. Two 0.5mm long adiabatic tapers were used to connect the input and output 10μm wide waveguide with the 500nm wide nanophotonic waveguide.

Assuming that the coupling efficiencies were the same for the couplers at both ends and neglecting the waveguide propagation losses, the coupling efficiency was obtained for different transversal holes period Λ_y and plotted in Fig. 5.6. With $\Lambda_y = 450nm$, we obtained 34% coupling efficiency at 1460nm with a 3dB bandwidth of 40nm. Limited by the wavelength range of our tunable laser, we could only measure the coupling efficiency down to 1440nm wavelength. The center wavelength of the coupler with $\Lambda_y = 400nm$ was obtained by curve fitting. The center wavelengths of the fabricated couplers were 1435nm, 1461nm and 1480nm for 400nm, 450nm and 500nm transversal period Λ_y respectively as shown in Fig. 5.6. The coupling efficiency was mainly limited by the bi-directional nature of diffraction. Adding a substrate mirror would further improve the performance. 69% coupling efficiency to slightly tilted optical fiber was measured in [15] for a shallow etched grating coupler with a metal bottom mirror. We expect this order of coupling efficiency to be attainable for the nanoholes grating coupler design. There also is a paper published more recently, which extended the bandwidth of the fully-etched grating coupler by employing the photonic crystal structure instead of nanoholes array [16].

5.4 Summary

The fully-etched grating couplers formed by an array of subwavelength nanoholes were proposed, fabricated and experimentally characterized. The grating couplers were fabricated in the same deep etch step as used for defining the waveguides, thus reducing the number of masks and fabrication steps needed. Despite the reduction in fabrication steps, we achieved coupling efficiencies

comparable with conventional grating couplers that use additional fabrication processes. The 34% coupling efficiency measured in the fabricated devices had a 40nm 3dB optical bandwidth for coupling between single-mode optical fiber and the silicon nanophotonic wire waveguides. The 3D FDTD simulation results had good agreement with the experimental results from the fabricated devices. Further improvement could be achieved by varying the grating strength to increase the field overlap with fiber mode [12] and adding a substrate mirror [15].

References:

[1] D. Taillaert, W. Bogaerts, P. Bienstman, T. F. Krauss, P. Van Daele, I. Moerman, S. Verstuyft, K. De Mesel, and R. Baets, "An out-of-plane grating coupler for efficient butt-coupling between compact planar waveguides and single-mode fibers," IEEE J. Quantum Electron., vol. 38, no. 7, pp. 949-955, Jul. 2002.

[2] D. Taillaert, F. Van Laere, M. Ayre, W. Bogaerts, D. Van Thourhout, P. Bienstman and R. Baets, "Grating couplers for coupling between optical fibers and nanophotonic waveguides," Jap. J. Appl. Phys., vol. 45, no. 8A, pp. 6071-6077, Aug. 2006.

[3] X. Chen, C. Li, and H. K. Tsang, "Fabrication-tolerant waveguide chirped grating coupler for coupling to a perfectly vertical optical fiber," *IEEE Photon. Technol. Lett.*, vol. 20, no. 23, pp. 1914-1916, Dec. 2008.

[4] S. Scheerlinck, J. Schrauwen, F. Van Laere, D. Taillaert, D. Van Thourhout, and R. Baets, "Efficient, broadband and compact metal grating couplers for silicon-on-insulator waveguides," *Opt. Express,* vol.15, no. 15, pp. 9625-9630, Jul. 2007.

[5] B. Wang, J. H. Jiang, and G. P. Nordin, "Embedded slanted grating for vertical coupling between fibers and silicon-on-insulator planar waveguides," *IEEE Photon. Technol. Lett.*, vol. 17, no.9, pp. 1884-1886, Sept. 2005.

[6] T. Shoji, T. Tsuchizawa, T. Watanabe, K. Yamada, and H. Morita, "Low loss mode size converter from 0.3μm^2 Si wire waveguides to single-mode fibers," *Electron. Lett.*, vol. 38, no. 25, pp. 1669-1670, Dec. 2002.

[7] D. Taillaert, H. Chong, P. I. Borel, L. H. Frandsen, R. M. De La Rue, and R. Baets, "A compact two-dimensional grating coupler used as a polarization splitter," *IEEE Photon. Technol. Lett.*, vol.15, no.9, pp.1249-1251, Sept. 2003.

[8] X. Chen, C. Li, and H. K. Tsang, "Etched waveguide grating variable 1X2 splitter/combiner and waveguide coupler," *IEEE Photon. Technol. Lett.*, vol.21, no.5, pp.268-270, Mar. 2009.

[9] Y. B. Tang, D. X. Dai, and S. L. He, "Proposal for a grating waveguide serving as both a polarization splitter and an efficient coupler for silicon-on-insulator nanophotonic circuits," *IEEE Photon. Technol. Lett.*, vol.21, no.4, pp.242-244, Feb. 2009.

[10] J. Feng and Z. Zhou, "Polarization beam splitter using a binary blazed grating coupler," Opt. Lett., vol.32, no.12, June 2007.

[11] J. H. Schmid, P Cheben, S. Janz, J. Lapointe, E. Post, and D. X. Xu, "Gradient-index antireflective subwavelength structures for planar waveguide facets," *Optics Lett.*, vol.32, no.13, pp.1794-1796, Jul. 2007.

[12] R. Halir, P. Cheben, S. Janz, D. X. Xu, I. Molina-Fernandez, and J. G. Wanguemert-Perez, "Waveguide grating coupler with subwavelength microstructures," *Optics Lett.*, vol.34, no.9, pp.1408-1410, May. 2009.

[13] R. Orobtchouk, A. Layadi, H. Gualous, D. Pascal, A. Koster, and S. Laval, "High-efficiency light coupling in a submicrometric silicon-on-insulator waveguide," *Applied Optcs*, vol.39, no.31, pp.5773-5777, Nov. 2000

[14] S. M. Rytov, "Electromagnetic properties of a finely stratified medium," *Sov. Phys. JETP*, vol.2, no.3, pp.466-475, 1956

[15] F. Van Laere, G. Roelkens, M. Ayre, J. Schrauwen, D. Taillaert, D. Van Thourhout, T. E. Krauss, and R. Baets, "Compact and highly efficient grating

couplers between optical fiber and nanophotonic waveguides," *J. Lightw. Technol.*, vol.25, no.1, pp.151-156, Jan. 2007.

[16] L. Liu, M. Pu, K. Yvind, and J.M. Hvam, "High-efficiency, large-bandwidth silicon-on-insulator grating coupler based on a fully-etched photonic crystal structure," *Applied Physics Letters*, vol.96, 051126 (2010)

6. Apodized grating couplers with Gaussian-like output profile

In this chapter, we describe a shallow-etched apodized waveguide grating coupler which achieves efficient coupling between single mode fiber and a silicon-on-insulator nanophotonic waveguide. By appropriate choice of waveguide/grating thicknesses (340nm top silicon thickness is used instead of 220nm as in the previous chapters) and varying the coupling strength of the grating coupler via tailoring its fill factor to optimize the mode matching, a coupling efficiency of 75.8% (-1.2dB) was obtained for each fiber/silicon waveguide interface with slightly titled optical fiber, which was the highest coupling efficiency reported hitherto for grating couplers between optical fibers and nanophotonic waveguides. Detailed design and experimental results are included. Efforts were also put to enhance the coupling efficiency for coupling with vertical optical fibers.

6.1 Introduction

SOI based photonic integrated circuits (PICs) have many promising applications [1]. Compared with the butt-coupling techniques [2] between optical fibers and nanophotonic waveguides, diffractive waveguide grating couplers [3-8] have been actively researched, because of their many advantages as introduced in the previous chapters. A coupling efficiency as high as -1.6dB (69%) was recently achieved with a polysilicon overlay [8]. However, the coupling efficiency for a grating coupler is still slightly less than those with butt-coupling techniques which are able to achieve a coupling efficiency that is normally higher that -1dB (79%).

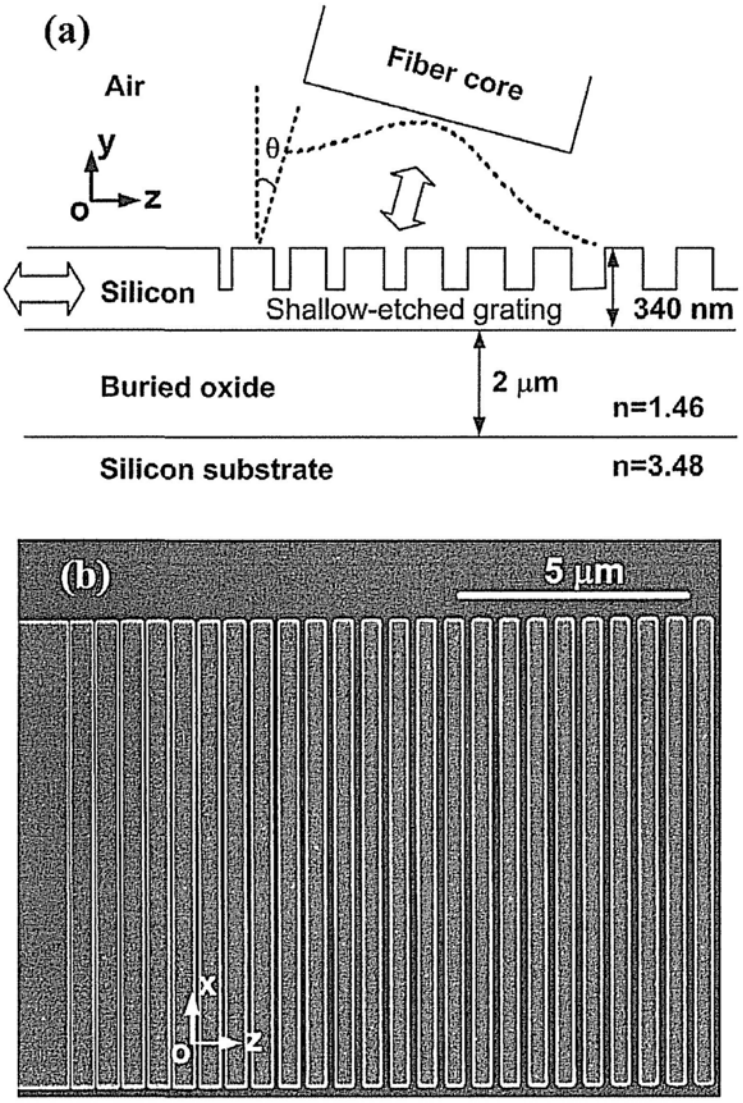

Fig. 6.1: (a) Schematic of the proposed waveguide diffractive grating coupler. (b) SEM image of the fabricated grating coupler with varied coupling strength on 10.4μm wide waveguide. A Gaussian-like field output is achieved to match the fiber mode.

Two main factors have limited the coupling efficiency of grating couplers. One is the poor directionality (defined as the portion of the light power coupled upwards normalized with respect to the total out-coupled optical power). Grating diffraction

tends to be bi-directional, so that half of it optical power would be loss to the substrate. Additional structures such as a substrate mirror [6] or a polysilicon overlay [7] were demonstrated to increase the portion of light coupling towards the fiber, but those structures require relatively complicated fabrication process. Another factor that limits the coupling efficiency is the mode mismatch between the field profiles of diffracted light from waveguide grating and the fiber mode. An exponentially decaying field profile is generally expected when the light diffracted from a uniform grating, and this would theoretically limit the coupling efficiency to a maximum of 80% for coupling to the Gaussian-like mode profile of an optical fiber [11]. By engineering the coupling strength (or leakage factor) of the grating structure, Gaussian-like profile from weak grating on polymer waveguides was demonstrated [9]. It was suggested that Gaussian-like output profile from SOI grating couplers may be achieved by varying the fill factor of the grating [4]. But this approach has not yet been implemented.

In this chapter, we describe the design and experimental measurement results of a novel highly efficient diffractive grating for coupling between optical fiber and nanophotonic waveguide as shown in Fig. 6.1. Two techniques were implemented for the first time to improve the coupling efficiency: We went beyond the strict single-mode waveguide thickness constraint and used a more optimum configuration to improve the directionality of the grating. Although the waveguide thickness used in this design (340nm) may support a first order mode, for most device applications, the grating coupler itself can act as an effective mode filter for both the input and output coupling and thus only the fundamental mode is present. Secondly by carefully designing the grating fill factor to vary the grating coupling strength, a Gaussian-like output field profile was realized with the shallow-etched SOI grating.

The grating coupler achieved a efficiency of 75.8% for coupling between a standard single mode optical fiber (~ 9 μm core diameters) and a 450nm (wide) by 340nm (thick) waveguide. This result is the highest coupling efficiency demonstrated to date for waveguide grating couplers. To verify our design, the coupling strength and effective refractive index of the shallow-etched waveguide diffractive gratings with different fill factors were also characterized. A small off-vertical tilt (θ=10°) of optical fiber was applied to reduce the large second order back reflection [3]. It is also possible to chirp the grating period instead of tilting the fiber to reduced back reflection, whilst keeping the fiber vertical to the chip surface [10].

6.2 Design and simulations

The grating couplers were optimized for coupling between single mode optical fibers with 10.4μm mode field diameter (MFD) and the fundamental TE (transverse electric) mode in the nanophotonic waveguides. They were fabricated on a SOI wafer using electron beam lithography with 340nm thick top silicon layer and 2μm thick buried oxide. The fundamental mode of the nanophotonic waveguide was first expanded laterally (in x-axis) by an adiabatic taper to a 10.4μm wide waveguide which has a lateral mode size similar to a single mode fiber. The light is diffracted vertically upwards into the optical fiber by the shallow-etched grating structure when the wavelength λ satisfies the phase matching condition [5]. Two dimensional Finite-Difference Time-Domain (2D FDTD) simulations were used to simulate the grating diffraction [10].

6.2.1 Optimizing the directionality of diffraction

According to simulations, the directionality of grating diffraction is mainly dependent on the thickness of waveguide and the etch depth of the grating structure, but not the fill factor. Thus we can investigate the directionality of diffraction by decomposition of the grating into interfaces between the teeth and grooves, and analyzing those interfaces separately. Simulation results of each tooth-to-groove and groove-to-tooth interface are shown in the following figures, with 340nm waveguide thickness. For the ease of explanation, the cladding is assumed to be oxide, so that the silicon waveguide initially has a symmetric structure sandwiched with oxide.

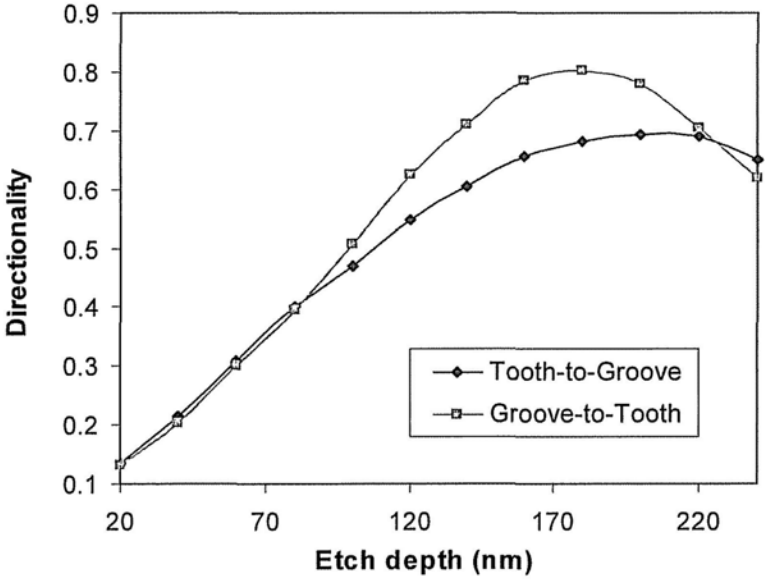

Fig. 6.2: Directionality of each tooth-to-groove and groove-tooth interface with different etch depth of the waveguide grating.

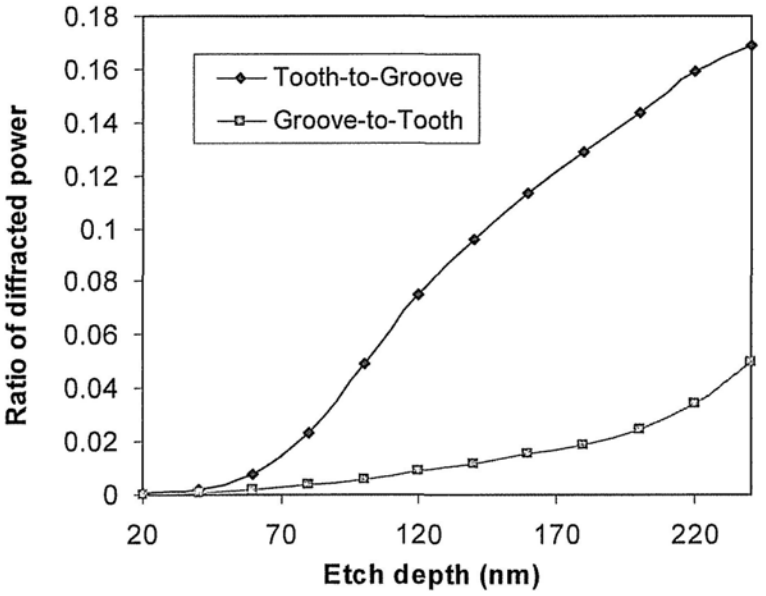

Fig. 6.3: The ratios of the diffracted power from each tooth-to-groove and groove-to-tooth interface to the total input with different etch depth of the waveguide grating. It can be found that the tooth-to-groove interface almost dominate the overall diffraction process.

The directionality of the different interfaces is plotted in Fig. 6.2, and the ratios of the diffracted power from each tooth-to-groove and groove-tooth interface to the total input are plotted in Fig. 6.3. Although the directionalities are slightly different for those two types of grating interfaces, the power diffracted from tooth-to-groove interfaces almost dominates the diffraction process as shown in Fig. 6.3. Thus, we will focus on the diffraction process at the tooth-to-groove interfaces to analyze the directionality of diffraction.

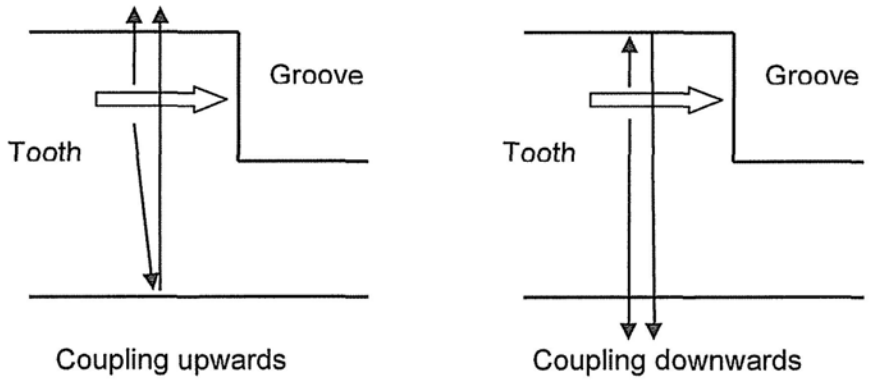

Fig. 6.4: Schematic illustration of the light power diffracted upwards and downwards. Light is partially blocked by the side wall of the groove and scattered from approximately the midpoint of the side wall.

Similar to the volume current method (VCM) [12], a clear picture of the underlying physical mechanism could be depicted by considering the light a kind of "current" that is partially blocked by the side wall of the groove as shown in Fig. 6.4. Light is generally scattered from the midpoint of the grooves' side walls. There are mainly two wave components interfering with each other during diffraction either upwards or downwards. One is direct scattered from the diffraction center and another is the wave scatter in an opposite direction and reflected back from the interface between silicon and oxide. When the etch depth increases from 0nm to around 210nm, the phase difference for those two up-coupled wave components approximately changes from 1.1π to 0.1π, whilst it changes form 0π to 1π for the down-coupled ones. Thus the up-coupling is initially suppressed by destructive interference and enhanced by constructive interference, when increasing the etch depth of the grating. This result matches the simulation data in Fig. 6.2.

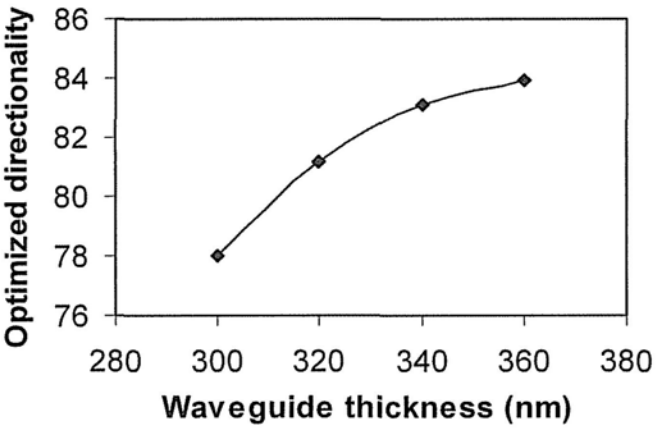

Fig. 6.5: The optimized coupling directionalities for waveguide grating couplers with different thicknesses of top silicon (period = 610nm, f = 0.4).

We also obtained the optimized directionalities by varying the etch depth of waveguide grating couplers with various top-silicon thicknesses as shown in Fig. 6.5. Higher directionality is achieved with increased waveguide thickness. However, the thickness need to be as small as possible (in 250nm – 400nm range) for a better light confinement, which is also an essential merit for photonic integrated circuits. A thickness of 340nm is chosen after making trade-off of those two factors.

The improved directionality can apply to the cases of either air cladding or silicon dioxide deposited on top of the waveguide as shown in Fig. 6.6(a). The directionality is improved further (to ~0.9 by simulation), when the lower interface of the buried oxide and silicon substrate is included in the calculation.

6.2.2 Achieving Gaussian-like mode profile

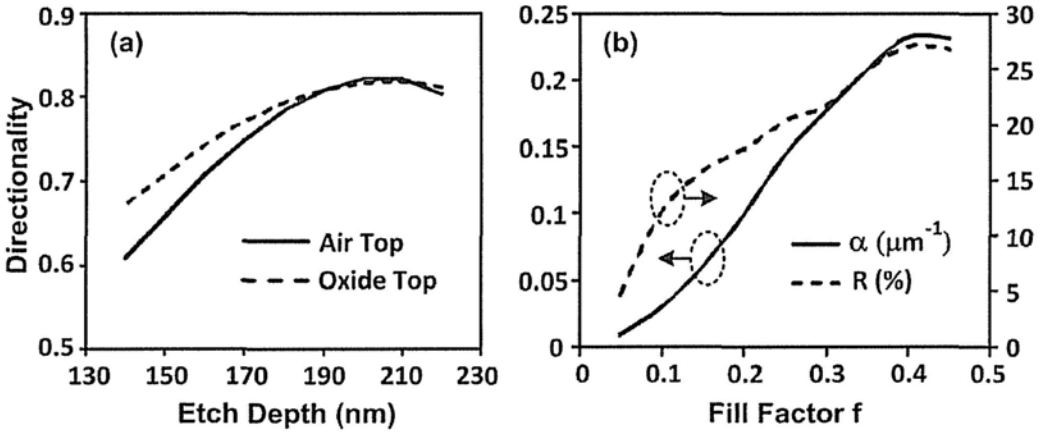

Fig. 6.6: (a) Directionality of the diffractive waveguide grating with different etching depths of grooves for SOI with 340nm thick top silicon (f = 0.5, period = 610nm). (b) Coupling strength of the 200nm shallow-etched waveguide grating with different fill factor f ($\theta = 10°$). The back reflection into waveguide for different f is also plotted.

For light diffracted from a uniform waveguide grating, the optical power confined in the waveguide structure may be described by:

$$P(z) = P_o \exp(-2\alpha z), \qquad (6.1)$$

where α is the coupling strength. The mode matching efficiency could only reach 80% with Gaussian-shaped fiber mode with optimized design, when α equals to around 0.13μm^{-1} for fiber with 10.4μm MFD [11]. Higher coupling efficiency could be achieved [4, 9] by vary the coupling strength along z-axis to obtain a Gaussian-shaped output field profile G(z), as:

$$dP(z)/dz = -2\alpha(z)P(z) = -G^2(z). \qquad (6.2)$$

α is then calculated by:

$$\alpha(z) = \frac{G^2(z)}{2\left(1 - \int_0^z G^2(t)dt\right)} \qquad (6.3)$$

Since the etch depth is determined by the condition to optimize the directionality as described above, we modified the fill factor *f* (defined as the ratio of the shallow-etched groove width to the grating period) to change the coupling strength. From the simulation results in Fig. 6.6(b), we find that the coupling strength α increases significantly with the fill factor when $f < 0.4$. If we increase the fill factor further, α will not change too much, until decreasing with the fill factor when $f > 0.6$. We thus use *f* ranging from 0.08 to 0.4 to engineer the coupling strength of the grating coupler along z-axis. The average effective index n_{eff} and the grating period would also change with *f*.

According to Eq. 6.3 and the phase matching condition (Eq. 2.1), the periods and *f* (in bracket) for the optimized design counting from the front end are: 548nm (0.08), 550nm (0.1), 556nm (0.13), 560nm (0.15), 564nm (0.17), 570nm (0.2), 574nm (0.22), 580nm (0.25), 586nm (0.28), 594nm (0.32), and 604nm (0.37), followed by a uniform grating with 610nm period ($f = 0.4$). For uniform gratings with large etch depth, the large refractive index step in each period of the grating can (in the case of gratings with a constant *f*) lead to a constructive build up of reflection losses, even with the off-vertical fiber tilt as shown in Fig. 6.6(b), and this would limit the coupling efficiency. However, by varying the fill factor according to Eq. 6.3, the constructive build up of reflections could also be suppressed, leading to a further improvement in the waveguide-to-fiber coupling efficiency. 84% coupling efficiency was obtained by simulation.

6.3 Experimental results

We characterized the fabricated grating couplers by measuring the fiber-waveguide-fiber insertion loss of light coupled via a pair of grating couplers coupling light into and out of a 450nm wide waveguide. A pair of adiabatic linear tapers, each with a length of 500μm, is used to connect the 10.4μm wide grating region and the 450nm wide waveguide section. The waveguide length was kept short (20μm) to have negligible propagation loss. The measured coupling loss per fiber-waveguide interface is thus only 1.2 dB (corresponding to 75.8% coupling efficiency) at the wavelength of 1533nm. The couplers had a 3dB (~50% coupling efficiency) optical bandwidth of about 45nm. The measured coupling efficiency is plotted in Fig. 6.7 together with the calculated results.

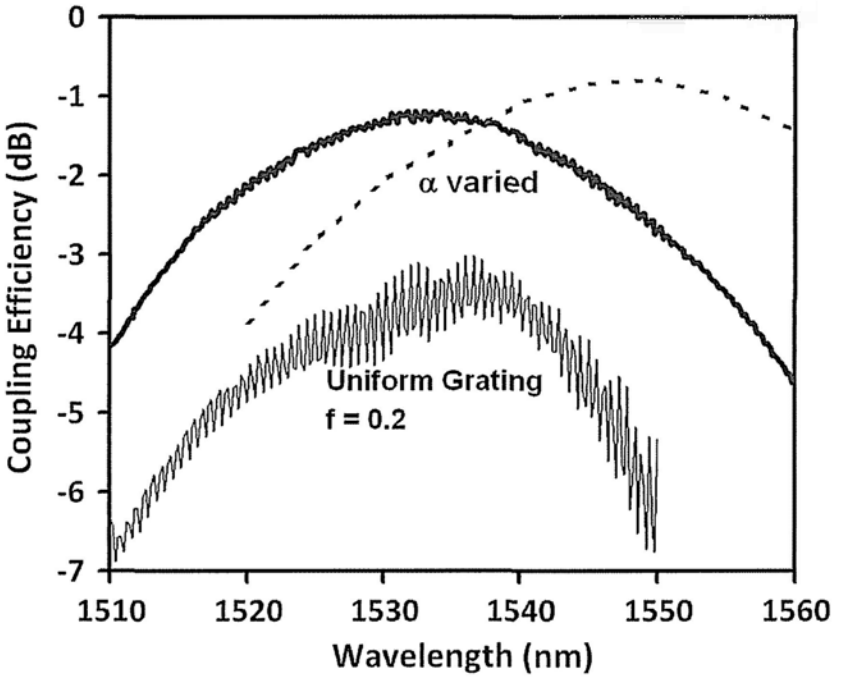

Fig. 6.7: Calculated (dotted line) and measured (solid line) coupling efficiency of the diffractive grating coupler with varied coupling strength. Up to -1.2dB efficiency was obtained at 1533nm experimentally. Over 2dB enhancement was demonstrate by the increased mode matching efficiency and reduced back reflection compared to uniform grating with f = 0.2.

The measured center wavelength of the coupling efficiency is clearly blue shifted. We believe this is because of the non-vertical side slope of the dry-etching process, which tend to increase the effective refractive index of the waveguide grating. The side slop is about 75° – 80° according to our previous measurement. The Fabry-Perot (FP) resonance of the fiber-to-fiber transmission at the center wavelength was less than 0.3dB for the apodized grating coupler, indicating that the back reflections into the waveguide was also suppressed successfully by variation in coupling strength. Compared to the coupling efficiency of a uniform grating with 0.2 fill factor plotted

in Fig. 6.7, or the grating coupler described in [7], around 1dB improvement could be achieved by the increased mode-matching efficiency of the Gaussian-like field output. Besides, the reduction of back reflection gives another enhancement of about 1dB.

To check the sensitivity of the proposed design to variations in the fabrication process, we varied the lithographic exposure energy to change the actual widths of the grooves for the devices (up to 10nm variation observed in SEM images). Ten waveguide samples were fabricated; all of them could achieve better than -2dB coupling efficiency.

The coupling strength α for gratings with different fill factor was characterized by moving one fiber to the positive direction of z-axis to collect the optical power diffracted out, while the fiber at input-end was fixed. Measured results are plotted in Fig. 6.8. For f = 0.1, 0.2, 0.3, and 0.4, which could also be treated as the matching efficiency between an exponential decaying curve (diffracted light from uniform grating) and a Gaussian curve (fundamental mode profile of optical fiber). The coupling strength α is measured to be around 0.013, 0.074, 0.19, and 0.31μm^{-1} respectively by curve fitting. The average effective refractive indices were also calculated with the measured peak coupling wavelength. These results agree with the simulation results.

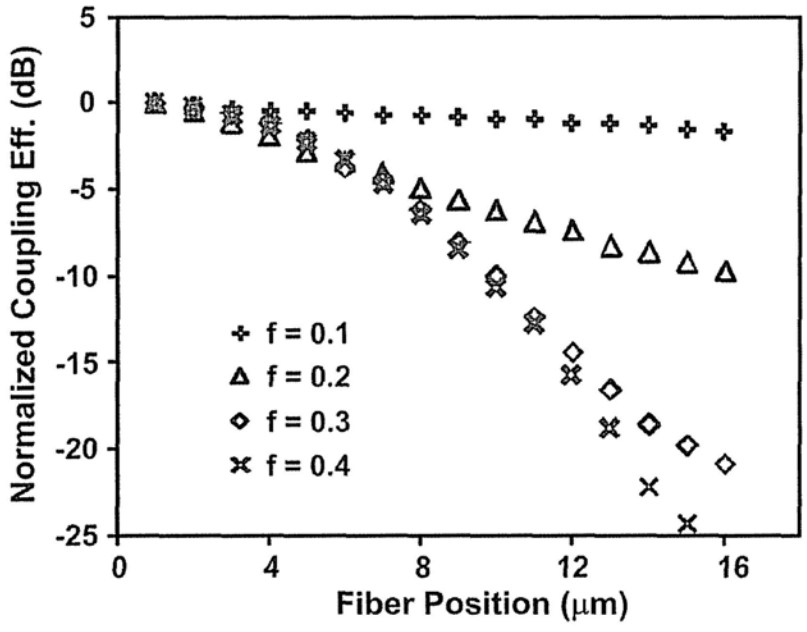

Fig. 6.8: Measured changes of coupling efficiency by moving one fiber towards the positive direction of z-axis, while keeping the other fiber fixed. Thus the decay rate of the diffracted output from the uniform grating with different f was obtained by curve fitting to calculate the coupling strength.

6.4 Apodized grating couplers for vertical optical fibers

With slightly tilted fiber (θ = 10° as shown in Fig. 6.1(a)), we found that the apodized grating is able to eliminate the small back reflection caused by the comparatively large index step of the grating. But back reflection would still dominate (> 80%) when we designed the gratings for coupling to fully vertical optical fibers (θ = 0°). Because the vertical coupling scheme without fiber tilting would be more preferable for low cost photonic packaging process, preliminary work on applying linearly chirped grating [10] to reduce the back reflection was carried out with the constraint of maintaining a Gaussian-like output profile and keeping the fiber vertical to the chip surface.

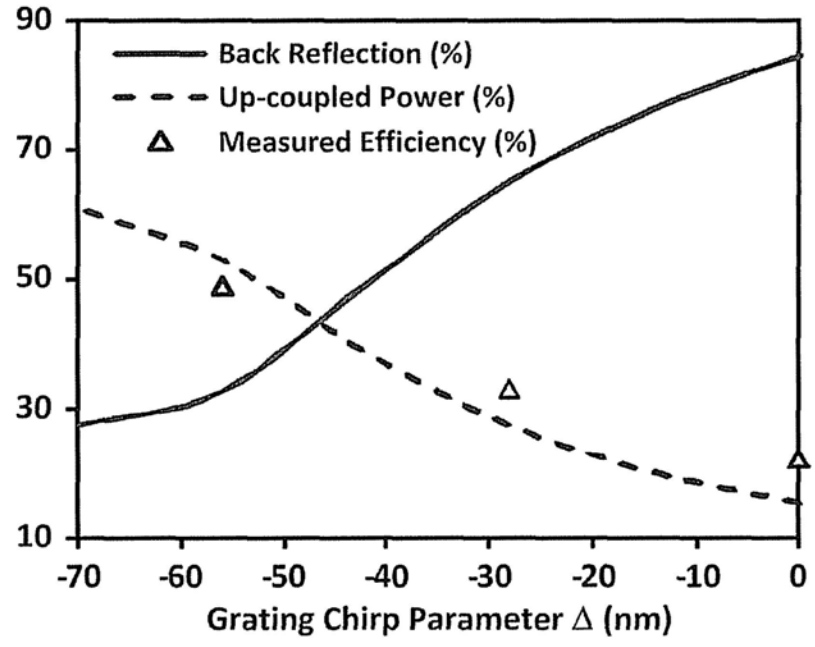

Fig. 6.9: Simulated back reflection and up-coupled power into fiber are plotted with different grating chirped parameter for apodized grating couplers. Experimentally measured coupling efficiencies are also plotted.

Simulation results for the apodized grating couplers with chirped periods are plotted in Fig. 6.9. We are using fill factor f (ratio of the width of etched grooves to the period) ranging from 0.08 to 0.4 to engineer the coupling strength of the grating coupler along z-axis. The average effective index of the grating region would also change with f. According to phase matching condition, the grating period Λ need to be initially changed from 520nm to 580nm for different f in the design for vertical coupling at 1550nm wavelength. Thereafter, we could define a grating chirp parameter Δ as the maximum deviation of the change applied to the first and last grating periods of the linearly chirped section (similar to [10]). The negative sign means the change of each period is decreasing. For example, if $\Delta = -40$nm, the first

period would be change from 520nm to 540nm, and the last period would be changed from 580nm to 560nm. By increasing the linearly chirping of the grating periods (reducing Δ from 0), the back reflection can be reduced significantly. The coupling efficiency is enhanced as shown in Fig. 6.9. Preliminary experimental results showed a 3dB coupling loss with $\Delta = -56$nm. The Fabry-Perot resonance was found to be reduced from 11dB to 2.6dB for a short waveguide with two grating couples at both ends, indicating a significant reduction of the back reflection. Further improvement of the design is under way, as we found that the coupling strength increased abruptly when reducing the coupling angle θ. Thus the output profile of the vertical grating coupler may be distorted.

6.5 Conclusion

We achieved a coupling efficiency of 75.8% (-1.2dB) between a standard single mode optical fiber and a 450nm wide SOI optical waveguide using a single etched grating structure, without any additional bottom mirrors or high index overlay. This result is the highest coupling efficiency reported hitherto for waveguide grating couplers. The coupling strength of the waveguide grating is varied to achieve a Gaussian-like mode field output along z-axis in order to match with the mode of optical fibers. Back reflection is also suppressed by the variation of coupling strength. The proposed structure is quite robust to fabrication process variations. The coupling strengths and average effective refractive indices for uniform gratings with different fill factors were characterized and the results agree with the simulation results.

We also achieved ~50% (-3dB) coupling efficiency by grating couplers with vertical optical fibers. In addition to the Gassian-like output mode profile from the apodized grating, back reflection was further reduced from ~80% to ~30% by a linear chirp of the grating period. Around 3dB enhancement was achieved by the chirp when coupling with vertical optical fibers. Further improvement is under way.

References:

[1] B. Jalali and S. Fathpour, "Silicon photonics", J. Lightwave Technol., vol.24, no.12, pp.4600-4615, Dec. 2006.

[2] T. Shoji, T. Tsuchizawa, T. Watanabe, K. Yamada, and H. Morita, "Low loss mode size converter from 0.3μm^2 Si wire waveguides to singlemode fibers," *Electron. Lett.*, vol.38, no.25, pp.1669-1670, Dec. 2002.

[3] D. Taillaert, W. Bogaerts, P. Bienstman, T. F. Krauss, P. Van Daele, I. Moerman, S. Verstuyft, K. De Mesel, and R. Baets, "An out-of-plane grating coupler for efficient butt-coupling between compact planar waveguides and single-mode fibers," IEEE J. Quantum Electron., vol.38, no.7, pp.949-955, Jul. 2002.

[4] D. Taillaert, P. Bienstman, and R. Baets, "Compact efficient broadband grating coupler for silicon-on-insulator waveguides," *Opt. Lett.*, vol.29, no.23, pp.2749-2751 Dec. 2004.

[5] D. Taillaert, F. Van Laere, M. Ayre, W. Bogaerts, D. Van Thourhout, P. Bienstman, and R. Baets, "Grating couplers for coupling between optical fibers and nanophotonic waveguides," Jap. J. Appl. Phys., vol.45, no.8A, pp.6071-6077, Aug. 2006.

[6] F. Van Laere, G. Roelkens, M. Ayre, J. Schrauwen, D. Taillaert, D. Van Thourhout, T. F. Krauss, and R. Baets, "Compact and highly efficient grating couplers between optical fiber and nanophotonic waveguides," *J. Lightw. Technol.*, vol.25, no.1, pp.151-156, Jan. 2007.

[7] G. Roelkens, D. Vermeulen, D. Van Thourhout, R. Baets, S. Brision, P. Lyan, P. Gautier, and J.-M. Fedeli, "High efficiency diffractive grating couplers for interfacing a single mode optical fiber with optical fiber with a nanophotonic silicon-on-insulator waveguide circuit," *Appl. Phys. Lett.*, vol.92, no.13, 131101, Mar. 2008.

[8] D. Vermeulen, S. Selvaraja, P. Verheyen, G. Lepage, W. Bogaerts, G. Roelkens, "High-efficiency Silicon-On-Insulator Fiber-to-Chip Grating Couplers Using a Silicon Overlay," IEEE 6th International Conference on Group IV Photonics, PDPF1, Sept. 2009.

[9] R. Waldhausl, B. Schnabel, P. Dannberg,, E.-B. Kley, A. Brauer, and W. Karthe, "Efficient coupling into polymer waveguides by gratings," *Appl. Opt.*, vol.36, no.36, pp.9383-9390, Dec. 1997.

[10] X. Chen, C. Li and H. K. Tsang, "Fabrication-tolerant waveguide chirped grating coupler for coupling to a perfectly vertical optical fiber," *IEEE Photon. Technol. Lett.*, vol.20, no.23, pp.1914-1916, Dec. 2008.

[11] R. Orobtchouk, A. Layadi, H. Gualous, D. Pascal, A. Koster, and S. Laval, "High-Efficiency Light Coupling in a Submicrometric Silicon-on-Insulator Waveguide," *Appl. Opt.*, vol.39, no.31, pp.5773-5777, Nov. 2000.

[12] C.A. Flory, "Analysis of directional grating-coupled radiation in waveguide structures," IEEE J. Quantum Electron., vol.40, no.7, pp.949-957, July 2004.

7. Grating couplers on silicon-on-sapphire for mid-infrared wavelength

Silicon-based photonic integrated circuits (PICs) have been developed rapidly in recent years in telecommunication range around 1.55μm. However, light in this wavelength range suffers form strong absorption by free carriers generated from two photon absorption in silicon, which would be eliminated when wavelength goes beyond about 2μm. In this chapter, we will extend our work to mid-infrared range, which targeted to demonstrate a silicon Raman laser beyond 3μm wavelength or some other sensing applications. We implemented a mid-IR laser source at around 2.75μm using a custom-designed Erbium and Praseodymium co-doped double cladding fluoride fiber. Silicon-on-sapphire (SOS) was used for the optical waveguide instead of silicon-on-insulator (SOI) due to the low absorption in mid-infrared range of sapphire substrate. The first shallow-etched grating coupler for silicon waveguides on SOS substrate was demonstrated at mid-infrared wavelength.

7.1 Introduction

Silicon photonic technology based on silicon-on-insulator (SOI) platform has been developed rapidly in recent years for applications at near infrared wavelengths (1.1-1.6μm), including optical interconnects, modulators, wavelength filters, variable optical attenuators and nonlinear optical signal processing, because it offers highly integrated waveguides, CMOS manufacturing compatibility and potentially very low cost. Applications of silicon photonics in mid-infrared (2 - 5μm) region for sensing

and nonlinear devices have recently attracted increasing interest for similar reasons [1, 2]. Mid-infrared light source in 2 - 5μm range are essential for many applications, such as remote chemical detection, bimolecular sensing, and infrared spectroscopy [1-3]. Various silicon waveguide structures have been demonstrated [4]. Cascaded silicon Raman laser has been proposed for mid-infrared operation [5]. Raman amplification in bulk silicon [2] and wavelength conversion in silicon waveguide [6] were also demonstrated in mid-infrared wavelength. However, the silicon based mid-infrared laser has not yet been demonstrated.

In this chapter, we describe the development of mid-infrared waveguides and fiber couplers as the first step towards making a mid-infrared silicon Raman laser. Various grating couplers for coupling light between single mode fiber and sub-micron sized silicon waveguides have already been demonstrated at the 1550nm telecom wavelength region [7, 8]. However the high absorption of silicon dioxide (for wavelength > 2.6μm) greatly limits their applications in mid-infrared region. Therefore, we designed and fabricated the silicon waveguides on silicon-on-sapphire (SOS) substrate; together with a grating coupler to couple light from mid-infrared fiber laser into the silicon waveguide on sapphire substrate. The mid-infrared fiber laser is implemented with Erbium (Er) and Praseodymium (Pr) co-doped ZBLAN double cladding fiber pumped by a diode laser array at 975nm. The simulation and experimental results of the grating coupler fabricated on SOS substrate are included.

7.2 Mid-infrared fiber laser

Fluorozirconate glass formed by a mixture of zirconium, barium, lanthanum, aluminum, and sodium fluorides (ZBLAN) is transparent up to 6μm wavelengths.

High power emissions at around 2.7μm through the $^4I_{11/2}$ to $^4I_{13/2}$ transition shown in Fig. 7.1 of Er ions doped in ZBLAN optical fiber been demonstrated [9, 10]. In this transition, the natural lifetime of the lower energy state ($^4I_{13/2}$) is longer than that of the upper state ($^4I_{11/2}$). Thus electrons will accumulate in the lower state, which inhibits efficient steady-state lasing at 2.75μm. Pr co-doping can solve this population bottleneck by introducing energy transfer (ET) process between Er ions and co-doped Pr ions [10]. The electron density in $^4I_{13/2}$ state is reduced through relaxation of energy states from Pr ions.

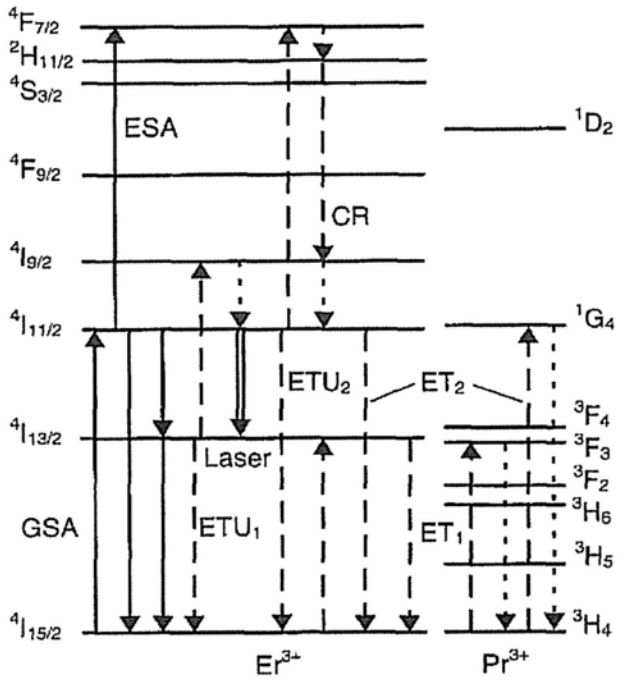

Fig. 7.1: Figure shows the schematic diagram of the energy-levels of erbium ions doped in ZBLAN optical fiber [10]. GSA: ground-state absorption. ESA: excited-state absorption. ETU: energy transfer up-conversion. ET: energy transfer. CR: cross relaxation.

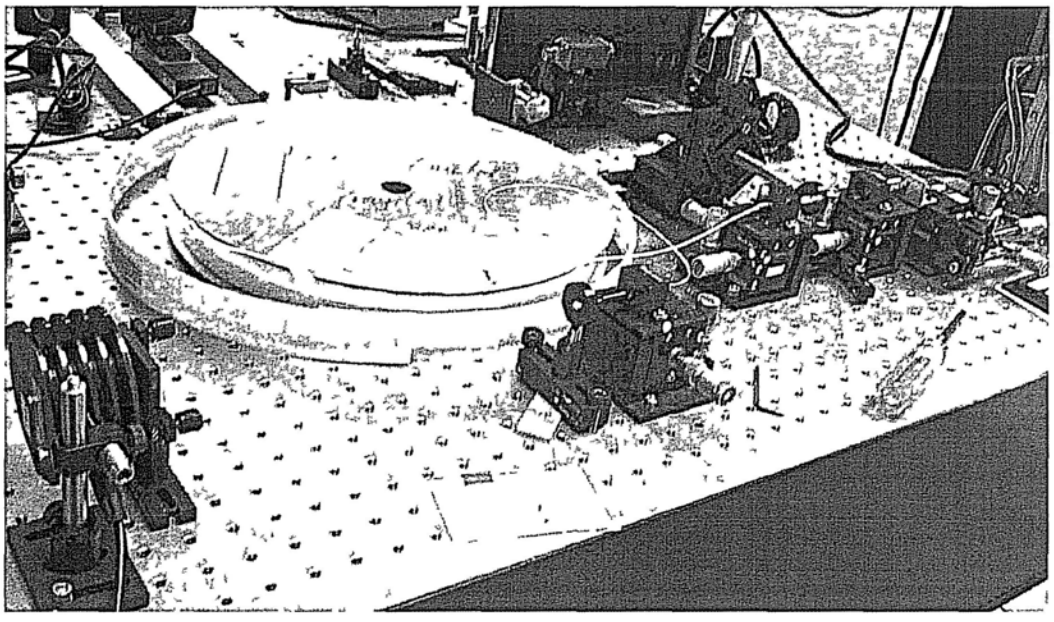

Fig. 7.2: Picture shows the experimental setup of the mid-infrared fiber laser. It mainly composited by a section of Er and Pr doped ZBLAN double cladding fiber and a high power laser diodes array at 975nm wavelength.

The doping concentration of Er and Pr ions were 30000ppm and 5000ppm respectively for the fiber core, with 9μm diameter and 0.25 numerical aperture (NA). A Bookham 975nm multimode laser diode module with 0.22 NA and 105μm diameter multi-mode fiber pigtail was used as the pump. The ZBLAN fiber was designed to be cladding pumped to allow good coupling efficiency with the pump laser and also to avoid thermal damage of the fiber by the high-intensity pump power. The outer cladding of the fiber is used to confine the pump light as shown in Fig.7.3

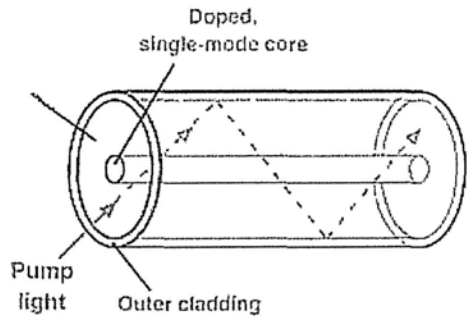

Fig. 7.3: Schematic diagram of the double cladding fiber.

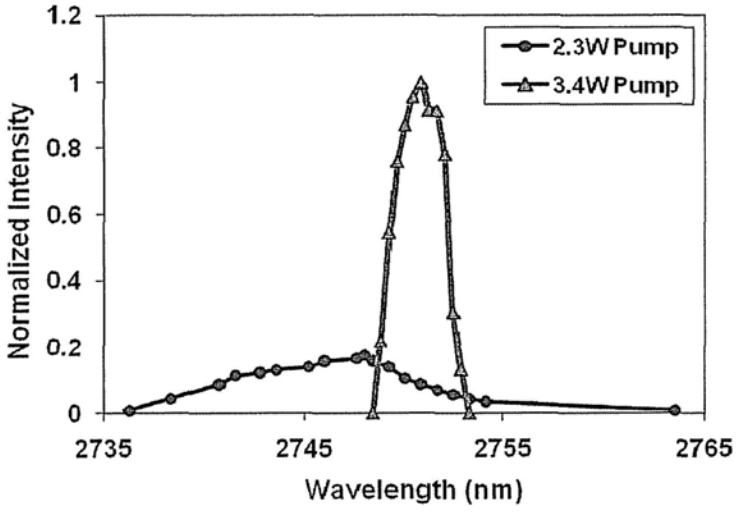

Fig.7.4: Spectra of the output from the diode pumped mid-infrared fiber laser with a threshold at ~2.5W pump power. The data plotted for 2.3W pump power was with 20 times magnification.

The inner cladding confined the mid-infrared light in the core area and acted as the waveguide core to guide the pump light. The diameter and NA of the inner cladding is 140μm and 0.5 respectively. The diameter of the outer cladding is 300μm. The laser cavity was constructed by ZBLAN fiber of 2m length and back reflections (~4%) on the cleaved fiber facets were used as feedback. The threshold of this fiber laser was about 2.5W pump power. The spectrum of the laser output with 3.4W

pump power was measured by monochromater and plotted in Fig. 7.4. The spectrum of fiber fluorescence with 2.3W pump power (before lasing) is also plotted.

7.3 Grating couplers and waveguides on silicon-on-sapphire

The waveguide was fabricated on a SOS wafer with top silicon thickness of 600nm. The width of the waveguide defined by deep etching (500nm etch depth) was 1μm with a waveguide length of 3mm. Similar to the waveguide grating couplers introduced in the previous chapters, adiabatic tapers were used to expand the width of the waveguide from 1μm to 10μm to match the mode size of the mid-infrared fiber laser. The length of the tapers is 1mm, which is designed to be sufficient long to eliminate the optical loss. The grating structure was 300nm shallow etched on top of the 10μm-width waveguide, whose SEM image was shown in Fig. 7.5(a). This etching depth was optimized by 2D FDTD simulations, followed a similar process as used for the grating couplers in communication band. The directionality of diffraction, coupling strength and back reflection were considered and made trade-off with each others.

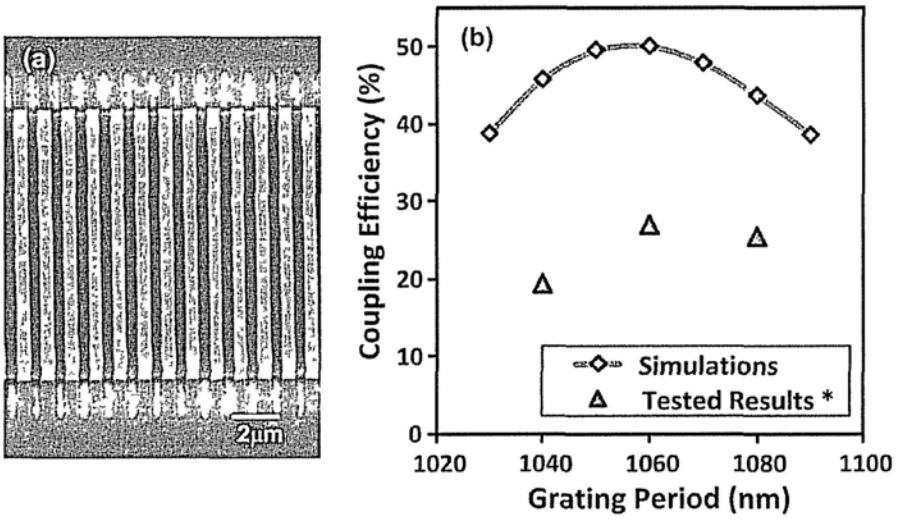

Fig. 7.5: (a) SEM image of the waveguide grating coupler on SOS wafer. (b) Coupling efficiency of the grating couplers at 2.75μm wavelength (* Waveguides was assumed to be lossless in the calculation, which implies the actual coupling efficiency should be higher.)

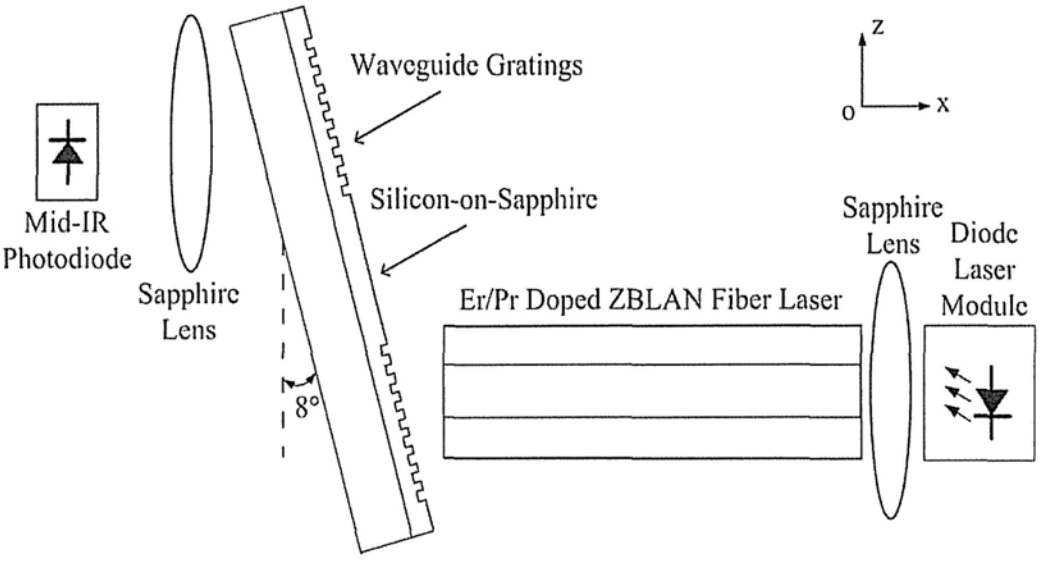

Fig.7.6: Experimental setup for testing the grating coupled waveguide on silicon-on-sapphire with mid-infrared fiber laser.

The whole experimental setup for characterization of the waveguides and gratings on SOS wafer is illustrated in Fig.7.6. The pump at 975nm was coupled into the inner cladding layer and the core of the ZBLAN fiber with a set of objective and sapphire lens. Then the other end of the ZBLAN fiber would be attached to the grating coupler to couple light into the waveguide. Camera with long distance objective lens (10×) was used to monitor the fiber-grating alignment. We introduced an 8 degree tilting of the fiber laser to the surface normal of the silicon-on-sapphire wafer to eliminate the light coupling back into the lasing cavity, which may change the lasing threshold. The mode of the light coupled into the 10μm-width waveguide was then converted to the mode of 1μm-width waveguide by the 1mm long taper and converted back after passing through a section of 3mm long waveguide.

We monitored the power of the light come from the back side of the silicon-on-sapphire wafer as shown in Fig. 7.6, which was collected by a sapphire lens. There is a constant power ratio (2.4) of the light diffracted upwards relative to the light diffracted downwards through the sapphire substrate. Thus, we could use the downward diffracted light at the waveguide output to measure the coupling efficiency of the grating coupler.

The period of the grating was calculated by the phase matching condition (Eq.2.1), where θ is 8° , which is the angle between the diffracted light and the normal of the wafer. n_{eff} is the effective index of the waveguide in the grating region, which is around 2.74 by calculation. Thus the grating period Λ is calculated to be around 1060nm for wavelength at 2.75μm. The SEM image of the fabricated grating coupler was shown in Fig. 7.5(a). Experimental measurements indicated that the coupling efficiency was 27%. In order to verify this design, we also fabricated grating coupler with 1040nm and 1080nm periods for testing. The measured

coupling efficiency was plotted in Fig. 7.5(b). Simulation results with different grating period by 2D FDTD simulation are also plotted for reference. The waveguide loss has not been considered in this stage, and the actual coupling efficiency can be higher than the numbers indicated in Fig. 7.5(b) if waveguide losses were taken into account. It's possible to demonstrate the focusing grating and 2D grating in the future on silicon-on-sapphire. However, it is much more difficult to achieve Gaussian-like output profile with apodized gratings on a silicon-on-sapphire wafer for mid-infrared wavelength. When the period of the grating increases with wavelength for diffraction, the number of periods in the area of fiber core that can be apodized is less than the one on SOI operated in communication band. Thus the output profile from the grating would be seriously distorted.

7.4 Conclusion

Grating couplers and waveguides on SOS wafer were fabricated and experimentally characterized, in order to explore the applications of silicon photonics in mid-infrared region. A ZBLAN fiber laser lasing at 2.75μm was constructed for experimental measurement. The waveguide grating coupler had a designed 50% coupling efficiency at 2.75μm wavelength between fiber laser and silicon waveguide. Measurement results on the fabricated device had a coupling efficiency of over 27%.

Reference:

[1] R.A. Soref, S.J. Emelett, and W.R. Buchwald, "Silicon waveguided components for the long-wave infrared region," J. Opt. A: Pure Appl. Opt., vol.8, no.10, pp.840-848, 2006.

[2] V. Raghunathan, D. Borlaug, R.R. Robert, and B. Jalali, "Demonstration of a mid-infrared silicon Raman amplifier," Opt. Express, vol.15, pp.14355-14362, 2007.

[3] M. Ebrahim-Zadeh and I.T. Sorokina, Mid-Infrared Coherent Sources and Applications (Springer, 2008)

[4] G.Z. Mashanovich, et al. "Silicon photonic waveguides for different wavelength regions," Semicond. Sci. Technol., vol.23, 064002, 2008.

[5] H. Rong, et al. "A cascaded silicon Raman laser," Nature Photonics, vol.2, pp.170-174, 2008.

[6] S. Zlatanovic, et al. "Mid-infrared wavelength conversion in silicon waveguides using ultacompact telecom-band-derived pump source," Nature Photonics, DOI: 10.1038/NPHOTON.2010.117, May 2010.

[7] D. Taillaert, W. Bogaerts, P. Bienstman, T. F. Krauss, P. Van Daele, I. Moerman, S. Verstuyft, K. De Mesel, and R. Baets, "An out-of-plane grating coupler for efficient butt-coupling between compact planar waveguides and single-mode fibers," *IEEE J. Quantum Electron.*, vol.38, pp.949-955, July 2002.

[8] X. Chen, C. Li and H. K. Tsang, "Fabrication-tolerant waveguide chirped grating coupler for coupling to a perfectly vertical optical fiber," *IEEE Photon. Technol. Lett.,* vol.20, no.23, pp.1914-1916, Dec. 2008.

[9] X.S. Zhu and R. Jain, "10-W-level diode-pumped compact 2.78μm ZBLAN fiber laser," Opt. Lett., vol.32, no.1, pp.26-28, 2007.

[10] M. Pollnau and S.D. Jackson, "Energy recycling versus lifetime quenching in erbium-doped 3-μm fiber lasers," IEEE J. Quantum Electron., vol.38, pp.162-169, 2002.

8. Conclusion

A summary of the work described in the thesis is presented in this chapter, including various grating couplers and nanophotonic devices. The comparison of those grating couplers is included. The prospect of future work related to the thesis is also discussed.

8.1 Summary and discussions

We first proposed and analyzed a linearly chirped grating for coupling light between a SOI nanophotonic waveguide and a vertical optical fiber. Vertical coupling is more preferable for photonic packaging process, because it enables a simpler optical alignment process that decouples adjustment of the fiber separation from the waveguide with the fiber position in the plane of the waveguide, and this can improve the speed for automatic alignment needed. Optimization of the chirped grating design can suppress the back reflection and increase coupling efficiency to about 42% with a 3dB bandwidth of 48nm by FDTD simulation. The fabrication steps required for the proposed chirped grating couplers are the same as the uniform grating couplers with titled fiber.

The optimized chirped grating couplers were fabricated with deep-UV photolithography. Using a two section design with a negative linear chirp in the front section, we obtained over 34% coupling efficiency experimentally for coupling light between TE mode in a submicron-sized SOI waveguide and a fully vertical optical fiber. The 3dB bandwidth was 45nm with center wavelength around 1550nm. Experimental measurements showed that the optimized chirped grating design is

robust and tolerant to variations in fabrication process parameters which may lead to a large (~20nm) random fluctuations in slot width and vary the duty cycle of the fabricated grating. The coupling efficiency of this grating coupler was mainly limited by the bi-directional nature of diffraction from the grating. Further improvement may be obtained by improving the diffraction directionality of the grating, such as adding waveguide bottom mirrors or optimize the thickness and etching depth

The design and measurement results of the focusing grating couplers between SOI waveguide and vertical optical fiber employing a section of linearly chirped grating are then described. The footprints of the grating couplers can be significantly reduced yet similar coupling efficiencies were obtained. These compact couplers are suitable for low cost packaging process of SOI chip using cleaved fiber or fiber array.

We also demonstrated 2D chirped grating couplers fabricated using deep-UV photolithography. Polarization independent operation was obtained. Measurements show that the chirped grating design could successfully suppress the second order back reflection into waveguide and enhance the coupling efficiency for 2D gratings couplers. We obtained over 30% coupling efficiency for coupling light between the quasi-TE mode in SOI nanophotonic waveguides and optical fibers. The coupling efficiency is slightly higher than the 2D grating couplers with tilted off-vertical optical fibers. According to the experimental measurement results, we found that the effective index of the grating region of the 2D grating could be predicted by simulation results for the 1D grating, when lateral fill factor of the shallow etched holes is larger than 0.5. This was explained by the effective medium theory and verified by 3D FDTD simulation. Similar to the 1D grating couplers, the coupling

efficiency of the demonstrated 2D grating couplers was mainly limited by the bi-directional nature of diffraction from the grating.

Based on the 2D grating couples and polarization splitter introduced, we then described the design and preliminary experimental results of an integrated polarization-diversity DPSK demodulator on SOI, which consist of the proposed 2D chirped grating couplers and two nominally identical microring resonators. It could potentially achieve polarization insensitive operation. The polarization-diversity scheme however places stringent fabrication tolerance on the microring resonators and we expect that thermal tuning of the micro-rings would be needed for the typical device fabricated using 193nm lithography in order to achieve fully polarization independent operation.

Besides, we demonstrated a Mach-Zehnder interferometer (MZI) on silicon-on-insulator (SOI) wafer. The measured extinction ratio of the fabricated MZI is over 20dB. The MZI is formed using novel 1×2 waveguide splitters/combiners that are based on shallow etched chirped gratings on the waveguides. The gratings could couple light directly from/into cleaved optical fibers while splitting/combining without excess loss. Over 36% coupling efficiency was experimental measured. The splitting ratio was widely tunable by adjusting the fiber position. The performance of the variable split-ratio was verified experimentally. The proposed splitter/combiner is a promising component for photonic integrated circuits because of its high efficiency and tunable splitting ratio. DPSK demodulation at 10Gb/s using the proposed MZI was also demonstrated. Opened-eye diagram was obtained from the demodulator. The device can be easily packaged with cleaved fiber or fiber arrays vertically attached to the wafer surface. This potentially low-cost packaging process and its high-quality performance would make the proposed device a promising

choice for the commercial market.

In addition to the designs and applications of various chirped grating couplers and nanophotonic devices, grating couplers formed by an array of fully-etched subwavelength nanoholes were proposed, fabricated and experimentally characterized. The grating couplers were fabricated in the same deep etch step as used for defining the waveguides, thus reducing the number of masks and fabrication steps needed. Despite the reduction in fabrication steps, we achieved coupling efficiencies comparable with conventional grating couplers that fabricated with additional fabrication processes. The 34% coupling efficiency measured in the fabricated devices had a 40nm 3dB optical bandwidth for coupling between single-mode optical fiber and the silicon nanophotonic wire waveguides. The 3D FDTD simulation results had good agreement with the experimental results from the fabricated devices. Further improvement could be achieved by varying the grating strength to increase the field overlap with fiber mode and adding a substrate mirror. However, compared with those shallow-etched grating couplers, the back reflection is still quite significant, which limits the performance and places more stringent requirements on the design and fabrication process.

All the waveguide gratings described in chapter 2 to 5 have a limit in coupling efficiency at about 35%, although we included the chirped gratings to reduce the packaging cost, the focusing gratings to reduce the device footprint, the fully-etched subwavelength structures to simplify the fabrication process, and bi-directional gratings or 2D gratings for varies practical applications. The limitation of coupling efficiency is posted by the bi-directional nature of light diffraction as significant part of light is coupled downwards into the substrate instead of the optical fibers, and also the mode field mismatch between the diffraction output and the fundamental mode

of optical fibers.

Therefore, as described in chapter 6, we optimized the waveguide thickness to improve the directionality of grating diffraction, and apodized the grating to enhance the mode-matching efficiency. We then achieved a coupling loss of 1.2dB between a standard single mode optical fiber and a 450nm wide SOI optical waveguide using a single etched grating structure, without any additional bottom mirrors or high index overlay. This result is the highest coupling efficiency reported to date for waveguide grating couplers. The coupling strength of the waveguide grating is varied to achieve a Gaussian-like mode field output along z-axis in order to match with the mode of optical fibers. Back reflection is also suppressed by the variation of coupling strength. The proposed structure is quite robust to fabrication process variations. The coupling strengths and average effective refractive indices for uniform gratings with different fill factors were characterized and the results agree with the simulation results.

We also achieved 3dB coupling loss with vertical optical fibers. In addition to the Gaussian-like output mode profile from the apodized grating, back reflection was further reduced from ~80% to ~30% by a linear chirp of the grating period. Around 3dB enhancement was achieved when coupling with vertical optical fibers. Further improvement is under way.

Finally, in order to explore the applications of silicon photonics in mid-infrared region, which is emerging for sensing and biomedical applications, grating couplers and waveguides were fabricated on SOS wafers and characterized. A ZBLAN fiber laser lasing at 2.75μm was constructed for experimental measurement. The waveguide grating coupler had a designed 50% coupling efficiency at 2.75μm

wavelength between fiber laser and silicon waveguide. Measurement results on the fabricated device had a coupling efficiency of over 27%.

8.2 Prospect of the future work

The best coupling efficiency (-1.2dB) demonstrated with apodized gratings and optimized diffraction directionality is only with slightly angled optical fibers. The attempt to achieve similar coupling efficiency with vertical optical fibers that is more preferable for low cost photonic packaging process was not quite successful at the current stage. Only around -3dB coupling efficiency was obtained as described in section 6.4. One of the possible reasons for comparatively lower efficiency is the back reflection, which is still quite significant (at about 30% by simulation). Strong FP resonance was measured experimentally with vertical optical fibers even with chirped grating periods. Another reason is the mode distortion caused by the chirp of grating periods. Coupling strength is changed with period. It means that the field pattern of the diffraction output may be no long Gaussian-like with chirped gratings for the apodized grating couplers. However, we believe the Gaussian-like field output from apodized gratings with eliminated back reflection can be eventually realized for vertical optical fibers. Further design work is still demanded to realize such high efficient and low-cost grating couplers.

Up to now, we only fabricated the most basic 1D apodized grating couplers with optimized diffraction directionality and Gaussian-like output field pattern, in order to demonstrate preliminarily the high coupling efficiency that could be possibly achieved with the shallow-etched grating couplers. Many more advanced and versatile functional components based on such apodized gratings could be explored and realized in principle, such as 2D grating couplers, various power and

polarization splitters, focusing grating couplers, etc. A range of photonic devices for PIC technology would also benefit from such enhancement in coupling efficiency between optical fibers and nanophotonic waveguides.

The limited bandwidth of the waveguide grating couplers is another issue that we need to deal with. The physical origin is the change of direction angle for different wavelength according to the phase matching condition. Only the light diffracted out in certain direction can efficiently coupled into the optical fibers, which is related to the NA of the fibers. Chirping and apodizing of the gratings would normally further decrease the bandwidth, as their optimization is also wavelength dependent. In order to increase the bandwidth of grating coupler, we probably need to modify the function of effective index of the grating structure against wavelength, or increase the NA of the optical fibers if possible.

Appendix A:

Basic simulation procedures of a grating coupler

We use commercially available software (*FullWAVE of RSoft Photonic CAD Suite, version 8.2*) to do 2D FDTD simulation for the grating couplers. A 12μm wide waveguide produces a lateral TE mode profile (in the plan of wafer surface) that is well-matched to conventional single mode optical fibers, thus 2D Simulations of the grating structures are accurate enough to evaluate the performance of the grating couplers [1].

The well-known finite-difference time-domain (FDTD) method is a rigorous solution to Maxwell's equations without any approximations or theoretical restrictions [2]. It is a direct solution of the Maxwell's curl equations in Cartesian coordinates as implemented in the software, which therefore includes many more effects than other approximate methods.

Here are the basic procedures for evaluate the performance of a grating coupler:

Step 1: Set the parameters used for the global setting of a new project, including the wavelength (1.55μm), refractive index of silicon (3.48) and Air (1), etc.

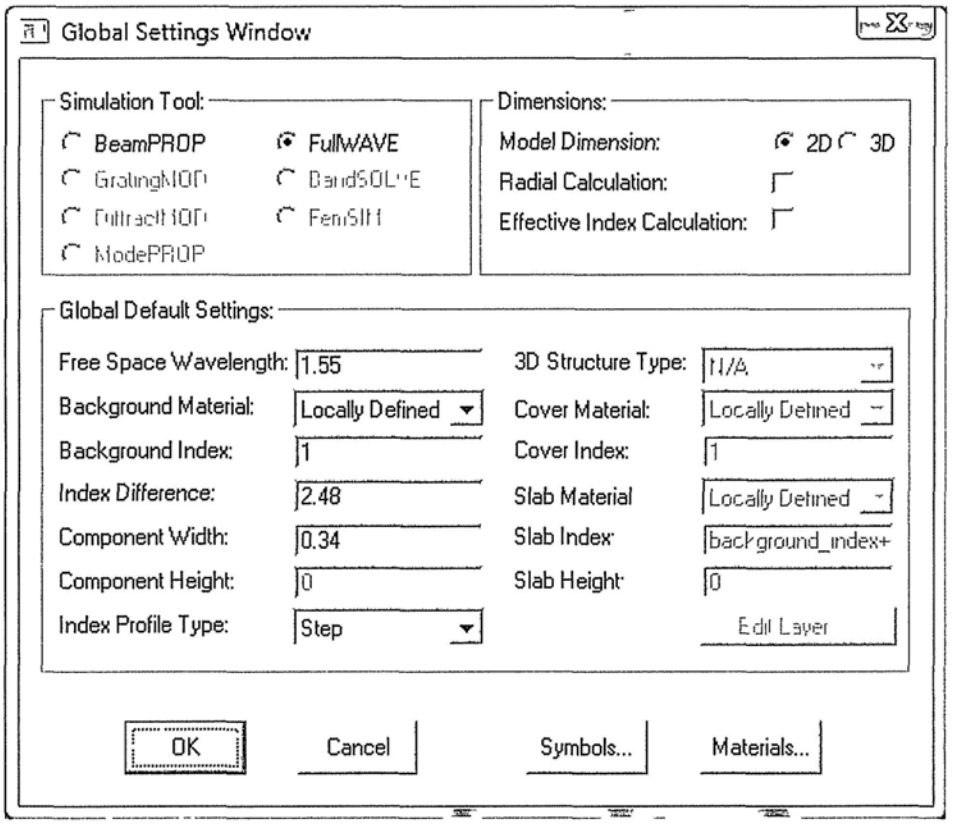

Step 2: Draw the grating coupler in the CAD. The launched field (light input) is placed on the waveguide with a slab mode. Power monitors are put at both side of the grating as shown in the following figure to monitor the directionality, and one on the waveguide behind the field launch position to monitor the back reflection of the grating.

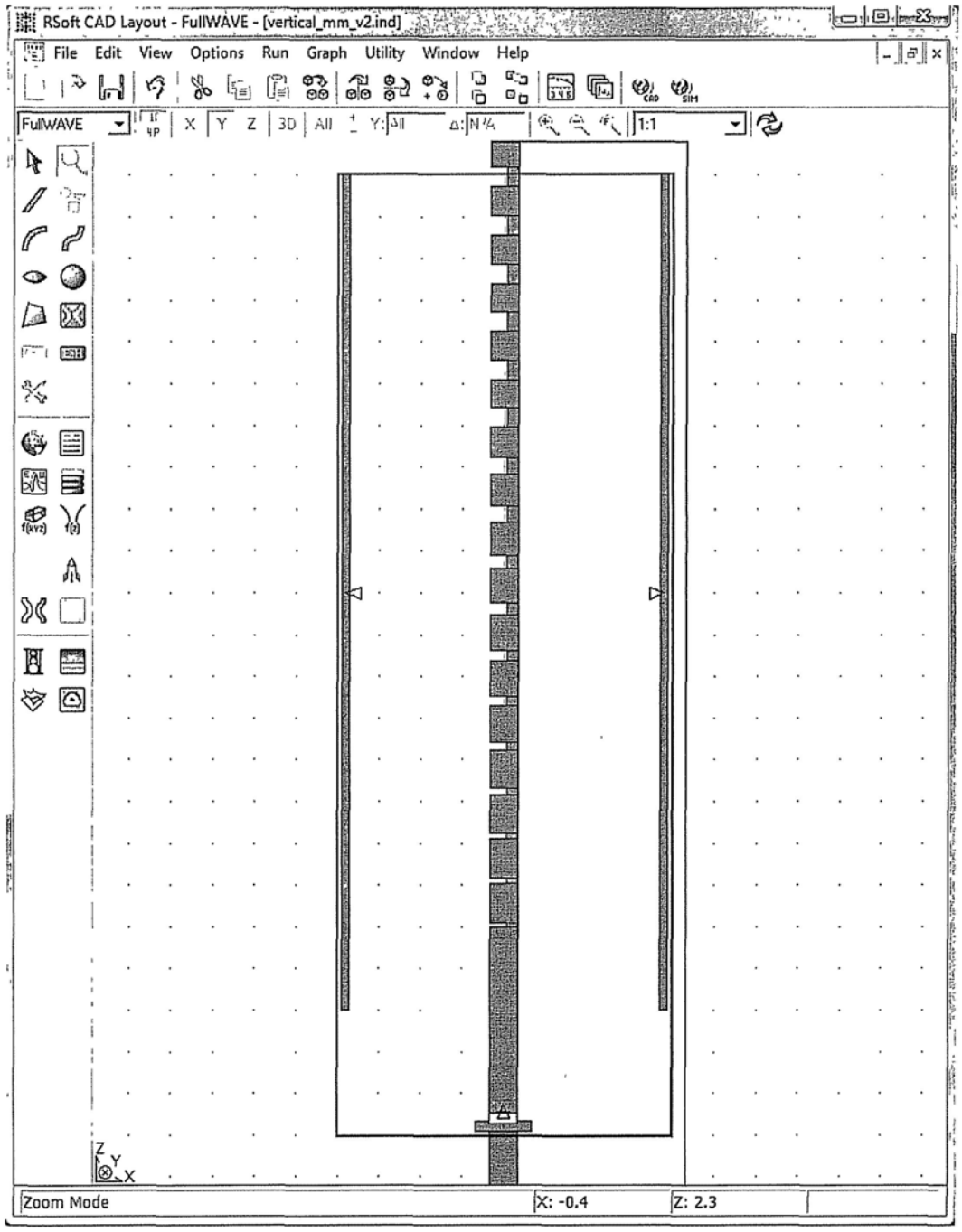

Step 3: Set the parameters and start the FDTD simulation. The grid size must be small enough to resolve the smallest feature of the structure. We will sometimes further reduce the grid size to evaluate the accuracy of the simulations.

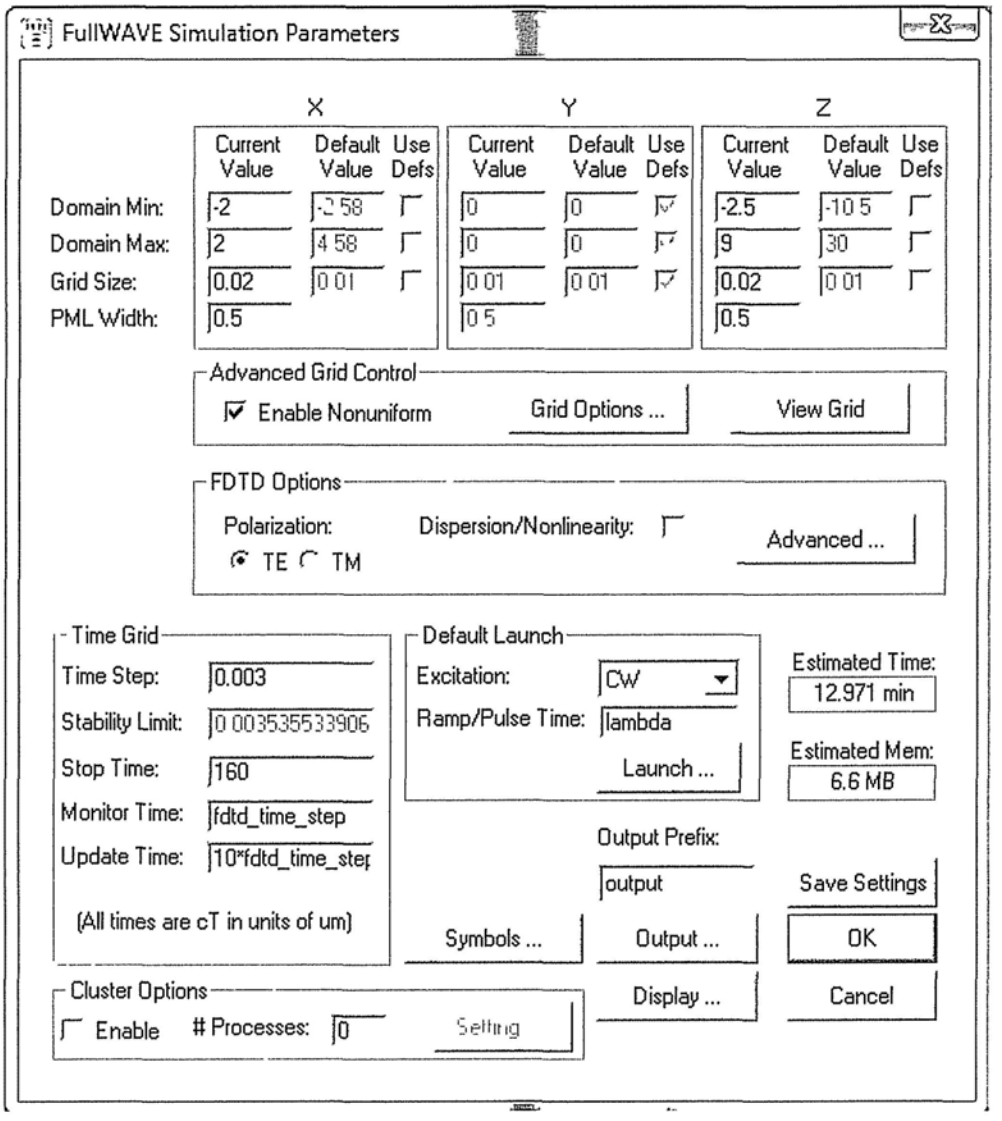

Step 4: The launch position of the field is changed to the left side of the grating (above the wafer surface) with a Gaussian mode input. A power monitor is placed on the waveguide to monitor percentage of power coupled into the waveguide mode.

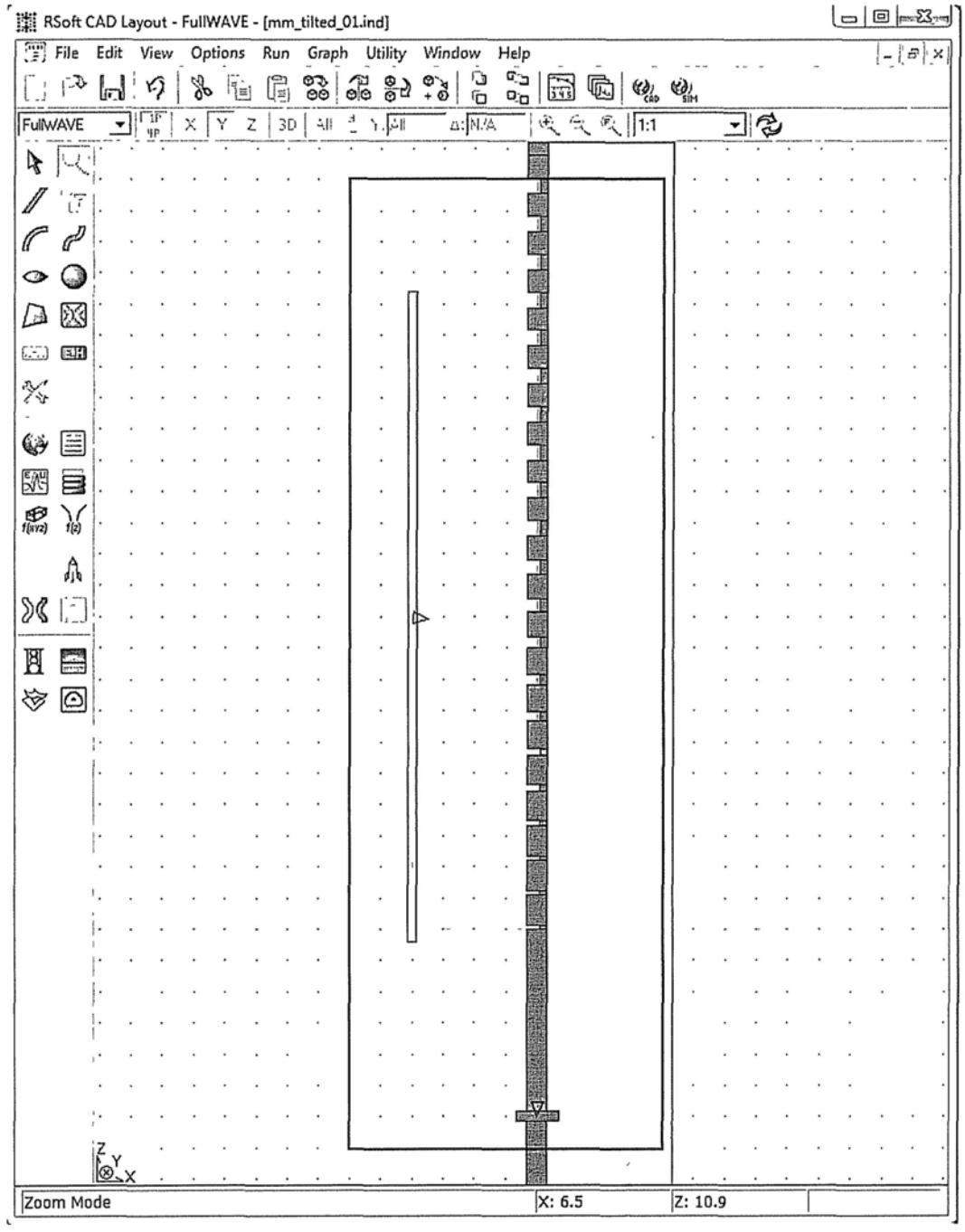

Step 5: The detailed parameters for the launched field. The mode of the input field is Gaussian with a full width of 10.4μm. The "Phi" sets the angle of input (90° + θ).

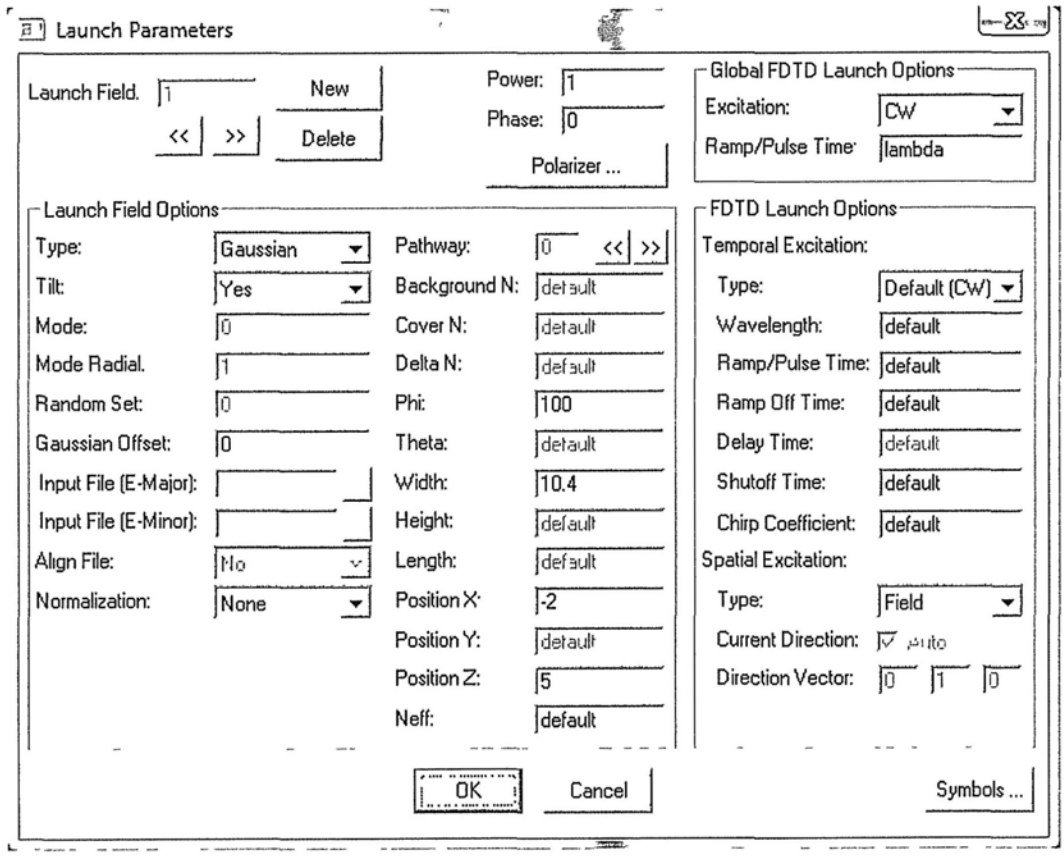

References:

[1] D. Taillaert, P. Bienstman, and R. Baets, "Compact efficient broadband grating coupler for silicon-on-insulator waveguides," *Opt. Lett.*, vol.29, no.23, pp.2749-2751 Dec. 2004.

[2] A. Taflove, Computational Electrodynamics, the Finite-Difference Time-Domain Method. Norwood, MA: Artech House, 1995.

Appendix B:

List of abbreviations

1D – One dimensional

2D – Two dimensional

AMI – Alternate mark inversion

BER – Bit-error rate

CMOS – Complementary metal-oxide-semiconductor

CR – Cross relaxation.

DPSK – Differential phase-shift keying

DQPSK – Differential-quadrature-phase-shift-keying

DWDM – Dense wavelength-division multiplexing

EMT – Effective medium theory

ESA – Excited-state absorption

ET – Energy transfer.

ETU – Energy transfer up-conversion.

FDTD – Finite difference time-domain

FP – Fabry-Perot

FSR – Free spectral range

FTTB – Fiber-to-the-building

FTTH – Fiber-to-the-home

GSA – Ground-state absorption

IC – Integrated circuit

MFD – Mode field diameter

Mid-IR – Mid-infrared

MOS – Metal-oxide-semiconductor

MZI – Mach-Zehnder interferometer

NA – Numerical aperture

OEIC – Optoeletronic integrated circuit

OOK – On-off-keying

PIC – Photonic integrated circuit

PLC – Planar lightwave circuit

PICs – Photonic integrated circuits

Q – Quality factor

ROF – Radio over fiber

SEM – Scanning electron microscope

SNR – Signal-to-noise ratio

SOI – Silicon-on-insulator

SOS – Silicon-on-sapphire

TE – Transverse electric

TM – Transverse magnetic

TPA – Two-photon absorption

ZBLAN – Fluorozirconate glass formed by a mixture of zirconium, barium, lanthanum, aluminum, and sodium fluorides

Appendix C:

Publication list

Journal Articles:

1. **X. Chen,** C. Li, C.K.Y. Fung, S.M.G. Lo, and H.K. Tsang, "Apodized grating couplers for efficient coupling to optical fibers," *IEEE Photon. Technol. Lett.*, vol.22, no.15, pp.1156-1158, Aug. 2010.
2. **X. Chen,** C. Li, and H.K. Tsang, "Two dimensional silicon waveguide chirped grating couplers for vertical optical fibers," *Optics Communications, vol.283, no.10, pp.2146-2149, May.* 2010.
3. **X. Chen** and H.K. Tsang, "Nanoholes grating couplers for coupling between silicon-on-insulator waveguides and optical fibers," *IEEE Photonics Journal*, vol.1, no.3, pp.184-190, Sept. 2009.
4. **X. Chen,** C. Li, and H.K. Tsang, "Etched waveguide grating variable 1X2 splitter/combiner and waveguide coupler," *IEEE Photon. Technol. Lett.*, vol.21, no.5, pp.268-270, Mar. 2009.
5. C. Li, **X. Chen**, Z. Sheng, and H.K. Tsang, "Chirped waveguide gratings for low-cost silicon photonic wire packaging and other applications "(Invited), *Proc. of SPIE*, vol.7219, 721903, Jan. 2009.
6. **X. Chen,** C. Li, and H.K. Tsang, "Fabrication-tolerant waveguide chirped grating coupler for coupling to a perfectly vertical optical fiber," *IEEE Photon. Technol. Lett.*, vol. 20, no. 23, pp. 1914-1916, Dec. 2008.

Patent:

7. **X. Chen,** C. Li, and H.K. Tsang, "Optical devices for coupling of light," United States Patent Application 20090290837.

Conference Papers:

8. L. Xu, C. Li, C.W. Chow, **X. Chen**, C.Y. Wong, S.M.G. Lo, and H.K.Tsang, "Frequency Quadrupling of Phase Modulated Signals," OECC (Accepted), Japan, July 2010.
9. H.K. Tsang, **X. Chen**, L. Xu, and C. Li, "Some Recent Developments in Silicon Photonics Enabled by ePIXfab," (Invited) The 15th European Conference on Integrated Optics (ECIO), Cambridge, UK. Apr. 2010.
10. **X. Chen**, C. Li, S.M.G. Lo, K. Fung, and H.K. Tsang, "Silicon waveguide grating couplers with engineered coupling strength for optimized coupling," The 15th European Conference on Integrated Optics (ECIO), Cambridge, UK, April 2010.
11. L. Xu, C. Li, **X. Chen**, and H.K. Tsang, "DQPSK demodulation using integrated silicon ring resonators," The 15th European Conference on Integrated Optics (ECIO), Cambridge, UK, April 2010.
12. **X. Chen**, C. Li, Y. Gao, L. Xu, H.K. Tsang, and C. Shu, "Characterization of Integrated Polarization-Diversity DPSK Demodulator with Two-Dimensional Chirped Grating Couplers and Ring Resonators," OFC/NFOEC 2010 in San Diego, California, USA, JWA26, Mar. 2010.
13. **X. Chen**, C. Li, and H.K. Tsang, "Non-uniform Focusing Grating for Coupling between Silicon Waveguide and Vertical Optical Fiber," The 22nd Annual Meeting of IEEE Photonics Society, Turkey, TuV3, Oct. 2009.
14. **X. Chen** and H.K. Tsang, "Characterization of Deep Etched Holes Arrays as Grating Couplers between Optical Fibers and Nanophotonic Waveguides," The 22nd Annual Meeting of IEEE Photonics Society, Turkey, ThL5, Oct. 2009.
15. **X. Chen**, C. Li, and H.K. Tsang, "Grating Coupler for Mid-infrared Silicon-on-Sapphire Waveguide," in ThG5, OECC, Hong Kong, July. 2009.
16. **X. Chen**, C. Li, L. Xu, and H.K. Tsang, "DPSK demodulation using mach-zehnder delay-interferometer on silicon-on-insulator integrated with diffractive grating structure," Asia Optical Fiber Communication and Optoelectronic Exposition and Conference, Shanghai, China, SuF3, Oct. 2008

17. **X. Chen**, C. Li, and H.K. Tsang, "Characterization of silicon-on-insulator waveguide chirped grating for coupling to a vertical optical fiber," IEEE/LEOS International Conference on Optical MEMs and Nanophotonics, Freiburg, Germany, pp. 56-57, Aug. 2008.

18. **X. Chen**, C. Li, and H.K. Tsang, "Chirped Grating for Efficient Coupling from a Silicon Waveguide to a Vertical Optical Fiber," 16th International Conference on Photonics in Switching, Sapporo, Japan, D-02-5, Aug. 2008.